The long non-coding RNA *GHSROS* reprograms prostate cancer cell lines toward a more aggressive phenotype

Patrick B. Thomas[1,2,3], Penny L. Jeffery[1,2,3], Manuel D. Gahete[4,5,6,7,8], Eliza J. Whiteside[9,10,†], Carina Walpole[1,3], Michelle L. Maugham[1,2,3], Lidija Jovanovic[3], Jennifer H. Gunter[3], Elizabeth D. Williams[3], Colleen C. Nelson[3], Adrian C. Herington[1,3], Raúl M. Luque[4,5,6,7,8], Rakesh N. Veedu[11], Lisa K. Chopin[1,2,3,*], Inge Seim[1,2,3,12,*]

[1] Ghrelin Research Group, Translational Research Institute- Institute of Health and Biomedical Innovation, School of Biomedical Sciences, Queensland University of Technology (QUT), Woolloongabba, Queensland 4102, Australia.

[2] Comparative and Endocrine Biology Laboratory, Translational Research Institute-Institute of Health and Biomedical Innovation, School of Biomedical Sciences, Queensland University of Technology, Woolloongabba, Queensland 4102, Australia.

[3] Australian Prostate Cancer Research Centre–Queensland, Institute of Health and Biomedical Innovation, School of Biomedical Sciences, Queensland University of Technology (QUT), Princess Alexandra Hospital, Translational Research Institute, Woolloongabba, Queensland 4102, Australia.

[4] Maimonides Institute of Biomedical Research of Cordoba (IMIBIC), Córdoba, 14004, Spain.

[5] Department of Cell Biology, Physiology and Immunology, University of Córdoba, Córdoba, 14004, Spain.

[6] Hospital Universitario Reina Sofía (HURS), Córdoba, 14004, Spain.

[7] CIBER de la Fisiopatología de la Obesidad y Nutrición (CIBERobn), Córdoba, 14004, Spain.

[8] Campus de Excelencia Internacional Agroalimentario (ceiA3), Córdoba, 14004, Spain.

[9] Centre for Health Research, University of Southern Queensland, Toowoomba, Queensland 4350, Australia.

[10] Institute for Life Sciences and the Environment, University of Southern Queensland, Toowoomba, Queensland 4350, Australia.

[11] Centre for Comparative Genomics, Murdoch University & Perron Institute for Neurological and Translational Science, Perth, Western Australia 6150, Australia.

[12] Integrative Biology Laboratory, College of Life Sciences, Nanjing Normal University, 1 Wenyuan Road, 210023, Nanjing, China.

[†] Present address: Moffitt Cancer Center and Research Institute, Tampa, FL, 33612, USA.

[*] Correspondence to inge@seimlab.org or l.chopin@qut.edu.au.

Short running title: *GHSROS* in prostate cancer

Key words: long non-coding RNA, antisense transcript, prostate cancer, tumour growth, gene expression

ABSTRACT

It is now appreciated that long non-coding RNAs (lncRNAs) are important players in the orchestration of cancer progression. In this study we characterized *GHSROS*, a human lncRNA gene on the opposite DNA strand (antisense) to the ghrelin receptor gene, in prostate cancer. The lncRNA was upregulated by prostate tumors from different clinical datasets. Consistently, transcriptome data revealed that *GHSROS* alters the expression of cancer-associated genes. Functional analyses *in vitro* showed that *GHSROS* mediates tumor growth, migration, and survival and resistance to the cytotoxic drug docetaxel. Increased cellular proliferation of *GHSROS*-overexpressing PC3, DU145, and LNCaP prostate cancer cell lines *in vitro* was recapitulated in a subcutaneous xenograft model. Conversely, *in vitro* antisense oligonucleotide inhibition of the lncRNA reciprocally regulated cell growth and migration, and gene expression. Notably, *GHSROS* modulates the expression of PPP2R2C, the loss of which may drive androgen receptor pathway-independent prostate tumor progression in a subset of prostate cancers. Collectively, our findings suggest that *GHSROS* can reprogram prostate cancer cells toward a more aggressive phenotype and that this lncRNA may represent a potential therapeutic target.

Keywords: long non-coding RNA, lncRNA, prostate cancer

INTRODUCTION

The human genome yields a multitude of RNA transcripts with no obvious protein-coding ability, collectively termed non-coding RNAs (ncRNAs)[1]. A decade of intensive research has revealed that many ncRNAs greater than 200 nucleotides in length have expression patterns and functions as diverse as protein-coding RNAs[1, 2]. These long non-coding RNAs (lncRNAs) have emerged as important regulators of gene expression, acting on nearby (*cis*) or distant (*trans*) protein-coding genes[2]. Although the vast majority of lncRNAs remain uncharacterized, it is clear that they play key regulatory roles in development, normal physiology, and disease.

We previously[3] identified *GHSROS* (also known as *AS-GHSR*), a 1.1-kb capped and polyadenylated lncRNA gene antisense to the intronic region of the ghrelin receptor gene (*GHSR*) (Fig. 1a). *GHSROS* harbors a putative human-specific promoter in a transposable element[3], a pattern frequently found in promoters of lncRNAs with high tissue specificity and low expression levels[4, 5]. It is now appreciated that many lncRNAs are equivalent to classical oncogenes or tumor suppressors and drive similar transcriptional programs in diverse cancer types[2]. Indeed, our earlier study showed that *GHSROS* is overexpressed in lung cancer and that its forced overexpression increases migration in lung adenocarcinoma cells lines[3]. We speculated that *GHSROS* plays a role in other cancers. Prostate cancer is a disease diagnosed in nearly 1.5 million men worldwide annually[6]. Intriguing recent studies have revealed that, like breast cancer, prostate cancer is a heterogeneous disease with multiple molecular phenotypes[7,8,9]. The identification of genes that drive or mediate these distinct phenotypes is crucial. Although a number of lncRNAs have been reported in prostate cancer, few have been functionally characterized or assessed as therapeutic targets[10]. Here, we report that *GHSROS* is highly expressed in a subset of prostate tumors. We provide evidence that this lncRNA

reprograms prostate cancer cells toward a more aggressive phenotype, possibly by repressing the expression of the tumor suppressor PPP2R2C to allow androgen-independent growth.

RESULTS

GHSROS is expressed in prostate cancer

Microarrays and RNA-sequencing are commonly used to assess the expression of genes. LncRNAs are often expressed at orders of magnitude lower than protein-coding transcripts, however, making them difficult to detect[5, 11,12,13,14,15]. Interrogation of exon arrays harboring four different strand-specific probes against *GHSROS* demonstrated that the lncRNA is actively transcribed, although expressed at very low levels in cancer cell lines and tissues (Supplementary Fig. S1), consistent with previous observations from Northern blotting and RT-PCR experiments[3]. The low expression across the *GHSROS* and *GHSR* loci in RNA-seq datasets is illustrated in Supplementary Fig. S2. Collectively, these data demonstrate that it is not currently possible to detect *GHSROS* in public genome-wide gene expression datasets.

We next evaluated *GHSROS* expression in a qRT-PCR tissue array of 18 cancers. This analysis revealed particularly high *GHSROS* expression in lung tumors, as previously reported[3], and elevated expression in prostate tumors (Fig. 1b). Analysis of additional prostate tissue-derived cDNA arrays revealed that *GHSROS* could be detected in approximately 41.7% of all normal prostate tissues (n=24), 55.7% of tumors (n=88), and 58.1% of other prostatic diseases (e.g. prostatitis; n=31) (Supplementary Table S1). *GHSROS* was highly expressed by a subset of prostate tumors (~11.4%; Z-score >1) (Fig. 1c) and elevated in tumors with Gleason scores 8-10 (Supplementary Fig. S3; Supplementary Table S1; Mann-Whitney-Wilcoxon test P=0.0021). To expand on these observations, we examined an independent cohort of eight normal prostate tissue specimens and 28 primary tumors with

high Gleason scores (18 of which had metastases at biopsy). Similarly, *GHSROS* expression was significantly elevated in tumors compared to normal prostate tissue (Mann-Whitney-Wilcoxon test, P=0.0070) (Fig. 1d; Supplementary Fig. S4; Supplementary Table S2).

As the functional thresholds of long non-coding RNAs are difficult to gauge and likely cell-context specific[16], we identified cell lines with a range of endogenous *GHSROS* expression. Compared to the RWPE-1 benign prostate-derived cell line, higher expression was observed in the PC3 (P=0.00040, Student's *t*-test) (Fig. 1e) and DuCaP prostate cancer cell lines (P=0.0024), and expression was similar to RWPE-1 in the DU145 (P=0.29) and LNCaP prostate cancer cell lines (P=0.49). We also assessed the expression of *GHSROS* in patient-derived xenografts (PDXs). Compared to RWPE-1, *GHSROS* was significantly upregulated ($P \leq 0.05$) in 4/6 of the LuCaP series of PDX lines[17] and in the BM18 femoral metastasis-derived androgen-responsive PDX line[18] (P=0.0005) (Fig. 1e).

GHSROS promotes growth and motility of prostate cancer cells _in vitro_

To gain insights into *GHSROS*, we assessed its function in three prostate-derived cell lines by stably overexpressing the lncRNA in PC3, DU145, and LNCaP cells (denoted PC3-GHSROS, DU145-GHSROS, and LNCaP-GHSROS) (Supplementary Fig. S5). Cell proliferation over 72 hours (measured by a xCELLigence real-time cell analysis instrument) was increased in PC3 (P=0.029, Student's t-test) and DU145 (P=0.026) *GHSROS*-overexpressing cells (Fig. 2a). LNCaP cells did not attach well to the gold electrodes of the xCELLigence instrument (data not shown), and we therefore utilized a WST-1 assay to assess this cell line. Similar to PC3 and DU145 cells overexpressing *GHSROS*, proliferation was also increased in LNCaP-GHSROS cells at 72 hours (P=0.040) (Fig. 2b). *GHSROS* overexpression also increased the rate of cell migration of PC3 (P=0.0064, Student's t-test),

DU145 (*P*=0.017), and LNCaP cells (*P*=0.00020) over 24 hours (Fig. 2c) (where LNCaP was assessed by a standard transwell migration assay; PC3 and DU145 by an xCELLigence instrument). To confirm the *in vitro* functional effects of *GHSROS*, we designed locked nucleic antisense oligonucleotides (LNA-ASOs) to strand-specifically silence endogenous *GHSROS* expression (Fig. 2d; Supplementary Fig. S6). Two LNA-ASOs targeting distinct regions of *GHSROS*, RNV124 and RNV104L, independently reduced the expression of *GHSROS* (percentage knockdown of ~63% and ~71%, respectively) in native PC3 cells 48 hours post transfection compared to scrambled control (*P*=0.0002 and *P*=0.0001, Student's *t*-test) (Fig. 2e). Moreover, *GHSROS* knockdown attenuated cell proliferation (RNV124, *P*=0.049; RNV104L, *P*=0.030) (Fig. 2f) and migration of PC3 cells over 18 hours (RNV124, *P*=0.0042) (Fig. 2g) – the reciprocal effects observed when *GHSROS* was forcibly overexpressed.

GHSROS is associated with cell survival and resistance to the cytotoxic drug docetaxel

Knockdown experiments also revealed that *GHSROS* protected PC3 prostate cancer cells from death by serum starvation (Supplementary Fig. S7). This observation led us to examine whether *GHSROS* contributes to cell survival following chemotherapy. The current treatment of choice for advanced, castration-resistant prostate cancer (CRPC; the fatal final stage of the disease) after the failure of hormonal therapy is the cytotoxic drug docetaxel, a semi-synthetic taxoid that induces cell cycle arrest. At the half maximal inhibitory concentration (IC_{50}) of docetaxel (5 nM for LNCaP[19]), survival was significantly increased in *GHSROS*-overexpressing LNCaP cells ($P \leq 0.05$, Student's *t*-test) (Fig. 3a) after 96 hours. A similar, less pronounced response was observed in LNCaP cells treated with enzalutamide, a hormonal therapy used to target the androgen receptor in metastatic, castration-resistant tumors[20] (Fig. 3a).

Survival pathways are induced after docetaxel treatment in prostate cancer[21, 22], and resistance may develop after chemotherapy (acquired resistance) or exist in treatment-naïve patients (innate resistance)[21]. The pronounced survival following docetaxel treatment in *GHSROS*-overexpressing LNCaP cells led us to speculate that endogenous *GHSROS* expression also contributed to drug resistance. Docetaxel significantly increased *GHSROS* expression in native LNCaP and PC3 cells – in a dose-dependent manner and at concentrations both above and below their respective IC_{50} values (Fig. 3b). The lncRNA was not differentially expressed in charcoal stripped serum (CSS), used to simulate androgen deprivation therapy, or following treatment with enzalutamide (Fig. 3c). In agreement with previous reports[23, 24], the gene coding for prostate specific antigen (PSA; *KLK3*) was downregulated by docetaxel and enzalutamide in LNCaP cells (-6.6-fold, P=0.00070, Student's *t*-test) (Fig. 3c). Taken together, these data suggest that *GHSROS* mediates tumor survival and resistance to the cytotoxic chemotherapy docetaxel.

GHSROS* potentiates tumor growth *in vivo

In order to firmly establish a role for *GHSROS* in tumor growth, we established subcutaneous *GHSROS*-overexpressing androgen-independent (PC3 and DU145) and androgen-responsive (LNCaP) cell line xenografts in NOD/SCIDIL2Rγ (NSG) mice. Subcutaneous graft sites allow easy implantation and monitoring of tumor growth (using calipers)[25] – ideal for exploring the role of a new gene such as *GHSROS in vivo*. Overexpression of *GHSROS* in xenografts was confirmed post-mortem by qRT-PCR (Supplementary Fig. S8). Compared to vector controls, xenograft tumor volumes were significantly greater at day 25 in PC3-GHSROS mice (P=0.0040, Mann-Whitney-Wilcoxon test) and at day 35 in DU145-GHSROS mice (P=0.0011) (Fig. 4a). While xenograft tumors were not palpable in LNCaP-

GHSROS mice *in vivo*, tumors were significantly larger by weight post-mortem (at 72 days) (P=0.042, Student's t-test) (Fig. 4b) – with a size increase similar to that seen for DU145-GHSROS xenografts (Fig. 4c). LNCaP-GHSROS tumors invaded the muscle of the flank and the peritoneum (data not shown) and were more vascularized than control tumors (observed grossly and estimated by $CD31^+$ immunostaining) (Fig. 4d). Representative Ki67 immunostaining for proliferating xenograft tumor cells is shown in Fig. 4e.

GHSROS modulates the expression of cancer-associated genes

Having established that *GHSROS* plays a role in regulating hallmarks of cancer – including cell proliferation, invasion, and migration[26] – we sought to determine the genes likely to mediate its function by examining the transcriptomes of cultured PC3 cells and LNCaP xenografts overexpressing this lncRNA.

High-throughput RNA-seq of cultured PC3-GHSROS cells (~50M reads) revealed that 400 genes were differentially expressed (168 upregulated, 232 downregulated, moderated t-test; cutoff set at $\log_2$ fold-change ± 1.5, $Q \leq 0.05$) (Supplementary Table S3) compared with empty vector control cells. In support of our functional data, gene ontology analysis using DAVID showed enrichment for cancer, cell motility, cell migration, and regulation of growth (Supplementary Tables S4 and S5). Given that *GHSROS* is not readily detectable by high-throughput sequencing and array technologies, we queried the 400 genes differentially expressed in PC3-GHSROS cells using Oncomine concept map analysis[27]. Enriched Oncomine concepts included poor clinical outcome and metastatic progression (Fig. 5a; Supplementary Table S6).

Complementary lower-coverage (~30M reads) RNA-seq data from LNCaP-GHSROS xenografts demonstrated that a surprisingly large number of genes were differentially expressed (1 961 upregulated, 2 372 downregulated, moderated *t*-test; cutoff set at $\log_2$ fold-change ± 1.5, $Q \leq 0.05$) (Supplementary Dataset 1). Selected genes with low expression counts were validated by qRT-PCR (Supplementary Fig. S9). In LNCaP-GHSROS xenografts, *GHSROS*-regulated genes were enriched for the androgen response (gene set enrichment analysis; NES = 2.71, $Q \leq 0.001$) (Fig. 5b), and included PSA (*KLK3*) (750.9-fold, $Q = 3.6 \times 10^{-6}$) and transmembrane protease serine 2 (*TMPRSS2*) (335.4-fold, $Q = 4.5 \times 10^{-6}$) (Supplementary Dataset 2). We also observed downregulation of numerous genes associated with cell migration and adhesion, epithelial–mesenchymal transition (EMT) (including *ZEB1;* -97.0-fold, $Q = 1.5 \times 10^{-5}$), and angiogenesis and vasculature development (Supplementary Dataset 3). As mentioned above, subcutaneous LNCaP-GHSROS xenografts infiltrated muscle of the flank and the peritoneum and were more vascularized at 72 days post injection in NSG mice, which may indicate that these tumors had completed EMT and angiogenesis at this time.

It is appreciated that the bone metastasis-derived, androgen-independent PC3 and the lymph node metastasis-derived, androgen-responsive LNCaP prostate cancer cell lines represent genetically and presumably metabolically distinct subtypes[28]. They are therefore useful for revealing broad, functional gene expression changes associated with aggressive disease in forced overexpression and knockdown experiments. Despite the differences between these cell lines, a quarter (25.3%; 101 genes) of genes differentially expressed by PC3 cells overexpressing *GHSROS* were also differentially expressed by LNCaP-*GHSROS* cells (Fig. 5c) ($P = 0.000020$, hypergeometric test). These genes represent candidate mediators of *GHSROS* function.

We interrogated the STRING database[29] to reveal protein interactions between the 101 genes regulated by *GHSROS* in both cell lines. A number of genes associated with cell-cell adhesion, migration, and growth were connected, indicating functional enrichment of these proteins in *GHSROS*-overexpressing prostate cancer cells (Fig. 5d). This included increased expression of epithelial cadherin (*CDH1*), occludin (*OCLN*), and claudin-7 (*CLDN7*); and decreased contactin 1 (*CNT1*), noggin (*NOG*), and transforming growth factor beta induced (*TGFBI*) in *GHSROS*-overexpressing cells. Of note, increased *CDH1* expression is associated with exit from EMT and growth of aggressive, metastatic prostate tumors[25]. A second, interesting upregulated network included anterior gradient 2 (*AGR2*) and trefoil factors 1 and 2 (*TFF1* and *TFF2*). Trefoil factors are small proteins associated with mucin glycoproteins. Their expression is increased in castration-resistant prostate cancer (CRPC) and may facilitate the acquisition of hormone independence[31, 32]. Similarly, *AGR2* has been associated with the propensity of a number of aggressive tumor types to metastasize, including prostate cancer[33, 34].

Ten out of the 101 genes were differentially expressed in metastatic tumors compared to primary tumors in two clinical prostate datasets: Grasso[35] (59 localized and 35 metastatic prostate tumors) and Taylor[36] (123 localized and 27 metastatic prostate tumors) (Supplementary Tables S7 and S8) ($Q \leq 0.25$, moderated *t*-test). *DIRAS1*, *FBXL16*, *TP53I11*, *TFF2*, and *ZNF467* were upregulated in both metastatic tumors and *GHSROS*-overexpressing PC3 and LNCaP cells, while *AASS*, *CHRDL1*, *CNTN1*, *IFI16*, and *MUM1L1* were downregulated. We investigated whether the expression of these genes contributes to adverse disease outcome by assessing survival in two independent datasets: the Taylor dataset and TCGA-PRAD. The latter a dataset of localized prostate tumors generated by The Cancer

Genomics Atlas (TCGA) consortium[37]. As overall survival data was available for a small number of patients in these datasets, we assessed disease-free survival (relapse). Relapse is a suitable surrogate for overall survival in prostate cancer given that recurrence of disease would be expected to contribute significantly to mortality, and metastatic disease is incurable. Unsupervised *k*-means clustering was employed to divide each dataset into two groups based on gene expression alone. Two genes, zinc finger protein 467 (*ZNF467*; which was induced by forced *GHSROS*-overexpression) and chordin-like 1 (*CHRDL1*; which was repressed), correlated with relapse in both datasets (Supplementary Table S9). Chordin-like 1 is a negative regulator of bone morphogenetic protein 4-induced migration and invasion in breast cancer[38]. It was downregulated in *GHSROS*-overexpressing cell lines and in metastatic tumors compared to localized tumors in the Taylor and Grasso datasets. Interrogation of the Chandran prostate cancer dataset (60 localized tumors and 63 adjacent, normal prostate)[39] suggests that *CHRDL1* is downregulated by prostate tumors in general. *CHRDL1* expression stratified the Taylor (*N*=150; 27 metastatic tumors) dataset into two groups with a significant, 438-day difference in overall disease-free survival (relapse; Cox *P*=0.0062, absolute hazard ratio (HR) = 2.5). A statistically significant, yet clinically negligible difference in relapse (9 days; Cox *P*=0.0071, absolute HR = 1.8) was observed in the TCGA-PRAD dataset (*N*=489; no metastatic tumors) (Supplementary Table S9). Survival analysis *P*-values (Kaplan-Meier and Cox proportional-hazard) and hazard ratios indicate whether there is a significant difference between two groups, but not the degree of difference. Evaluating statistically significant differences in survival (e.g. in days) between groups is therefore subjective. Given these data, we propose that *CHRDL1* may play an important role in metastatic tumors.

In contrast to *CHRDL1*, *ZNF467* stratified patients into clusters with an obvious difference in overall median survival (relapse) between groups in both the Taylor (697 days; Cox

285 *P*=0.0039, HR = 2.7) and TCGA-PRAD datasets (139 days; Cox *P*=0.000026, HR = 2.5)
286 (Supplementary Table S9). ZNF467 has not been functionally characterized, however, a
287 recent study suggests that it is a transcription factor which clusters in close proximity to the
288 androgen receptor in a network associated with breast cancer risk[40], indicating that ZNF467
289 and AR regulate similar pathways. Clustering of patients into groups of either low or high
290 *ZNF467* expression revealed that elevated expression of the gene associated with a worse
291 relapse outcome (Supplementary Fig. S10a-c). In agreement, *ZNF467* gene expression can
292 distinguish low (≤ 6) from high (≥ 8) Gleason score prostate tumors in a Fred Hutchinson
293 Cancer Research Center prostate cancer dataset (381 localized and 27 metastatic prostate
294 tumors)[41]. *ZNF467* expression is also elevated in chemotherapy-resistant ovarian cancer[42] and
295 breast cancer[43] cell lines.
296
297 The 101 *GHSROS*-regulated genes were visualized in a scatter plot to reveal genes with
298 particularly distinct (≥ 8-fold) differential expression in *GHSROS*-overexpressing prostate
299 cancer cell lines – putative fundamental drivers of the observed tumorigenic phenotypes. This
300 revealed that *PPP2R2C* (Fig. 5e), a gene encoding a subunit of the holoenzyme phosphatase
301 2A (PP2A)[44,45], was downregulated by forced overexpression of *GHSROS*. In the PC3-
302 GHSROS RNA-seq dataset, *PPP2R2C* was the third most downregulated gene (-29.9-fold,
303 moderated *t*-test $Q=3.4 \times 10^{-10}$) (Supplementary Table S3). Consistently, forced
304 overexpression or knockdown of *GHSROS* in prostate cancer cell lines reciprocally regulated
305 endogenous *PPP2R2C* expression (Fig. 5f; Supplementary Figs. S9 and S11).
306
307 We observed that *GHSROS* was also able to reciprocally regulate androgen receptor (*AR*)
308 expression in some prostate cancer cell lines (downregulated upon *GHSROS* overexpression
309 in PC3 and LNCaP; upregulated upon *GHSROS* knockdown in DUCaP) (Fig. 5f). LNCaP-

GHSROS xenografts showed a variable *AR* expression pattern, which may be linked to differences in available androgen, however, *PPP2R2C* expression was still significantly repressed *in vivo* (-3.7-fold, Student's *t*-test $P=7.9 \times 10^{-3}$) (Supplementary Fig. S9). Similarly, while *AR* could not be detected in DU145 cells, *GHSROS*-overexpression decreased *PPP2R2C* expression in this cell line (Fig. 5f). The androgen receptor is also expressed by ovarian and lung cancer tumors and cell lines[46, 47]. Forced overexpression of *GHSROS* in the A549 lung adenocarcinoma cell line decreased *AR* and *PPP2R2C* expression (Student's *t*-test, $P \leq 0.0001$). *GHSROS* knockdown in the ES-2 ovarian clear cell carcinoma cell line, which does not express *PPP2R2C*, increased the expression of *AR* (Student's *t*-test, $P=0.0029$ and $P=0.0022$) (Fig. 5f; Supplementary Fig. S11).

DISCUSSION

Very recent work suggests that a small proportion (~3%) of long non-coding RNA genes are dysregulated in tumors and mediate cell growth[48]. Herein, we demonstrate that the lncRNA *GHSROS* is one such gene. *GHSROS* expression is elevated across many different cancers, suggesting that it is a so-called pan-cancer lncRNA[49,50]. In prostate cancer *GHSROS* is detectable in normal tissue and expressed at higher levels in a subset (~10%) of tumors. We have yet to narrow down on particular prostate tumor strata with elevated *GHSROS*, however.

From assessing the function of *GHSROS* in immortalized prostate cancer cell lines, the following observations were made: Forced overexpression of *GHSROS* enhances *in vivo* tumor growth, and *in vitro* cell viability and motility. We also demonstrate that forced overexpression of *GHSROS* facilitates survival and recalcitrance to the cytotoxic chemotherapy drug docetaxel. Critically, we show that endogenous *GHSROS* is elevated following docetaxel treatment. Docetaxel is commonly prescribed for late-stage, metastatic

CRPC patients, but large, randomized trials suggest that it is also effective against recently-diagnosed, localized prostate tumors[51]. These data suggest that *GHSROS* acts as a cell survival factor in prostate cancer. While the underlying mechanisms are unknown, two genes associated with chemotherapy resistance, *ZNF467* and *PPP1R1B* (also known as *DARPP-32*), were upregulated in PC3 and LNCaP cells overexpressing *GHSROS*. *PPP1R1B* is a potent anti-apoptotic gene which confers resistance in cancer cell lines to several chemotherapeutic agents when overexpressed[52].

The expression and function of *GHSROS* in prostate cancer suggests that it belongs to a growing list of lncRNAs that function as *bona fide* oncogenes. Notable examples associated with aggressive cancer and adverse outcomes include *HOTAIR* (HOX transcript antisense RNA), which is upregulated in a range of cancers[2], and the prostate cancer-specific *SCHLAP1* (SWI/SNF Complex Antagonist Associated With Prostate Cancer 1)[53]. To better understand how *GHSROS* mediates its effects in prostate cancer, we examined transcriptomes of prostate cancer cell lines with forced *GHSROS* overexpression: PC3 cells in culture (*in vitro*) and subcutaneous LNCaP xenografts in mice (*in vivo*). The 101 common differentially expressed genes included several transcription factors with established roles in prostate cancer and genes associated with metastasis and poor prognosis. Our study not only highlights genes modulated by *GHSROS*, but also genes (such as *ZNF467*, *CHRDL1*, and *PPP2R2C*) that may be generally relevant to prostate cancer progression.

Reactivation of the androgen receptor (*AR*) has long been considered a seminal event; supporting renewed tumor growth in a majority of metastatic CRPC patients[54, 55]. However, it is now increasingly recognized that, similar to other endocrine-related cancers, several subtypes of prostate cancer exist[7,8,9]. These include subtypes characterized by androgen

pathway-independent growth[44, 56]. In this context, our results on *PPP2R2C*, a gene which encodes a PP2A substrate-binding regulatory subunit, is of interest. We demonstrate that *PPP2R2C* expression in prostate cancer cell lines is repressed by forced *GHSROS* overexpression and increased by *GHSROS* knockdown. There is emerging evidence that inactivation of PP2A mediates CRPC in a subset of patients who display resistance to AR-targeting therapies[44, 45]. Loss of *PPP2R2C* expression alone is thought to reprogram prostate tumors towards AR pathway-independent growth and survival[44]. Several independent lines of evidence suggest that *PPP2R2C* is a critical tumor suppressor involved in many cancers. Loss of *PPP2R2C* expression has been attributed to esophageal adenocarcinoma tumorigenesis[57], and *PPP2R2C* downregulation by distinct microRNAs positively correlates with increased proliferation of cultured cancer cells derived from the prostate[58], nasopharynx[59], and ovary[60]. *PPP2R2C* also has a classical growth-inhibiting tumor suppressor role in brain cancers[61]. A subtype of medulloblastoma, pediatric brain tumors, are characterized by high expression of the chemokine receptor CXCR4 and concordant suppression of *PPP2R2C*[62]. Similarly, the gene is ablated in A2B5^{+} glioma stem-like cells, a population which mediates a particularly aggressive chemotherapy-resistant glioblastoma phenotype[63]. Although seemingly paradoxical, *GHSROS* repression of *AR* and *PPP2R2C* in prostate cancer cell lines can be rationalized. Knockdown of *PPP2R2C* using small interfering RNA in cultured LNCaP and VCaP cells did not alter the expression of *AR*[44]. In contrast, *AR* knockdown in androgen-independent LP50 cells[64] (a cell line derived from LNCaP) markedly decreased *PPP2R2C* expression (Supplementary Fig. S12) – suggestive of an adaptive response to loss of androgen receptor expression (and function). Precisely how *GHSROS* mediates *PPP2R2C* downregulation and its effects on tumor growth remains to be determined, however, *GHSROS* is the first lncRNA shown to downregulate this critical tumor suppressor, suggesting a role in adaptive survival pathways and CRPC development. Taken

385 together, we speculate that *GHSROS* prime prostate tumors for androgen receptor-
386 independent growth.
387
388 In this study, the growth of *GHSROS*-overexpressing prostate cancer cell lines was assessed
389 using subcutaneous prostate cancer cell lines xenografts. We appreciate that other models
390 (including orthotopic xenografts) are critical for firmly establishing roles for a gene in cancer
391 processes, including invasion and metastasis[25], and we will assess these in a future study. The
392 interaction between *GHSROS* and genomic regions, proteins, and other RNA transcripts also
393 requires further elucidation. While this study firmly establishes that *GHSROS* plays a role in
394 prostate cancer, the mechanism by which it reprograms gene expression remains unknown.
395 LncRNAs are now considered critical components of the cellular machinery[1]. Unlike protein-
396 coding genes, which typically require sequence conservation to maintain function, the
397 mechanisms of action of lncRNAs are usually not obvious and uncovering their precise,
398 sometimes subtle, function remains a challenge[1]. For example, some lncRNAs modulate the
399 epigenetic regulation of gene expression and interact with chromatin, acting as scaffolds to
400 guide other molecules (including RNA, proteins, and epigenetic enzymes) to influence gene
401 expression[1, 2].
402
403 Although cancers are highly heterogeneous diseases and few therapies target molecular
404 phenotypes, lncRNAs provide a largely untapped source for new molecular targets[2]. Here, we
405 developed antisense oligonucleotides targeting *GHSROS* and assessed them in cultured
406 cancer cells. We are in the process of refining our oligonucleotides for targeting *in vivo*
407 xenografts. Targeting *GHSROS* may present an opportunity for clinical intervention,
408 however, it is appreciated that translational and regulatory challenges exist for
409 oligonucleotide therapies[65].

In summary, we propose that *GHSROS* is an oncogene that regulates cancer hallmarks and the expression of a number of genes, including the tumor suppressor *PPP2R2C* – the loss of which is an emerging alternative driver of prostate cancer. Further studies are needed to elucidate the expression and function of *GHSROS* in more detail and to determine whether pharmacological targeting of this lncRNA could prove useful for treating cancer.

MATERIALS AND METHODS

Assessment of *GHSROS* transcription in public high-throughput datasets

To expand on Northern blot and qRT-PCR analyses which suggest that the lncRNA *GHSROS* is expressed at low levels[3], we interrogated ~4,000 oligonucleotide microarrays with probes for known and predicted exons (Affymetrix GeneChip Exon 1.0 ST). For illustrative purposes, an RNA-sequencing dataset averaging ~160M reads from metastatic castration-resistant prostate cancer was also examined. See Supplementary information and Supplementary Table S10.

Cell culture and treatments

Prostate-derived cell lines (PC3, DU145, LNCaP, C4-2B[66], 22Rv1, DUCaP[67], RWPE-1, and RWPE-2), the ES-2 ovarian cancer cell line, and the A549 lung cancer cell line were obtained from ATCC (Rockville, MD, USA), except where indicated by a reference. See Supplementary information for details.

Patient-derived xenografts

Patient-derived xenograft (PDX) lines were obtained in-house (see Supplementary information).

435 **Production of *GHSROS* overexpressing cancer cell lines**

436 See Supplementary information for details.

437

438 **RNA extraction, reverse transcription, and quantitative reverse transcription**

439 **Polymerase Chain Reaction (qRT-PCR)**

440 See Supplementary information for details. Primers are listed in Supplementary Table S11.

441

442 **Locked Nucleic Acid-Antisense Oligonucleotides (LNA-ASO)**

443 Two distinct LNA ASOs complementary to different regions of *GHSROS*, RNV104L and

444 RNV124 (see Supplementary Fig. S6), were designed in-house (by R.N.V.) and synthesized

445 commercially (Exiqon, Vedbæk, Denmark). See Supplementary information for details.

446

447 ***In vitro* cell assays**

448 Proliferation and migration assays were performed using an xCELLigence real-time cell

449 analyzer (RTCA) DP instrument (ACEA Biosciences, San Diego, CA). Cell viability was

450 assessed using a WST-1 cell proliferation assay (Roche, Nonnenwald, Penzberg, Germany).

451 See Supplementary information for details.

452

453 **Mouse subcutaneous *in vivo* xenograft models**

454 PC3, DU145, and LNCaP cells overexpressing *GHSROS* (or empty vector control) were

455 injected subcutaneously into the flank of 4-week-old male NSG mice (obtained from Animal

456 Resource Centre, Murdoch, WA, Australia). All mouse studies were carried out with approval

457 from the University of Queensland and the Queensland University of Technology Animal

458 Ethics Committees performed in accordance with relevant guidelines and regulations. See

459 Supplementary information for details.

460 **RNA-sequencing of *GHSROS* overexpressing PC3 and LNCaP cells**

461 See Supplementary information for details. Raw and processed RNA-sequencing
462 (transcriptome) data have been deposited in Gene Expression Omnibus (GEO) with the
463 accession codes GSE86097 (*GHSROS* overexpression in cultured PC3 cells) and GSE103320
464 (*GHSROS* overexpression in LNCaP xenografts).

465

466 **LP50 prostate cancer cell line *AR* knockdown microarray**

467 We interrogated microarray data (NCBI GEO accession no. GSE22483) from androgen-
468 independent late passage LNCaP cells (LP50) subjected to androgen receptor (*AR*)
469 knockdown by shRNA[64]. See Supplementary information for details.

470

471 **Survival analysis in clinical gene expression datasets**

472 Non-hierarchical *k*-means clustering was used to partition patients into groups (k=2) of
473 samples with similar gene expression patterns. Kaplan-Meier and Cox proportional-hazard
474 model were utilized to generate survival probabilities and hazard ratios (HRs). See
475 Supplementary information for details.

476

477 **Code**

478 Code is available in a repository at https://github.com/sciseim/GHSROS_MS.

479

480 **CONFLICT OF INTEREST**

481 The author(s) declare no competing interests.

482

483

484

ACKNOWLEDGEMENTS

This work was supported by the National Health and Medical Research Council Australia (1002255 and 1059021; to P.L.J., A.C.H., L.K.C., and I.S.), the Cancer Council Queensland (1098565; to A.C.H., R.N.V., L.K.C., and I.S.), the Australian Research Council (grant no DP140100249; to A.C.H., and L.K.C.), a QUT Vice-Chancellor's Senior Research Fellowship (to I.S.), the Movember Foundation and the Prostate Cancer Foundation of Australia through a Movember Revolutionary Team Award, the Australian Government Department of Health, and the Australian Prostate Cancer Research Center, Queensland (L.K.C., A.C.H., J. H. G., E.D.W., and C.C.N.), Queensland University of Technology, the Instituto de Salud Carlos III (co-funded by European Union ERDF/ESF, "Investing in your future" grant no. PI13-00651; to R.M.L.), a Miguel Servet grant (CP15/00156; to M.D.G.), Junta de Andalucía (grant no. BIO-0139 to R.M.L.), and CIBERobn (CIBER is an initiative of Instituto de Salud Carlos III, Ministerio de Sanidad, Servicios Sociales e Igualdad, Spain; to R.M.L.). We acknowledge the use of the high-performance computational facilities at the Queensland University of Technology and the technical assistance of the Translational Research Institute Histology core and Biological Resource Facility.

AUTHOR CONTRIBUTIONS

PBT, IS, PLJ and LKC conceived and designed the study, and interpreted the data. PBT, MM, MDG, CW, LJ and PLJ performed laboratory experiments. IS and PBT performed computational biology analyses. PBT, LKC, PLJ and IS wrote the article. All authors (PBT, PLJ, MDG, EJW, CW, MM, LJ, JHG, EDW, CCN, RML, RNV, LKC and IS) contributed to the conception and design of the study, interpretation of the data and writing of the manuscript.

REFERENCES

1 Mattick J.S., Rinn J.L. Discovery and annotation of long noncoding RNAs. *Nat Struct Mol Biol* 2015; **22**: 5-7.

2 Huarte M. The emerging role of lncRNAs in cancer. *Nat Med* 2015; **21**: 1253-1261.

3 Whiteside E.J. *et al*. Identification of a long non-coding RNA gene, growth hormone secretagogue receptor opposite strand, which stimulates cell migration in non-small cell lung cancer cell lines. *Int J Oncol* 2013; **43**: 566-574.

4 Saxonov S., Berg P., Brutlag D.L. A genome-wide analysis of CpG dinucleotides in the human genome distinguishes two distinct classes of promoters. *Proc Natl Acad Sci U S A* 2006; **103**: 1412-1417.

5 Derrien T. *et al*. The GENCODE v7 catalog of human long noncoding RNAs: analysis of their gene structure, evolution, and expression. *Genome Res* 2012; **22**: 1775-1789.

6 Fitzmaurice C. *et al*. The Global Burden of Cancer 2013. *JAMA Oncol* 2015; **1**: 505-527.

7 Tosoian J.J., Antonarakis E.S. Molecular heterogeneity of localized prostate cancer: more different than alike. *Transl Cancer Res* 2017; **6**: S47-S50.

8 Shoag J., Barbieri C.E. Clinical variability and molecular heterogeneity in prostate cancer. *Asian J Androl* 2016; **18**: 543-548.

9 Dagogo-Jack I., Shaw A.T. Tumour heterogeneity and resistance to cancer therapies. *Nat Rev Clin Oncol* 2018; **15**: 81-94.

10 Mouraviev V. *et al*. Clinical prospects of long noncoding RNAs as novel biomarkers and therapeutic targets in prostate cancer. *Prostate Cancer Prostatic Dis* 2016; **19**: 14-20.

11 Ruiz-Orera J., Messeguer X., Subirana J.A., Alba M.M. Long non-coding RNAs as a source of new peptides. *eLife* 2014; **3**: e03523.

12 Kutter C. *et al*. Rapid turnover of long noncoding RNAs and the evolution of gene expression. *PLoS Genet* 2012; **8**: e1002841.

13 Cabili M.N. *et al*. Integrative annotation of human large intergenic noncoding RNAs reveals global properties and specific subclasses. *Genes Dev* 2011; **25**: 1915-1927.

14 Necsulea A. *et al*. The evolution of lncRNA repertoires and expression patterns in tetrapods. *Nature* 2014; **505**: 635-640.

15 Wang K.C. *et al*. A long noncoding RNA maintains active chromatin to coordinate homeotic gene expression. *Nature* 2011; **472**: 120-124.

16 Geisler S., Coller J. RNA in unexpected places: long non-coding RNA functions in diverse cellular contexts. *Nat Rev Mol Cell Biol* 2013; **14**: 699-712.

17 Nguyen H.M. *et al*. LuCaP Prostate Cancer Patient-Derived Xenografts Reflect the Molecular Heterogeneity of Advanced Disease and Serve as Models for Evaluating Cancer Therapeutics. *Prostate* 2017; **77**: 654-671.

18 McCulloch D.R., Opeskin K., Thompson E.W., Williams E.D. BM18: A novel androgen-dependent human prostate cancer xenograft model derived from a bone metastasis. *Prostate* 2005; **65**: 35-43.

19 Komura K. *et al*. Resistance to docetaxel in prostate cancer is associated with androgen receptor activation and loss of KDM5D expression. *Proc Natl Acad Sci U S A* 2016; **113**: 6259-6264.

20 Drake C.G., Sharma P., Gerritsen W. Metastatic castration-resistant prostate cancer: new therapies, novel combination strategies and implications for immunotherapy. *Oncogene* 2014; **33**: 5053-5064.

21 Sonpavde G., Wang C.G., Galsky M.D., Oh W.K, Armstrong A.J. Cytotoxic chemotherapy in the contemporary management of metastatic castration-resistant prostate cancer (mCRPC). *BJU Int* 2015; **116**: 17-29.

22 Chandrasekar T., Yang J.C., Gao A.C., Evans C.P. Mechanisms of resistance in castration-resistant prostate cancer (CRPC). *Transl Androl Urol* 2015; **4**: 365-380.

23 Lee H.Y. *et al*. Clinical predictor of survival following docetaxel-based chemotherapy. *Oncol Lett* 2014; **8**: 1788-1792.

24 Tran C. *et al*. Development of a second-generation antiandrogen for treatment of advanced prostate cancer. *Science* 2009; **324**: 787-790.

25 Lin D. *et al*. Next generation patient-derived prostate cancer xenograft models. *Asian J Androl* 2014; **16**: 407-412.

26 Hanahan D., Weinberg R.A. Hallmarks of cancer: the next generation. *Cell* 2011; **144**: 646-674.

27 Rhodes D.R. *et al*. Oncomine 3.0: genes, pathways, and networks in a collection of 18,000 cancer gene expression profiles. *Neoplasia* 2007; **9**: 166-180.

28 Seim I., Jeffery P.L., Thomas P.B., Nelson C.C., Chopin L.K. Whole-genome sequence of the metastatic PC3 and LNCaP human prostate cancer cell lines. *G3 (Bethesda)* 2017; **7**: 1731-1741.

29 Szklarczyk D. *et al*. The STRING database in 2017: quality-controlled protein-protein association networks, made broadly accessible. *Nucleic Acids Res* 2017; **45**: D362-D368.

30 Putzke A.P. *et al*. Metastatic progression of prostate cancer and e-cadherin regulation by ZEB1 and SRC family kinases. *Am J Pathol* 2011; **179**: 400-410.

31 Legrier M.E. *et al*. Mucinous differentiation features associated with hormonal escape in a human prostate cancer xenograft. *Br J Cancer* 2004; **90**: 720-727.

32 Vestergaard E.M., Borre M., Poulsen S.S., Nexo E., Torring N. Plasma levels of trefoil factors are increased in patients with advanced prostate cancer. *Clin Cancer Res* 2006; **12**: 807-812.

33 Kani K. *et al*. Anterior gradient 2 (AGR2): blood-based biomarker elevated in metastatic prostate cancer associated with the neuroendocrine phenotype. *Prostate* 2013; **73**: 306-315.

34 Zweitzig D.R., Smirnov D.A., Connelly M.C., Terstappen L.W., O'Hara S.M., Moran E. Physiological stress induces the metastasis marker AGR2 in breast cancer cells. *Mol Cell Biochem* 2007; **306**: 255-260.

35 Grasso C.S. *et al*. The mutational landscape of lethal castration-resistant prostate cancer. *Nature* 2012; **487**: 239-243.

36 Taylor B.S *et al*. Integrative genomic profiling of human prostate cancer. *Cancer Cell* 2010; **18**: 11-22.

37 Cancer Genome Atlas Research Network. The Molecular Taxonomy of Primary Prostate Cancer. *Cell* 2015; **163**: 1011-1025.

38 Cyr-Depauw C. *et al*. Chordin-Like 1 suppresses bone morphogenetic protein 4-induced breast cancer cell migration and invasion. *Mol Cell Biol* 2016; **36**: 1509-1525.

39 Chandran U.R., Dhir R., Ma C., Michalopoulos G., Becich M., Gilbertson J. Differences in gene expression in prostate cancer, normal appearing prostate tissue adjacent to cancer and prostate tissue from cancer free organ donors. *BMC Cancer* 2005; **5**: 45.

40 Castro M.A. *et al*. Regulators of genetic risk of breast cancer identified by integrative network analysis. *Nat Genet* 2016; **48**: 12-21.

41 Jhun M.A. *et al*. Gene expression signature of Gleason score is associated with prostate cancer outcomes in a radical prostatectomy cohort. *Oncotarget* 2017; **8**: 43035-43047.

42 Zhu L., Hu Z., Liu J., Gao J., Lin B. Gene expression profile analysis identifies metastasis and chemoresistance-associated genes in epithelial ovarian carcinoma cells. *Med Oncol* 2015; **32**: 426.

43 Davies G.F. *et al*. TFPI1 mediates resistance to doxorubicin in breast cancer cells by inducing a hypoxic-like response. *PLoS One* 2014; **9**: e84611.

44 Bluemn E.G. *et al*. PPP2R2C loss promotes castration-resistance and is associated with increased prostate cancer-specific mortality. *Mol Cancer Res* 2013; **11**: 568-578.

45 Gonzalez-Alonso P., Cristobal I., Manso R., Madoz-Gurpide J., Garcia-Foncillas J., Rojo F.. PP2A inhibition as a novel therapeutic target in castration-resistant prostate cancer. *Tumour Biol* 2015; **36**: 5753-5755.

46 Zhu H., Zhu X., Zheng L., Hu X., Sun L., Zhu X. The role of the androgen receptor in ovarian cancer carcinogenesis and its clinical implications. *Oncotarget* 2017; **8**: 29395-29405.

47 Harlos C., Musto G., Lambert P., Ahmed R., Pitz M.W. Androgen pathway manipulation and survival in patients with lung cancer. *Horm Cancer* 2015; **6**: 120-127.

48 Liu S.J. *et al*. CRISPRi-based genome-scale identification of functional long noncoding RNA loci in human cells. *Science* 2017; **355**.

49 Chiu H.S. *et al*. Pan-Cancer Analysis of lncRNA Regulation Supports Their Targeting of Cancer Genes in Each Tumor Context. *Cell Rep* 2018; **3**: 297-312.

50 Cabanski C.R. *et al*. Pan-cancer transcriptome analysis reveals long noncoding RNAs with conserved function. *RNA Biol* 2015; **12**: 628-642.

51 Puente J., Grande E., Medina A., Maroto P., Lainez N., Arranz J.A. Docetaxel in prostate cancer: a familiar face as the new standard in a hormone-sensitive setting. *Ther Adv Med Oncol* 2017; **9**: 307-318.

52 Belkhiri A., Zhu S., El-Rifai W. DARPP-32: from neurotransmission to cancer. *Oncotarget* 2016; **7**: 17631-17640.

53 Prensner J.R. *et al*. The long noncoding RNA SChLAP1 promotes aggressive prostate cancer and antagonizes the SWI/SNF complex. *Nat Genet* 2013; **45**: 1392-1398.

54 Ferraldeschi R., Welti J., Luo J., Attard G., de Bono J.S. Targeting the androgen receptor pathway in castration-resistant prostate cancer: progresses and prospects. *Oncogene* 2015; **34**: 1745-1757.

55 Wyatt A.W., Gleave M.E. Targeting the adaptive molecular landscape of castration-resistant prostate cancer. *EMBO Mol Med* 2015; **7**: 878-894.

56 Bluemn E.G. *et al*. Androgen receptor pathway-independent prostate cancer is sustained through FGF signaling. *Cancer Cell* 2017; **32**: 474-489.

57 Peng D. *et al*. Integrated molecular analysis reveals complex interactions between genomic and epigenomic alterations in esophageal adenocarcinomas. *Sci Rep* 2017; **7**: 40729.

58 Bi D., Ning H., Liu S., Que X., Ding K. miR-1301 promotes prostate cancer proliferation through directly targeting PPP2R2C. *Biomed Pharmacother* 2016; **81**: 25-30.

59 Yan L., Cai K., Liang J., Liu H., Liu Y., Gui J. Interaction between miR-572 and PPP2R2C, and their effects on the proliferation, migration, and invasion of nasopharyngeal carcinoma (NPC) cells. *Biochem Cell Biol* 2017; **95**: 578-584.

60 Wu A.H. *et al*. miR-572 prompted cell proliferation of human ovarian cancer cells by suppressing PPP2R2C expression. *Biomed Pharmacother* 2016; **77**: 92-97.

61 Fan Y.L., Chen L., Wang J., Yao Q., Wan J.Q. Over expression of PPP2R2C inhibits human glioma cells growth through the suppression of mTOR pathway. *FEBS Lett* 2013; **587**: 3892-3897.

62 Sengupta R. *et al*. CXCR4 activation defines a new subgroup of Sonic hedgehog-driven medulloblastoma. *Cancer Res* 2012; **72**: 122-132.

63 Auvergne R.M. *et al*. Transcriptional differences between normal and glioma-derived glial progenitor cells identify a core set of dysregulated genes. *Cell Rep* 2013; **3**: 2127-2141.

64 Gonit M. *et al*. Hormone depletion-insensitivity of prostate cancer cells is supported by the AR without binding to classical response elements. *Mol Endocrinol* 2011; **25**: 621-634.

65 Stein C.A., Castanotto D. FDA-Approved Oligonucleotide Therapies in 2017. *Mol Ther* 2017; **25**: 1069-1075.

66 Thalmann G.N. *et al*. Androgen-independent cancer progression and bone metastasis in the LNCaP model of human prostate cancer. *Cancer Res* 1994; **54**: 2577-2581.

67 Lee Y.G., Korenchuk S., Lehr J., Whitney S., Vessela R., Pienta K.J. Establishment and characterization of a new human prostatic cancer cell line: DuCaP. *In Vivo* 2001; **15**: 157-162.

FIGURES

Figure 1. Overview of the lncRNA *GHSROS* and its expression in cancer. **(a)** Overview of the *GHSR* and *GHSROS* gene loci. *GHSR* exons (black), *GHSROS* exon (red), repetitive elements (orange), introns (lines). **(b)** *GHSROS* expression in 19 cancers (TissueScan Cancer Survey Tissue qPCR panel). N (black) denotes normal tissue; T tumor (red). For each cancer, data are expressed as mean fold change using the comparative $2^{-\Delta\Delta Ct}$ method against a non-malignant control tissue. Normalized to β-actin (*ACTB*). **(c)** Relative gene expression of *GHSROS* in OriGene cDNA panels of tissues from normal prostate (n=24; blue), primary prostate cancer (n=88; red), and other prostatic diseases (n=31; orange). Determined by qRT-PCR, normalized to ribosomal protein L32 (*RPL32*), and represented as standardized expression values (Z-scores). **(d)** *GHSROS* expression in an Andalusian Biobank prostate tissue cohort. Absolute expression levels were determined by qRT-PCR and adjusted by a normalization factor calculated from the expression levels of three housekeeping genes (*HPRT*, *ACTB*, and *GAPDH*). NP denotes non-malignant prostate. *$P\leq0.05$, Mann-Whitney-Wilcoxon test. **(e)** Expression of *GHSROS* in immortalized, cultured cell lines and patient-derived xenograft (PDX) lines. Mean ± s.e.m. (n=3). *$P\leq0.05$, **$P\leq0.01$, ***$P\leq0.001$,

692 Student's *t*-test. Normalized as in (b) to the RWPE-1 non-malignant cell line. Androgen-
693 independent lines are labeled in orange.
694
695 **Figure 2.** *GHSROS* promotes human prostate cancer cell line growth and motility *in vitro*. **(a,**
696 **b)** Increased proliferation by *GHSROS*-overexpressing cells. PC3 and DU145 cells were
697 assessed using an xCELLigence real-time cell analyzer for 72 hours; LNCaP using a WST-1
698 assay at 72 hours. Vector denotes empty control plasmid. Mean ± s.e.m. (n=3). *$P \leq 0.05$,
699 **$P \leq 0.01$, ***$P \leq 0.001$, Student's *t*-test. **(c)** Increased migration by *GHSROS*-overexpressing
700 cells. PC3 and DU145 cells were assessed using an xCELLigence real-time cell analyzer for
701 24 hours; LNCaP using a transwell assay (at 24 hours; n=3). Parameters and annotations as in
702 (a). **(d)** *GHSROS* RNA secondary structure prediction. The location of locked nucleic
703 antisense oligonucleotides (LNA-ASOs) that target the lncRNA are shown in red. MFE
704 denotes minimum free energy. **(e)** LNA ASOs reduced *GHSROS* expression by PC3 cells
705 (measured 48 hours post-transfection). Fold-enrichment of *GHSROS* normalized to *RPL32*
706 and compared to scrambled control (n=3). Parameters and annotations as in (a). **(f)** *GHSROS*
707 knockdown reduces PC3 proliferation (n=3). Parameters and annotations as in (a). **(g)**
708 *GHSROS* knockdown reduces PC3 migration. Left panel: representative plot of cell index
709 impedance measurements from 0 to 20 hours after transfection of LNA-ASO RNV124 (n=3).
710 Right panel: RNV124 reduced cell migration at 18 hours (n=3). Parameters and annotations
711 as in (c).
712
713 **Figure 3.** *GHSROS* mediates cell survival and resistance to the cytotoxic drug docetaxel. **(a)**
714 Viability of *GHSROS*-overexpressing LNCaP cells under different culture conditions. Cell
715 number was assessed using WST-1. Cells were treated with enzalutamide (ENZ; 10 μM) or
716 docetaxel (DTX; 5 nM) for 96 hours and grown in either 2% FBS or 5% charcoal stripped

717 serum (CSS) RPMI-1640 media (*n*=3). Mean ± s.e.m. *$P \leq 0.05$, ***$P \leq 0.001$, Student's *t*-test.
718 **(b)** *GHSROS* expression of native PC3 and LNCaP cells treated with docetaxel. Cells were
719 grown in RPMI-1640 media with 2% FBS and treated with 1-20 nM docetaxel (DTX) for 48
720 hours (*n*=3). Fold-enrichment of *GHSROS* normalized to *RPL32* and compared to empty
721 vector control. Parameters and annotations as in (a). **(c)** *GHSROS* and PSA (*KLK3*)
722 expression of native LNCaP cells treated with ENZ (10 µM in 2% FBS or 5% CSS RPMI-
723 1640) or DTX (5 nM in 2% FBS RPMI-1640) for 48 hours (*n*=3). Parameters and annotations
724 as in (a).
725
726 **Figure 4.** *GHSROS* promotes human prostate cancer cell line growth *in vivo*. **(a)** Left panel:
727 time course for PC3-GHSROS (*n*=8) and vector control (*n*=4) xenograft tumor volumes.
728 Right panel: DU145-GHSROS (*n*=6) and vector control (*n*=4). Mean ± s.e.m. *$P \leq 0.05$,
729 **$P \leq 0.01$, ***$P \leq 0.001$, two-way ANOVA with Bonferonni's *post hoc* analysis. Tumors
730 were measured with digital calipers. **(b)** Tumor weights of LNCaP (left panel; *GHSROS*-
731 overexpressing *n*=9, vector *n*=8) or DU145 (right panel; see (a)). *$P \leq 0.05$, Mann-Whitney-
732 Wilcoxon test. **(c)** Size comparisons of DU145 (top panel) and LNCaP (bottom panel)
733 xenografts overexpressing *GHSROS* or empty vector. **(d)** Representative morphology of
734 LNCaP xenografts overexpressing *GHSROS* or empty vector. Tissue was stained with
735 hematoxylin and eosin (H&E), Masson's Trichrome (MT; collagen; blue) and CD31
736 (endothelial marker; brown immunoreactivity). Scale bar = 20 µm. **(e)** Representative Ki67
737 immunostaining of PC3 xenografts (top), DU145 xenografts (middle), and LNCaP xenografts
738 (bottom). Scale=20 µm.
739
740 **Figure 5.** *GHSROS* overexpression modulates the expression of cancer-associated genes. **(a)**
741 Oncomine network representation of genes differentially expressed by cultured PC3-

GHSROS cells visualized using Cytoscape. Node sizes (gene overlap) reflect the number of genes per molecular concept. Nodes are colored according to concept categories indicated in the left corner. Edges connect enriched nodes (odds ratio ≥3.0) and darker edge shading indicates a higher odds ratio. **(b)** Gene set enrichment analysis (GSEA) of genes differentially expressed by LNCaP-GHSROS xenografts reveals enrichment for the androgen response. The normalized enrichment score (NES) and GSEA false-discovery corrected *P*-value (*Q*) are indicated. **(c)** Venn diagram of differentially expressed genes (DEG) in LNCaP-GHSROS and PC3-GHSROS cells. Symbols of 101 overlapping genes are indicated in text boxes. **(d)** Interaction of 101 genes differentially expressed in PC3-GHSROS and LNCaP-GHSROS cells (see (c)). Lines represent protein-protein interaction networks from the STRING database. Genes induced (red) or repressed (blue) by *GHSROS*-overexpression are indicated. **(e)** Gene expression scatter plot comparing *GHSROS*-overexpressing PC3 and LNCaP cells. Differentially expressed genes (DEGs) in both datasets shown in red (induced) and blue (repressed); of which ≥8-fold ($\log_2$ cutoff at -3 and 3) DEGs are highlighted by a green box. **(f)** Heat map of gene expression in *GHSROS*-perturbed cells. Each row shows the relative expression of a single gene and each column a sample (biological replicate). Fold-enrichment of each gene normalized to *RPL32* and compared to empty vector control (overexpression) or scrambled control (LNA-ASO knockdown). Fold-changes were $\log_2$-transformed and are displayed in the heat map as the relative expression of a gene in a sample compared to all other samples (*Z*-score).

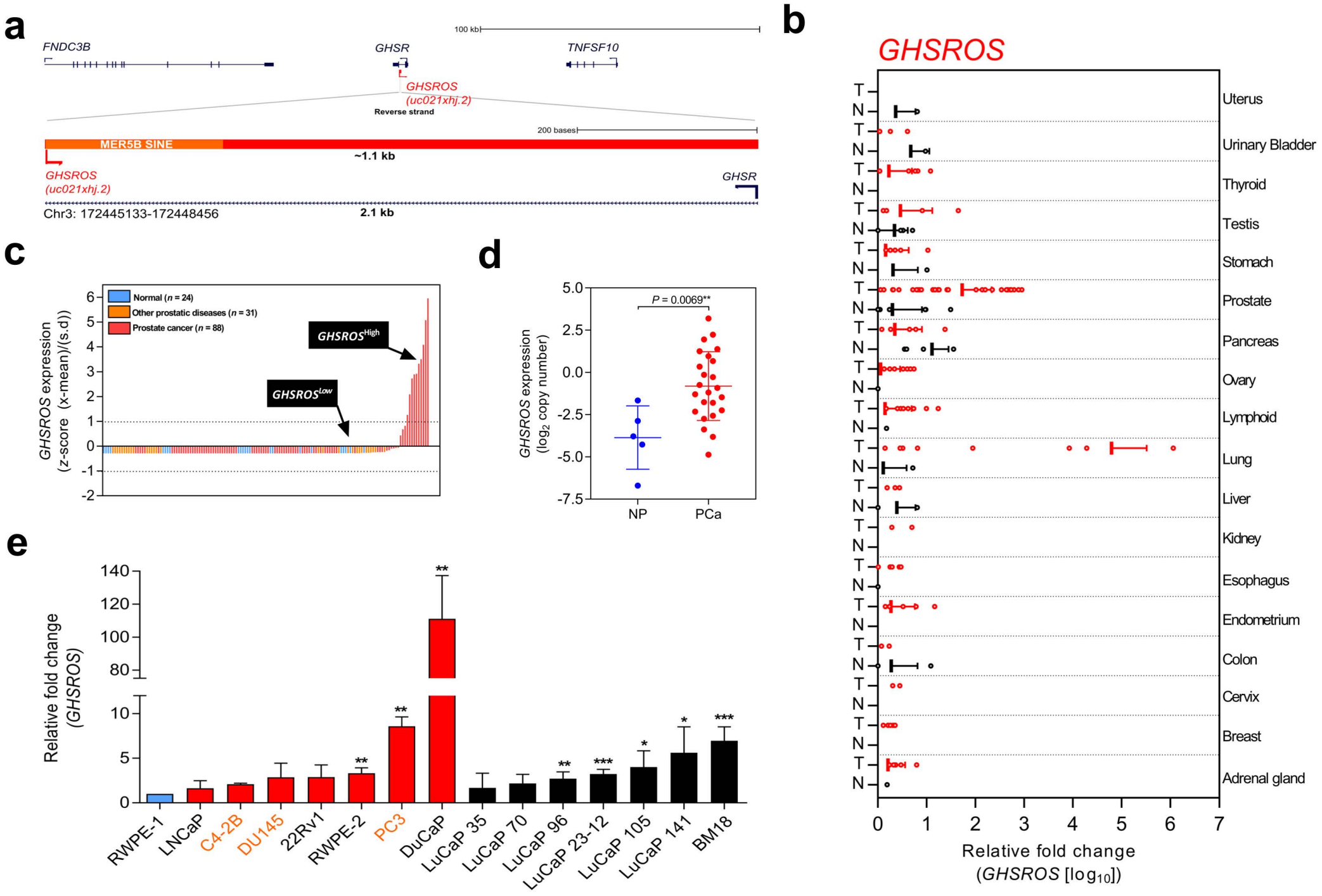
a
100 kb
FNDC3B
GHSR
TNFSF10
GHSROS
(uc021xhj.2)
Reverse strand
200 bases
MER5B SINE
~1.1 kb
GHSROS
(uc021xhj.2)
GHSR
Chr3: 172445133-172448456
2.1 kb
b
GHSROS
T
N
Uterus
Urinary Bladder
Thyroid
Testis
Stomach
Prostate
Pancreas
Ovary
Lymphoid
Lung
Liver
Kidney
Esophagus
Endometrium
Colon
Cervix
Breast
Adrenal gland
0 1 2 3 4 5 6 7
Relative fold change
(GHSROS [log10])
c
Normal (n = 24)
Other prostatic diseases (n = 31)
Prostate cancer (n = 88)
GHSROS High
GHSROS Low
GHSROS expression
(z-score (x-mean)/(s.d))
6 5 4 3 2 1 0 -1 -2
d
P = 0.0069**
GHSROS expression
(log2 copy number)
5.0 2.5 0.0 -2.5 -5.0 -7.5
NP
PCa
e
Relative fold change
(GHSROS)
140 120 100 80 10 5 0
**
**
**
**
***
*
*
***
RWPE-1
LNCaP
C4-2B
DU145
22Rv1
RWPE-2
PC3
DuCaP
LuCaP 35
LuCaP 70
LuCaP 96
LuCaP 23-12
LuCaP 105
LuCaP 141
BM18

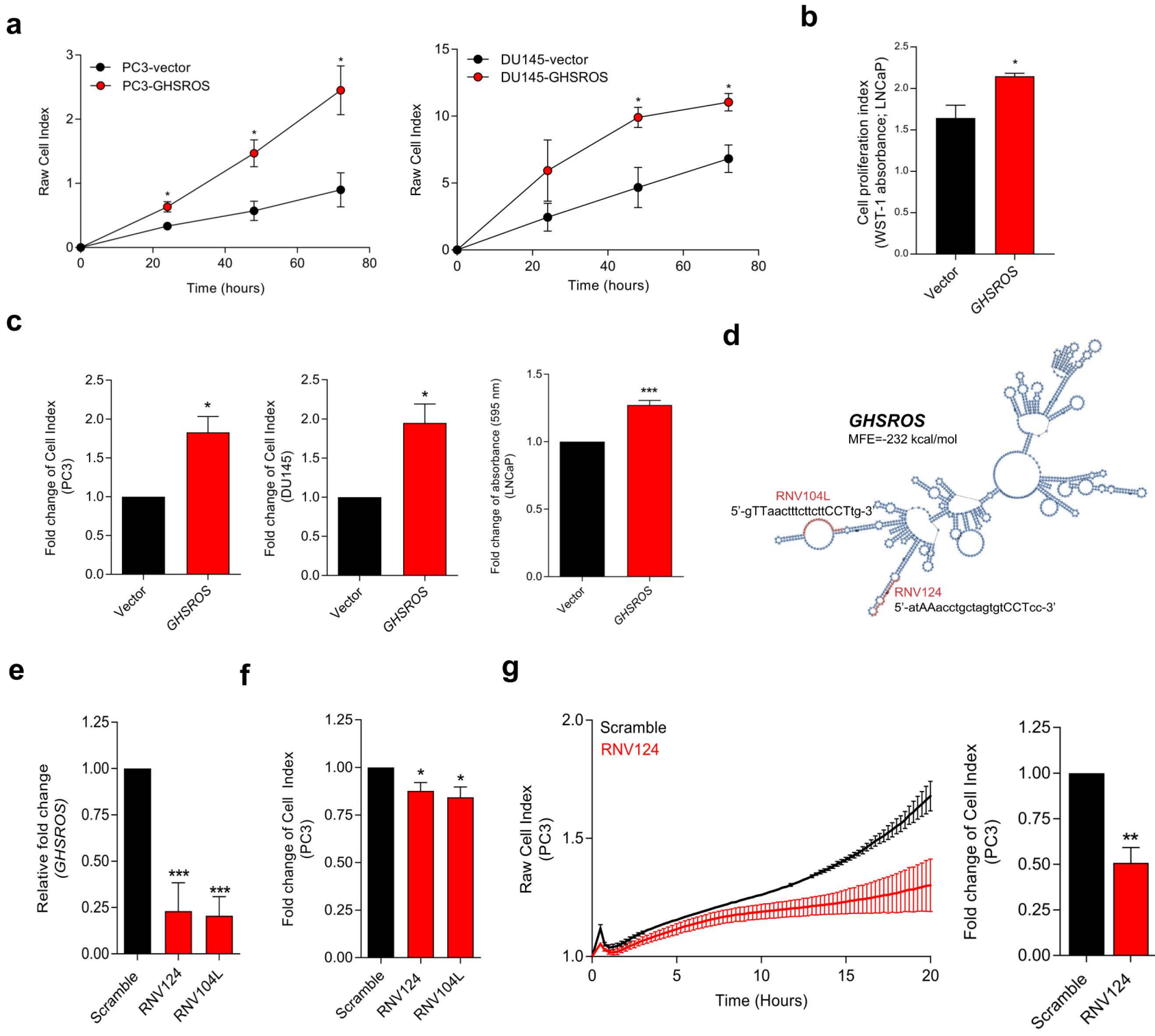
a
PC3-vector
PC3-GHSROS
Raw Cell Index
Time (hours)
DU145-vector
DU145-GHSROS
Raw Cell Index
Time (hours)
b
Cell proliferation index (WST-1 absorbance; LNCaP)
Vector
GHSROS
c
Fold change of Cell Index (PC3)
Vector
GHSROS
Fold change of Cell Index (DU145)
Vector
GHSROS
Fold change of absorbance (595 nm) (LNCaP)
Vector
GHSROS
d
GHSROS
MFE=-232 kcal/mol
RNV104L
5'-gTTaactttcttcttCCTtg-3'
RNV124
5'-atAAacctgctagtgtCCTcc-3'
e
Relative fold change (GHSROS)
Scramble
RNV124
RNV104L
f
Fold change of Cell Index (PC3)
Scramble
RNV124
RNV104L
g
Scramble
RNV124
Raw Cell Index (PC3)
Time (Hours)
Fold change of Cell Index (PC3)
Scramble
RNV124

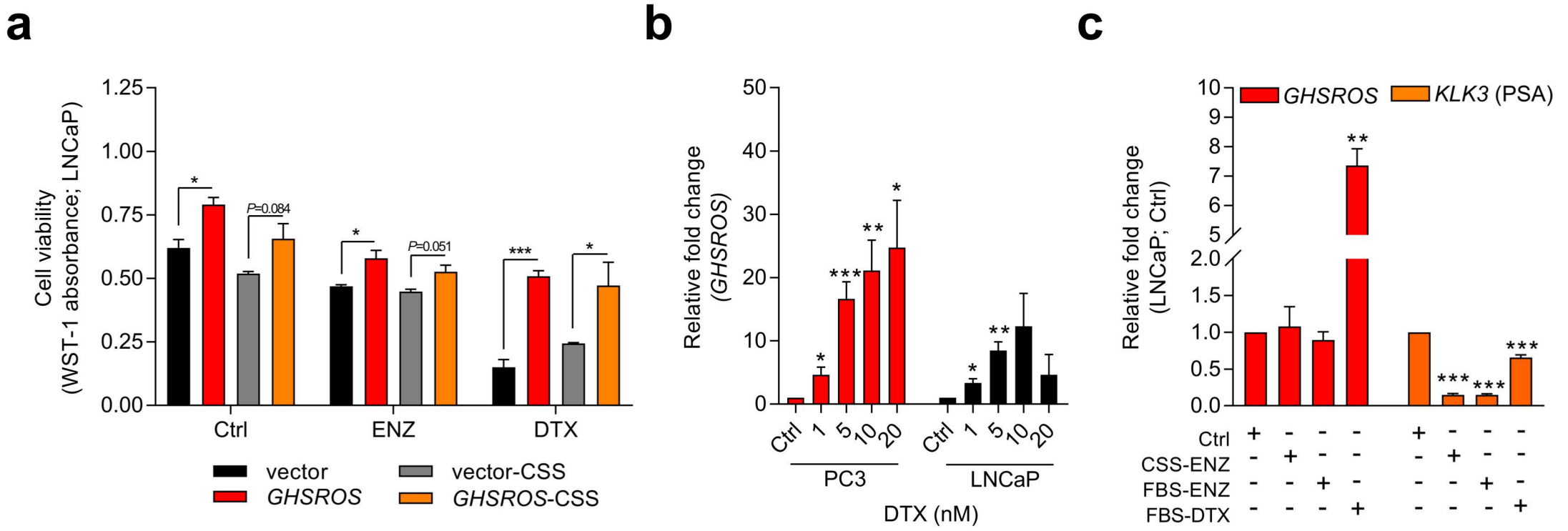
a
Cell viability
(WST-1 absorbance; LNCaP)
1.25
1.00
0.75
0.50
0.25
0.00
*
P=0.084
*
P=0.051
***
*
Ctrl
ENZ
DTX
vector
GHSROS
vector-CSS
GHSROS-CSS
b
Relative fold change
(GHSROS)
50
40
30
20
10
0
*
***
**
*
*
**
Ctrl
1
5
10
20
Ctrl
1
5
10
20
PC3
LNCaP
DTX (nM)
c
GHSROS
KLK3 (PSA)
Relative fold change
(LNCaP; Ctrl)
10
9
8
7
6
5
2.0
1.5
1.0
0.5
0.0
**
***
***
***
Ctrl
CSS-ENZ
FBS-ENZ
FBS-DTX

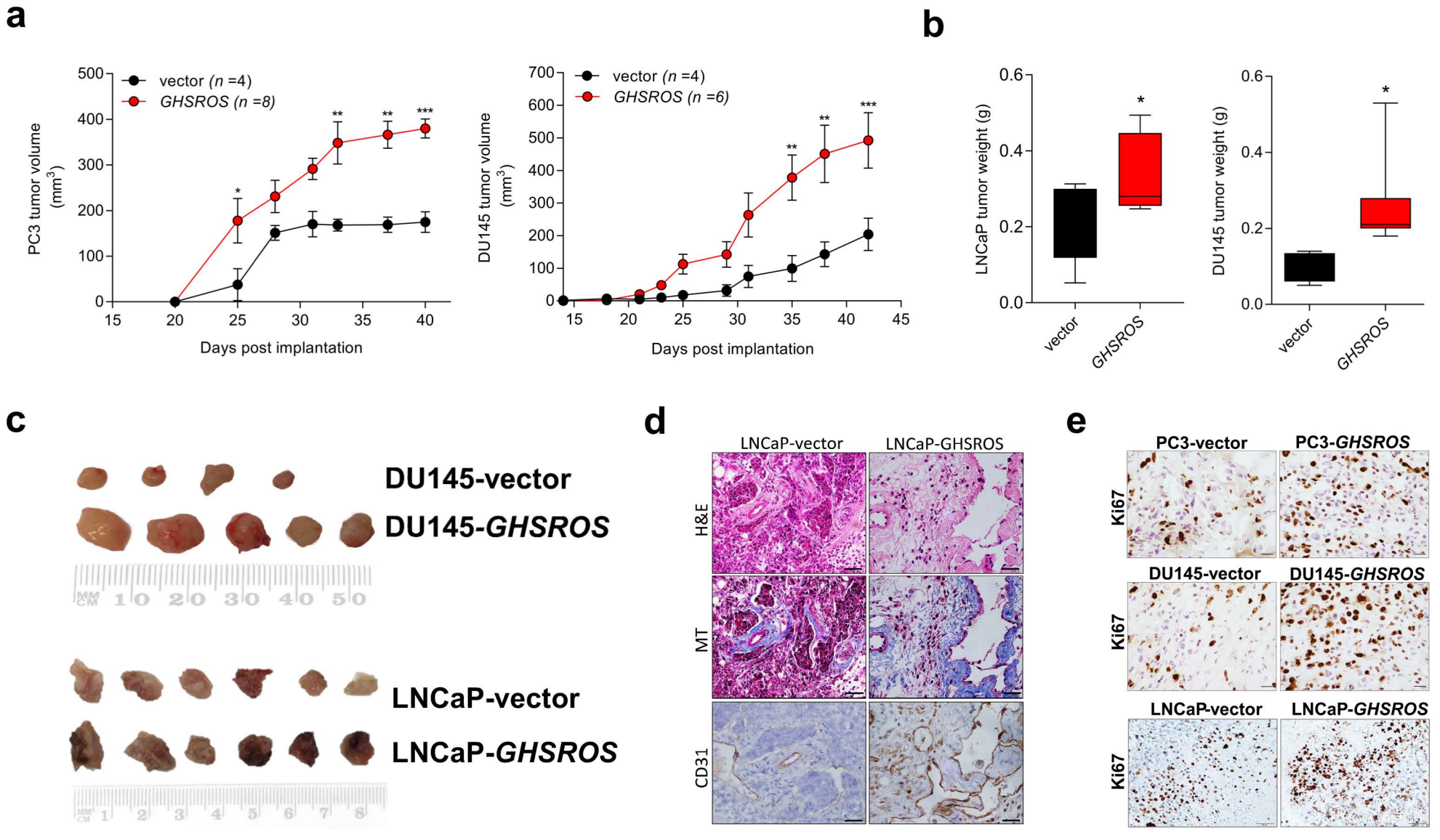
a
vector (n =4)
GHSROS (n =8)
PC3 tumor volume (mm3)
Days post implantation
vector (n =4)
GHSROS (n =6)
DU145 tumor volume (mm3)
Days post implantation
b
LNCaP tumor weight (g)
DU145 tumor weight (g)
vector
GHSROS
c
DU145-vector
DU145-GHSROS
LNCaP-vector
LNCaP-GHSROS
d
LNCaP-vector
LNCaP-GHSROS
H&E
MT
CD31
e
PC3-vector
PC3-GHSROS
DU145-vector
DU145-GHSROS
LNCaP-vector
LNCaP-GHSROS
Ki67

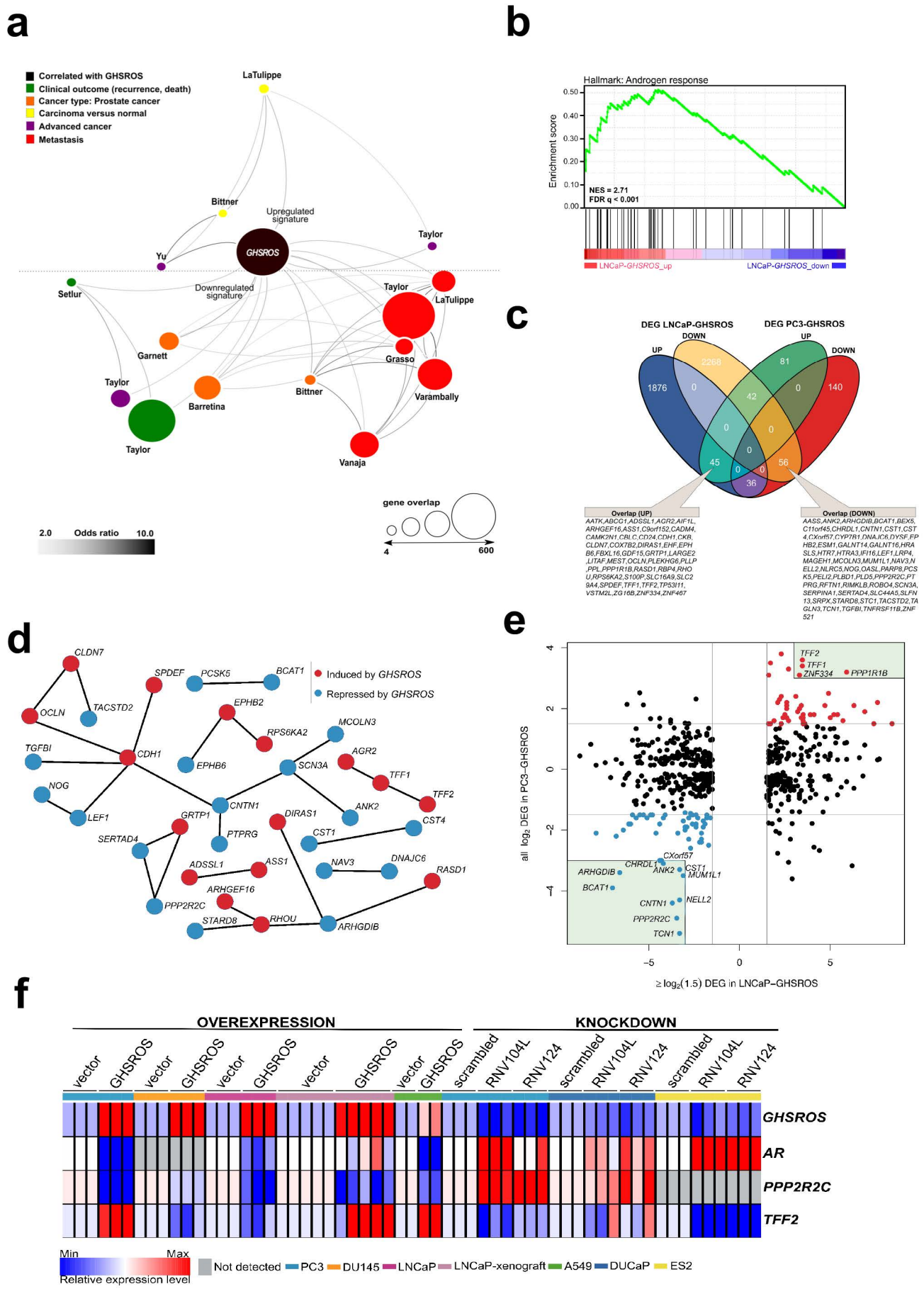
a
Correlated with GHSROS
Clinical outcome (recurrence, death)
Cancer type: Prostate cancer
Carcinoma versus normal
Advanced cancer
Metastasis
LaTulippe
Bittner
Upregulated signature
Yu
GHSROS
Taylor
Setlur
Downregulated signature
Taylor
LaTulippe
Garnett
Grasso
Taylor
Barretina
Bittner
Varambally
Taylor
Vanaja
gene overlap
4
600
2.0
Odds ratio
10.0
b
Hallmark: Androgen response
Enrichment score
0.50
0.40
0.30
0.20
0.10
0.00
NES = 2.71
FDR q < 0.001
LNCaP-GHSROS_up
LNCaP-GHSROS_down
c
DEG LNCaP-GHSROS
DEG PC3-GHSROS
UP
DOWN
UP
DOWN
1876
0
2268
42
81
0
140
0
0
0
0
45
0
36
56
Overlap (UP)
AATK,ABCC1,ADSSL1,AGR2,AIF1L,ARHGEF16,AS1,C9orf152,CADM4,CAMK2N1,CBLC,CD24,CDH1,CK8,CLDN7,COX7B2,DIRAS1,EHF,EPHB6,FBXL16,GDF15,GRTP1,LARGE2,LITAF,MEST,OCLN,PLEKHG6,PLLP,PPL,PPP1R1B,RASD1,RBP4,RHOU,RPS6KA2,S100P,SLC16A9,SLC29A4,SPDEF,TFF1,TFF2,TP53I11,VSTM2L,ZG16B,ZNF334,ZNF467
Overlap (DOWN)
AASS,ANK2,ARHGDIB,BCAT1,BEX5,C11orf45,CHRDL1,CNTN1,CST1,CST4,CXorf57,CYP7B1,DNAJC6,DYSF,FPHB2,ESM1,GALNT14,GALNT16,HRASLS,HTR7,HTRA3,IFI16,LEF1,LRP4,MAGEH1,MCOLN3,MUM1L1,NAV3,NELL2,NLRC5,NOG,OASL,PARP8,PCSK5,PELI2,PLBD1,PLD5,PPP2R2C,PTPRG,RFTN1,RIMKLB,ROBO4,SCN3A,SERPINA1,SERTAD4,SLC4A5,SLFN13,SRPX,STARD8,STC1,TACSTD2,TAGLN3,TCN1,TGFBI,TNFRSF11B,ZNF521
d
CLDN7
SPDEF
PCSK5
BCAT1
Induced by GHSROS
Repressed by GHSROS
OCLN
TACSTD2
EPHB2
RPS6KA2
MCOLN3
TGFBI
CDH1
EPHB6
SCN3A
AGR2
TFF1
NOG
TFF2
CNTN1
ANK2
LEF1
GRTP1
DIRAS1
CST4
PTPRG
CST1
SERTAD4
ADSSL1
AS1
NAV3
DNAJC6
RASD1
ARHGEF16
PPP2R2C
STARD8
RHOU
ARHGDIB
e
all log2 DEG in PC3−GHSROS
≥ log2(1.5) DEG in LNCaP−GHSROS
TFF2
TFF1
ZNF334
PPP1R1B
CXorf57
CHRDL1
ANK2
CST1
MUM1L1
ARHGDIB
BCAT1
CNTN1
NELL2
PPP2R2C
TCN1
f
OVEREXPRESSION
KNOCKDOWN
vector
GHSROS
scrambled
RNV104L
RNV124
GHSROS
AR
PPP2R2C
TFF2
Min
Max
Relative expression level
Not detected
PC3
DU145
LNCaP
LNCaP-xenograft
A549
DUCaP
ES2

Supplementary information.

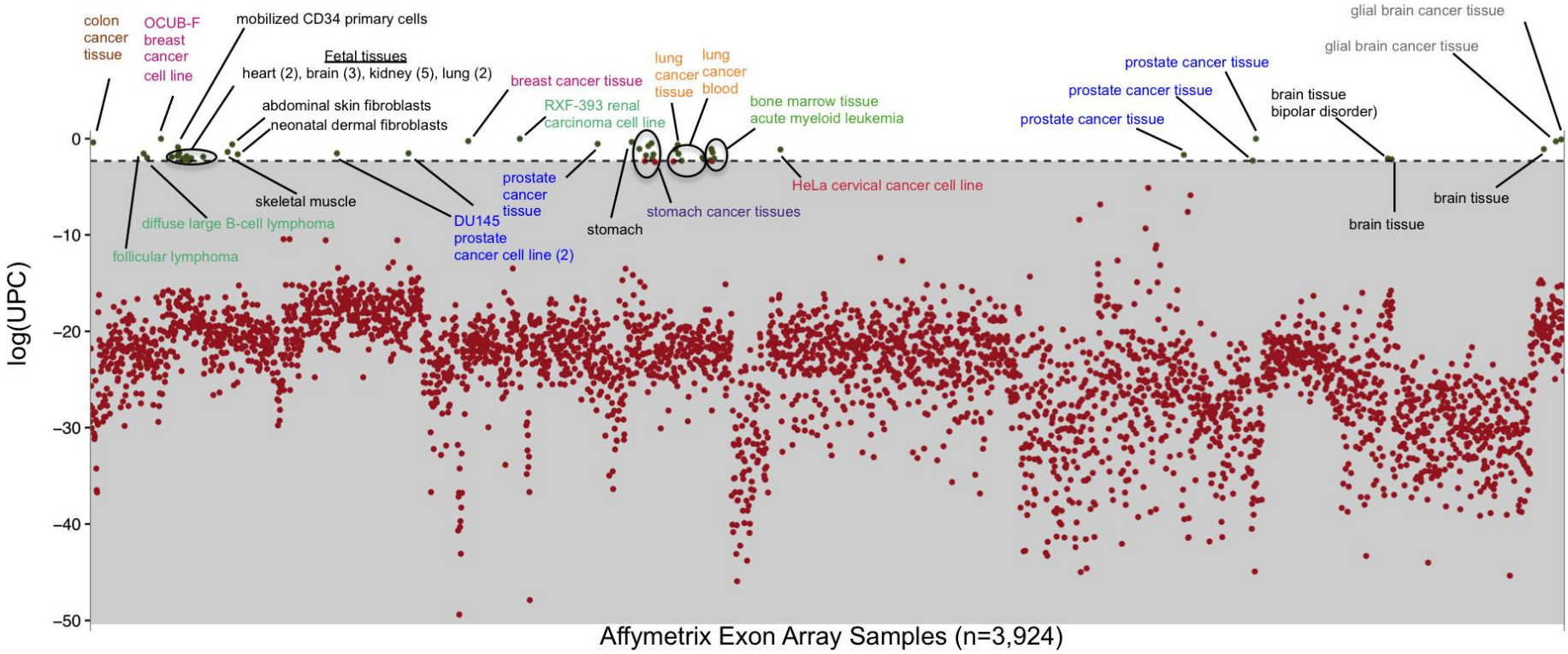

Supplementary Fig. S1. Scatterplot of *GHSROS* Universal exPression Code values in publicly available exon array datasets. The scatter plot shows the log of Universal exPression Code (UPC) values, an estimate on whether a gene is actively transcribed in exon array samples. The dotted horizontal line separates samples with a UPC ≥ 0.1.

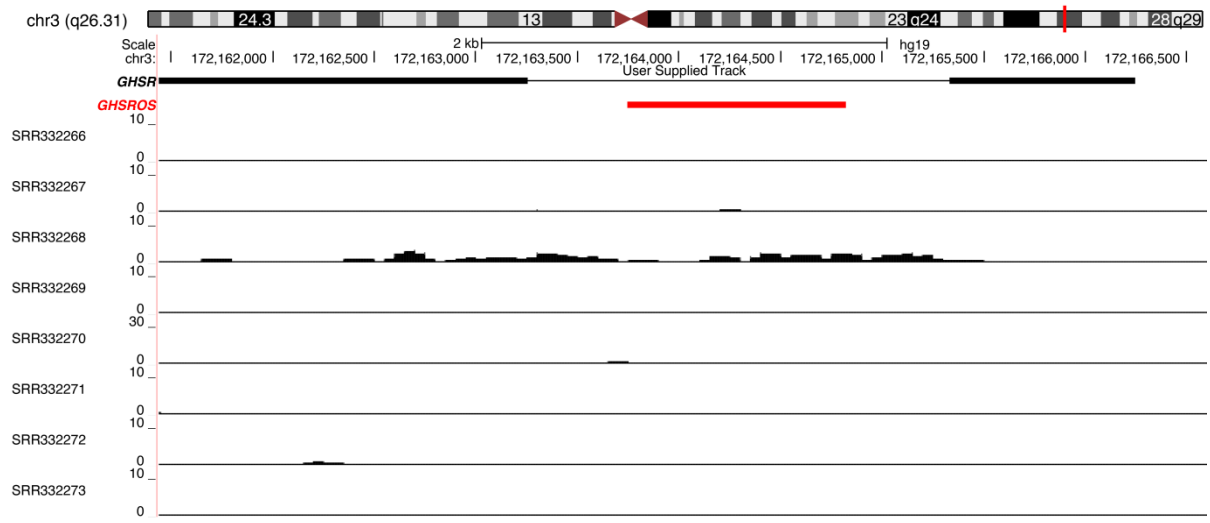

Supplementary Fig. S2. UCSC genome browser visualization of *GHSR*/*GHSROS* locus expression in castration-resistant prostate cancer. *GHSR* exons (black), antisense *GHSROS* exon (red). SRR332266 to SRR332273 denote NCBI Sequence Read Archive (SRA) database accession numbers. The *y*-axis represents read counts normalized to sequencing depth.

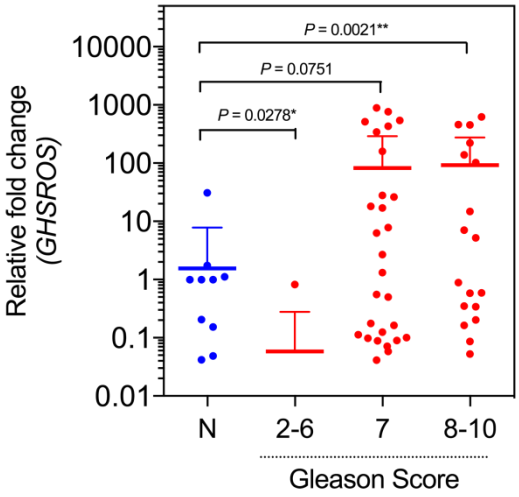

**Supplementary Fig. S3. *GHSROS* expression in OriGene TissueScan Prostate Cancer Tissue qPCR panels stratified by Gleason score. ****P* ≤ 0.05, ***P* ≤ 0.01, Mann-Whitney-Wilcoxon test. Expression was normalized to the housekeeping gene *RPL32* and relative to a normal prostate sample.

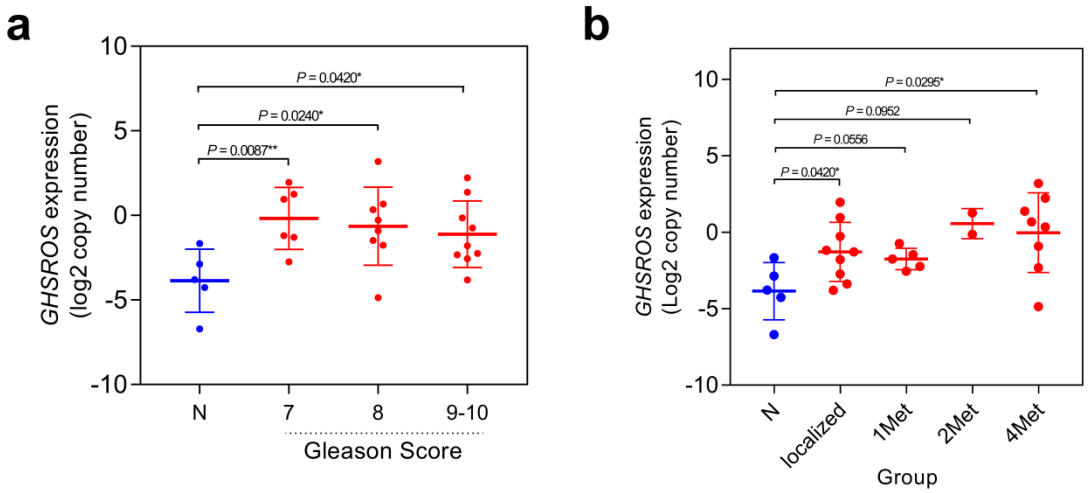

Supplementary Fig. S4. *GHSROS* expression in the Andalusian Biobank prostate tissue cohort. *GHSROS* expression in the Andalusian Biobank prostate tissue cohort stratified by (**a)** Gleason score and **(b)** number of metastatic sites. 1 Met denotes one and ≥ 2 Met two or more metastatic sites. Absolute expression levels were determined by qRT-PCR and adjusted by a normalization factor calculated from the expression levels of three housekeeping genes (*HPRT*, *ACTB*, and *GAPDH*). N denotes normal prostate. *$P \leq 0.05$, **$P \leq 0.01$, Mann-Whitney-Wilcoxon test.

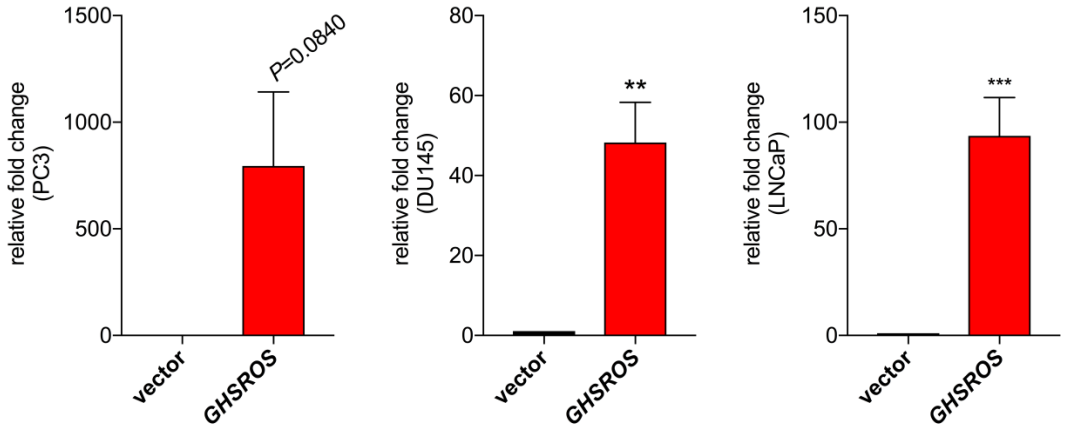

Supplementary Fig. S5. Confirmation of *GHSROS* overexpression in prostate cancer-derived cell lines. Bar graphs show qRT-PCR quantification of the relative expression levels of *GHSROS* when overexpressed in prostate-derived (PC3, DU145, and LNCaP) cancer cell lines. Expression was normalized to the housekeeping gene *RPL32* using the comparative $2^{-\Delta\Delta Ct}$ method of quantification. Results are relative to the respective vector control. Mean ± s.e.m., n=3, $^{**}P \leq 0.01$, $^{***}P \leq 0.001$, Student's t-test.

Supplementary Fig. S6. Sequence of the lncRNA *GHSROS* and regions targeted by oligonucleotides. The 1.1kb *GHSROS* sequence. Locked nucleic antisense oligonucleotide (LNA-ASO) locations are highlighted in red and the qRT-PCR amplicon in yellow.

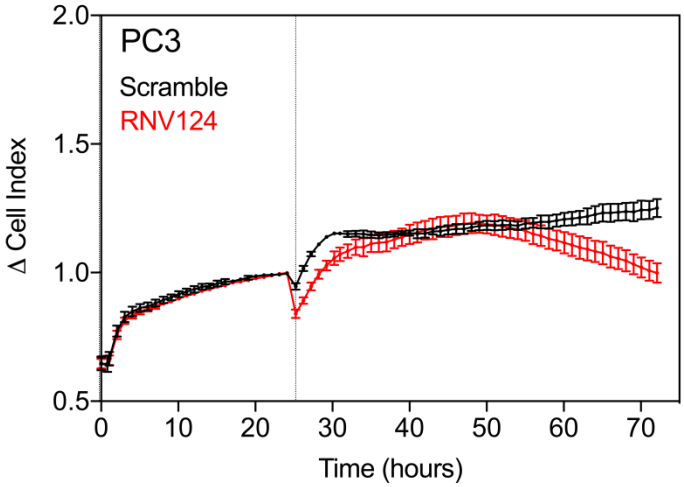

Supplementary Fig. S7. *GHSROS* knockdown attenuates PC3 cell survival upon serum starvation. Cells were transfected with the LNA-ASO RNV124 and grown for 24 hours (indicated by a vertical dotted line) prior to serum starvation. Results are relative to scrambled control. Mean ± s.e.m., *n*=3. At 48 hours after serum starvation, (72 hours after cells transfected as indicated on the x-axis), there was a significant difference in survival ($P = 0.049$, Student's *t*-test).

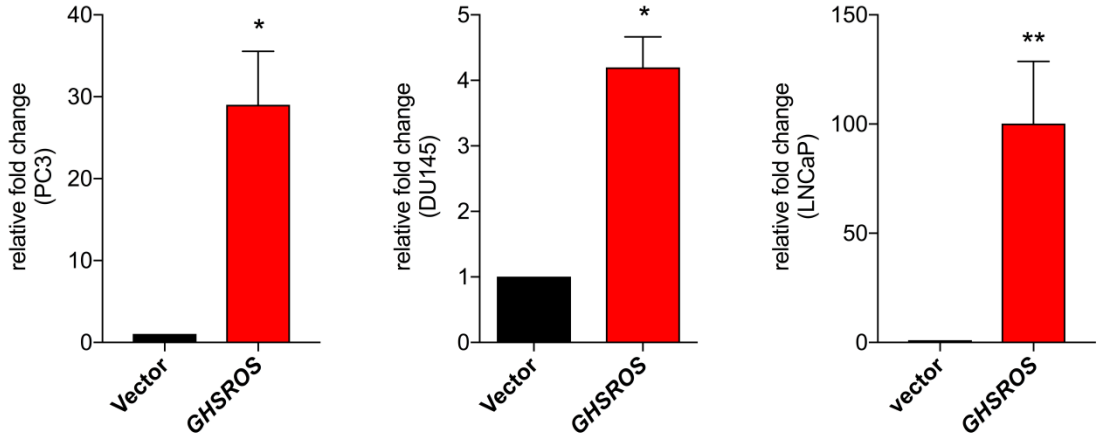

Supplementary Fig. S8. Validation of *GHSROS* overexpression in PC3, DU145, and LNCaP tumor xenografts by qRT-PCR. Expression changes were measured from excised PC3 (*n*=2 vector, *n*=3 *GHSROS*), DU145 (*n*=2 vector, *n*=3 *GHSROS*), and LNCaP xenografts (*n*=8 vector, *n*=5 *GHSROS*) at *in vivo* endpoint. Expression was normalized to the housekeeping gene *RPL32*. Results are relative to the respective vector control. Mean ± s.e.m., *n*=3, **P* ≤ 0.05, ***P* ≤ 0.01, Student's *t*-test.

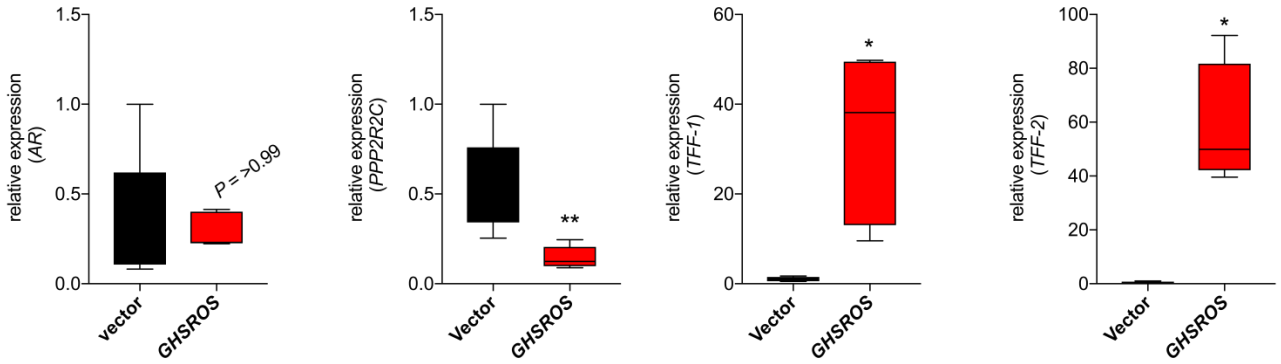

Supplementary Fig. S9. Expression of selected genes in LNCaP tumor xenografts overexpressing *GHSROS*. Expression changes were measured by qRT-PCR from excised LNCaP (*n*=4-8 vector, *n*=4-5 *GHSROS*) at *in vivo* endpoint. Expression was normalized to the housekeeping gene *RPL32*. Results are relative to the respective vector control. Mean, *n*=3, $*P \leq 0.05$, $***P \leq 0.01$, Student's *t*-test.

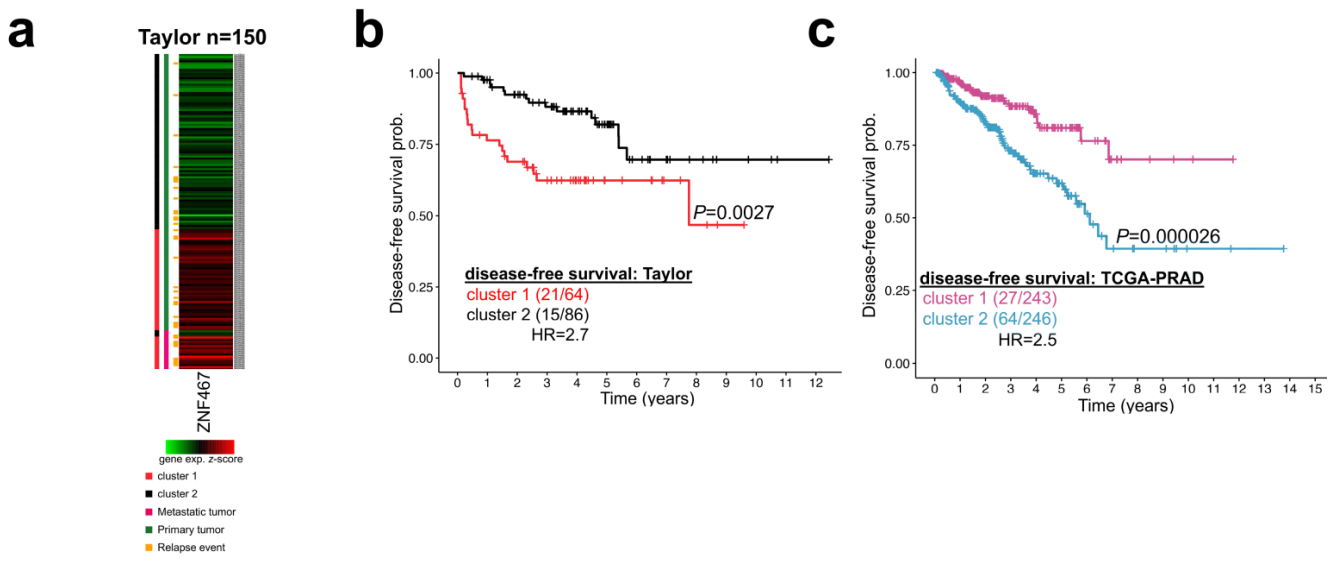

Supplementary Fig. S10. Zinc finger protein 467 (*ZNF467*), a gene induced by forced *GHSROS*-overexpression, is upregulated by metastatic tumors and associated with adverse relapse outcome. (a) Heat map of *ZNF467* expression in the Taylor cohort normalized to depict relative values within rows (samples) with high (red) and low expression (green). Vertical bars show patient grouping by *k*-means clustering (cluster 1, red; cluster 2, black), tumor type (primary, green; metastatic pink), and relapse status (relapse event, orange). **(b)** Kaplan-Meier analyses of *ZNF467* in the Taylor cohort. Patients were stratified by *k*-means clustering, as described in (a). **(c)** Kaplan-Meier analyses of *ZNF467* in the TCGA-PRAD cohort of 489 localized prostate tumors. Patients were stratified by *k*-means clustering (cluster 1, purple; cluster 2, turquoise).

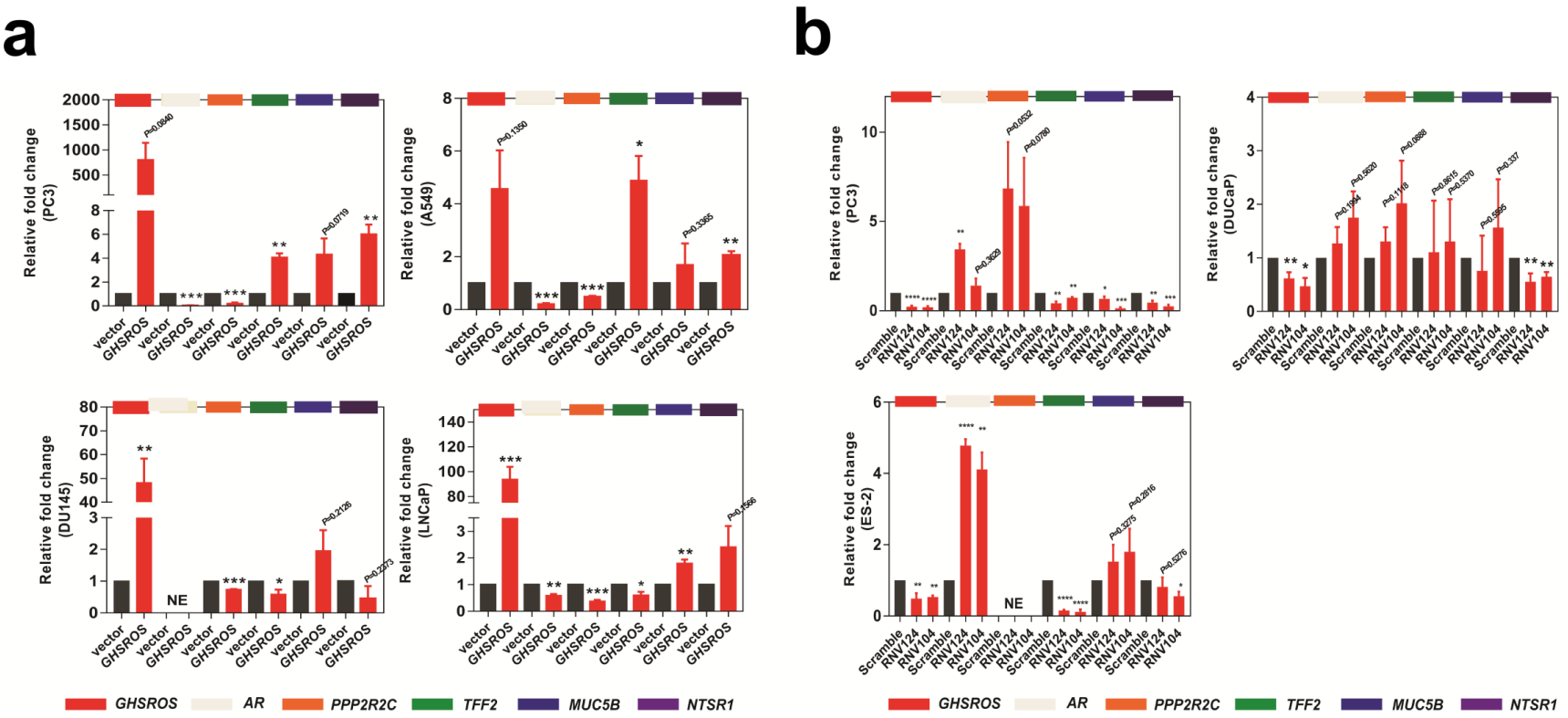

Supplementary Fig. S11. Effects of *GHSROS* perturbation in cultured cells assessed by qRT-PCR. (a) qRT-PCR validation of 5 genes regulated by *GHSROS*. Expression was normalized to the housekeeping gene RPL32. Results are relative to the respective vector control. Coloured bars indicate individual genes. Genes that were not expressed represented as no expression (NE). Mean ± s.e.m., n=3, $*P \leq 0.05$, $**P \leq 0.01$, $***P \leq 0.001$, Student's t-test. **(b)** qRT-PCR validation of regulated genes following knockdown of *GHSROS* by transfection with LNA-ASOs for 48 hours. Expression was normalized to the housekeeping gene *RPL32*. Results are relative to the respective scrambled control. Annotated as in (a).

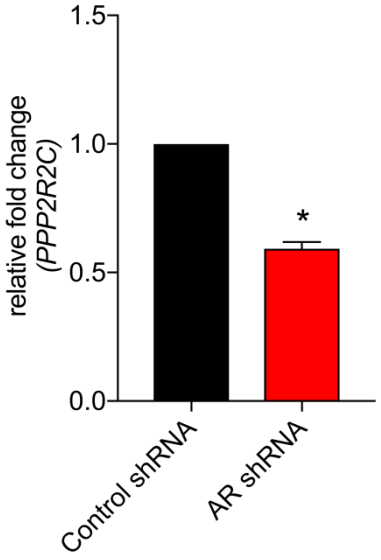

Supplementary Fig. S12. Effect of androgen receptor (AR) perturbation in LP50 prostate cancer cells on *PPP2R2C* expression. Assessed by microarray (NCBI GEO accession no. GSE22483). Mean ± s.e.m. n=2, *$Q \leq 0.05$, moderated t-test.

Supplementary Table S1. Correlation between *GHSROS* expression and clinicopathological parameters in OriGene TissueScan Prostate Cancer Tissue qPCR panels. Six samples were excluded due to missing clinical information. Relative *GHSROS* expression in tumors (T) stratified by clinical stage and Gleason score was compared to a normal prostate sample (N). *P*-values were calculated using the Mann-Whitney-Wilcoxon test. NA = not applicable, PD = other prostatic diseases.

Clinicopathological parameters	**Sample number (*n*)**	***P*-value**
Age at diagnosis (mean ± SD)	62.2 ± 7.80	
N/ T	24/88	0.1413
PD/ T	31/88	0.8001
N/ PD	24/31	0.0691
Clinical stage		
N (normal prostate)	24	
I	0	NA
II	47	0.311
III	33	0.0855
IV	3	0.0185
Gleason score		
N (normal prostate)	24	
2-6	15	0.0278
7	47	0.0751
8-10	25	0.00210

Supplementary Table S2. Correlation between *GHSROS* expression and clinicopathological parameters in the Andalusian Biobank prostate tissue cohort. Absolute levels of *GHSROS* expression in tumors were stratified by Gleason score and the number of metastatic tumor sites were compared to normal prostate (N). Tumors positive or negative for extraprostatic extension and perineural infiltration were compared to each other. *P*-values were calculated using the Mann-Whitney-Wilcoxon test. NA = not applicable.

Clinicopathological parameters	**Sample number (*n*)**	***P*-value**
Age at diagnosis (mean ± SD)	73.7 ± 9.81	
Gleason score		
N (normal prostate)	8	
7	6	0.00870
8	9	0.0240
9-10	13	0.0420
Number of metastatic sites		
N (normal prostate)	8	
primary prostate tumor: 0/localized	10	0.0420
primary prostate tumor: 1 metastatic site	6	0.0556
primary prostate tumor: ≥2 metastatic sites	12	0.0127
Extraprostatic extension		
-	16	0.379
+	11	
Perineural infiltration		
-	8	0.415
+	20	

Supplementary Table S3. Differentially expressed genes in PC3-GHSROS cells compared to empty vector control. Red: higher expression in PC3-GHSROS cells; Black: lower expression in PC3-GHSROS cells. Fold-changes are log_2 transformed; *Q*-value denotes the false discovery rate (FDR; Benjamini-Hochberg)-adjusted *P*-value (cutoff ≤ 0.05).

Gene Symbol	**Gene Name**	**log_2 Fold Change**	***P*-value**	***Q*-value**
AADACP1	arylacetamide deacetylase pseudogene 1	-1.9	8.2E-08	1.3E-06
AASS	aminoadipate-semialdehyde synthase	-2.4	2.5E-08	5.3E-07
AATK	apoptosis associated tyrosine kinase	1.8	5.1E-08	8.9E-07
ABCC3	ATP binding cassette subfamily C member 3	1.8	7.7E-13	7.1E-10
ABCG1	ATP binding cassette subfamily G member 1	2.1	1.7E-09	7.5E-08
ACHE	acetylcholinesterase (Cartwright blood group)	2.5	4.3E-10	3.0E-08
ACSS1	acyl-CoA synthetase short-chain family member 1	-1.9	7.4E-11	9.6E-09
ADAM23	ADAM metallopeptidase domain 23	-2.7	5.3E-10	3.5E-08
ADAM8	ADAM metallopeptidase domain 8	2.7	5.5E-14	1.5E-10
ADD2	adducin 2	-3.2	2.1E-09	8.8E-08
ADSSL1	adenylosuccinate synthase like 1	1.5	6.2E-08	1.0E-06
AFF2	AF4/FMR2 family member 2	-3.9	1.1E-11	3.0E-09
AGR2	anterior gradient 2, protein disulphide isomerase family member	2.1	3.9E-12	1.7E-09
AGTR1	angiotensin II receptor type 1	-2.1	3.6E-08	7.0E-07
AIF1L	allograft inflammatory factor 1 like	1.6	2.7E-08	5.6E-07
AMOT	angiomotin	-3.1	2.3E-11	4.7E-09
ANGPT1	angiopoietin 1	-2.8	1.0E-08	2.7E-07
ANGPTL4	angiopoietin like 4	1.6	2.0E-08	4.5E-07
ANK1	ankyrin 1	1.5	9.3E-06	5.5E-05
ANK2	ankyrin 2, neuronal	-3.1	2.4E-09	9.5E-08
ANOS1	anosmin 1	1.9	6.1E-09	1.8E-07
ANXA10	annexin A10	-2.3	1.1E-09	5.7E-08
APOBEC3G	apolipoprotein B mRNA editing enzyme catalytic subunit 3G	2.0	3.3E-08	6.5E-07
AR	androgen receptor	-3.6	1.4E-09	6.6E-08
ARHGAP44	Rho GTPase activating protein 44	-2.1	1.6E-08	3.8E-07
ARHGDIB	Rho GDP dissociation inhibitor beta	-3.4	5.3E-11	7.7E-09
ARHGEF16	Rho guanine nucleotide exchange factor 16	2.4	7.8E-10	4.6E-08
ARNT2	aryl hydrocarbon receptor nuclear translocator 2	-1.6	1.0E-07	1.5E-06
ASS1	argininosuccinate synthase 1	1.8	2.2E-08	4.8E-07
B3GALT5	beta-1,3-galactosyltransferase 5	-2.0	2.1E-06	1.7E-05

B3GALT5-AS1	B3GALT5 antisense RNA 1	-2.2	6.1E-09	1.8E-07
B3GNT7	UDP-GlcNAc:betaGal beta-1,3-N-acetylglucosaminyltransferase 7	1.6	4.2E-09	1.4E-07
B4GALNT1	beta-1,4-N-acetyl-galactosaminyltransferase 1	-1.8	8.8E-11	1.1E-08
BCAT1	branched chain amino acid transaminase 1	-3.9	1.5E-11	3.4E-09
BEX2	brain expressed X-linked 2	-1.8	4.2E-07	4.4E-06
BEX4	brain expressed X-linked 4	-1.8	1.1E-08	2.9E-07
BEX5	brain expressed X-linked 5	-1.7	8.1E-07	7.5E-06
BIK	BCL2 interacting killer	1.8	2.1E-06	1.6E-05
BLMH	bleomycin hydrolase	-1.8	6.6E-13	6.5E-10
BMP6	bone morphogenetic protein 6	-2.3	5.1E-09	1.6E-07
BTBD11	BTB domain containing 11	-3.1	5.7E-10	3.6E-08
BTG3	BTG family member 3	-2.0	1.1E-10	1.3E-08
C11orf45	chromosome 11 open reading frame 45	-1.8	2.0E-08	4.5E-07
C20orf166-AS1	C20orf166 antisense RNA 1	1.8	3.0E-07	3.5E-06
C9orf152	chromosome 9 open reading frame 152	1.8	5.3E-07	5.4E-06
CA9	carbonic anhydrase 9	2.5	3.1E-08	6.2E-07
CACNA2D2	calcium voltage-gated channel auxiliary subunit alpha2delta 2	-1.6	2.6E-08	5.5E-07
CADM4	cell adhesion molecule 4	2.3	8.8E-10	5.0E-08
CADPS2	calcium dependent secretion activator 2	-2.0	8.9E-12	2.6E-09
CALB1	calbindin 1	3.3	2.1E-10	1.9E-08
CAMK2N1	calcium/calmodulin dependent protein kinase II inhibitor 1	3.3	4.1E-12	1.7E-09
CAPN6	calpain 6	-2.5	3.3E-08	6.5E-07
CAV1	caveolin 1	1.6	5.2E-13	6.0E-10
CBLC	Cbl proto-oncogene C	1.8	2.8E-07	3.3E-06
CCBE1	collagen and calcium binding EGF domains 1	1.5	1.5E-08	3.7E-07
CCDC160	coiled-coil domain containing 160	-2.5	1.6E-08	3.8E-07
CCNB3	cyclin B3	-2.1	5.3E-08	9.2E-07
CD24	CD24 molecule	1.5	2.9E-12	1.5E-09
CD33	CD33 molecule	-2.0	5.7E-08	9.7E-07
CD70	CD70 molecule	-2.1	6.3E-07	6.2E-06
CDH1	cadherin 1	2.2	4.1E-08	7.8E-07
CDH12	cadherin 12	-1.6	8.8E-10	5.0E-08
CDH3	cadherin 3	2.0	1.5E-07	2.1E-06
CEACAM6	carcinoembryonic antigen related cell adhesion molecule 6	1.7	6.2E-07	6.1E-06
CEND1	cell cycle exit and neuronal differentiation 1	-2.0	2.4E-07	2.9E-06
CHD7	chromodomain helicase DNA binding protein 7	-1.6	1.1E-06	9.6E-06
CHRDL1	chordin-like 1	-3.0	5.4E-10	3.5E-08
CKB	creatine kinase B	1.8	2.6E-11	5.0E-09
CLDN7	claudin 7	2.1	1.4E-07	1.9E-06
CLMN	calmin (calponin-like, transmembrane)	-2.4	4.9E-09	1.6E-07

CNKSR2	connector enhancer of kinase suppressor of Ras 2	-2.4	9.2E-09	2.5E-07
CNTN1	contactin 1	-4.4	4.2E-11	6.6E-09
COBL	cordon-bleu WH2 repeat protein	-4.6	1.0E-11	2.9E-09
COL21A1	collagen type XXI alpha 1 chain	-1.9	1.2E-07	1.7E-06
COL5A1	collagen type V alpha 1	2.1	1.9E-09	8.2E-08
COX7B2	cytochrome c oxidase subunit 7B2	3.8	1.8E-09	7.6E-08
CPA6	carboxypeptidase A6	-2.3	1.5E-08	3.5E-07
CPEB1	cytoplasmic polyadenylation element binding protein 1	-2.5	5.4E-11	7.7E-09
CPZ	carboxypeptidase Z	1.6	1.7E-09	7.5E-08
CRABP1	cellular retinoic acid binding protein 1	4.1	1.1E-11	3.0E-09
CRABP2	cellular retinoic acid binding protein 2	2.4	1.1E-12	7.8E-10
CREB3L1	cAMP responsive element binding protein 3 like 1	4.0	2.4E-13	3.4E-10
CRIP1	cysteine rich protein 1	2.2	1.4E-10	1.5E-08
CRIP2	cysteine rich protein 2	2.3	9.6E-12	2.8E-09
CSMD2	CUB and Sushi multiple domains 2	-2.5	7.9E-09	2.2E-07
CST1	cystatin SN	-3.3	1.3E-10	1.4E-08
CST4	cystatin S	-2.6	1.8E-09	7.6E-08
CXADR	coxsackie virus and adenovirus receptor	-2.8	4.0E-11	6.5E-09
CXADRP2	coxsackie virus and adenovirus receptor pseudogene 2	-1.8	3.5E-07	3.9E-06
CXCL5	C-X-C motif chemokine ligand 5	1.5	1.0E-06	9.0E-06
CXorf57	chromosome X open reading frame 57	-3.0	4.7E-10	3.2E-08
CYP4F35P	cytochrome P450 family 4 subfamily F member 35, pseudogene	-1.5	1.4E-07	2.0E-06
CYP4V2	cytochrome P450 family 4 subfamily V member 2	-2.6	2.3E-09	9.1E-08
CYP7B1	cytochrome P450 family 7 subfamily B member 1	-2.3	2.2E-08	4.8E-07
DEPTOR	DEP domain containing MTOR-interacting protein	-1.7	6.7E-08	1.1E-06
DGKG	diacylglycerol kinase gamma	-2.7	1.0E-10	1.2E-08
DIRAS1	DIRAS family GTPase 1	2.2	2.8E-10	2.2E-08
DLX3	distal-less homeobox 3	-1.6	1.7E-06	1.4E-05
DMD	dystrophin	-3.0	4.0E-10	2.8E-08
DNAH5	dynein axonemal heavy chain 5	-1.7	3.3E-09	1.2E-07
DNAJA4	DnaJ heat shock protein family (Hsp40) member A4	-2.0	1.8E-08	4.1E-07
DNAJC6	DnaJ heat shock protein family (Hsp40) member C6	-2.4	4.6E-10	3.1E-08
DOCK3	dedicator of cytokinesis 3	-1.5	9.4E-09	2.6E-07
DPY19L2P1	DPY19L2 pseudogene 1	-1.9	1.2E-06	1.1E-05
DTX4	deltex 4, E3 ubiquitin ligase	-1.8	1.1E-08	2.8E-07
DYSF	dysferlin	-2.0	5.9E-11	8.3E-09
EDA	ectodysplasin A	-3.0	6.2E-09	1.8E-07
EGF	epidermal growth factor	-2.5	9.1E-10	5.1E-08
EGLN3	egl-9 family hypoxia inducible factor 3	-1.8	1.3E-07	1.8E-06
EHD2	EH domain containing 2	2.3	9.7E-09	2.6E-07
EHF	ETS homologous factor	1.9	8.5E-09	2.4E-07
ENTPD3	ectonucleoside triphosphate diphosphohydrolase 3	-1.8	1.1E-08	2.8E-07

EOMES	eomesodermin	-2.1	1.2E-09	6.1E-08
EPHB2	EPH receptor B2	-1.5	2.6E-10	2.1E-08
EPHB6	EPH receptor B6	1.7	1.4E-10	1.5E-08
ESM1	endothelial cell specific molecule 1	-1.8	4.3E-11	6.7E-09
EYA1	EYA transcriptional coactivator and phosphatase 1	-3.5	1.5E-10	1.6E-08
F2RL2	coagulation factor II thrombin receptor like 2	-1.6	2.0E-07	2.6E-06
FAM110C	family with sequence similarity 110 member C	-3.0	1.6E-10	1.6E-08
FAM131B	family with sequence similarity 131 member B	1.5	1.7E-11	3.6E-09
FAM134B	family with sequence similarity 134 member B	-1.5	6.3E-08	1.0E-06
FAM20A	family with sequence similarity 20 member A	2.0	1.3E-07	1.9E-06
FAM50B	family with sequence similarity 50 member B	1.7	8.5E-08	1.3E-06
FAM89A	family with sequence similarity 89 member A	-1.6	5.1E-08	8.9E-07
FBP1	fructose-bisphosphatase 1	2.5	3.1E-11	5.6E-09
FBXL16	F-box and leucine rich repeat protein 16	2.0	1.4E-08	3.5E-07
FBXL7	F-box and leucine rich repeat protein 7	-1.7	1.6E-08	3.7E-07
FCGBP	Fc fragment of IgG binding protein	-3.1	1.5E-10	1.6E-08
FEZF1-AS1	FEZF1 antisense RNA 1	-2.0	1.1E-06	9.8E-06
FGF13	fibroblast growth factor 13	-1.8	1.7E-08	4.0E-07
FNDC4	fibronectin type III domain containing 4	2.0	4.2E-08	7.9E-07
FOXL1	forkhead box L1	1.6	4.1E-10	2.9E-08
FOXRED2	FAD dependent oxidoreductase domain containing 2	3.6	2.3E-12	1.5E-09
FRMD4B	FERM domain containing 4B	-1.9	5.5E-09	1.7E-07
GAL	galanin and GMAP prepropeptide	-3.2	1.5E-09	6.7E-08
GALNT12	polypeptide N-acetylgalactosaminyltransferase 12	2.1	9.9E-10	5.3E-08
GALNT14	polypeptide N-acetylgalactosaminyltransferase 14	-1.6	1.3E-08	3.3E-07
GALNT16	polypeptide N-acetylgalactosaminyltransferase 16	-1.7	1.2E-06	1.0E-05
GAS6	growth arrest specific 6	1.6	2.1E-09	8.8E-08
GBP7	guanylate binding protein 7	-1.5	2.9E-06	2.1E-05
GCNT1	glucosaminyl (N-acetyl) transferase 1, core 2	-1.6	1.4E-07	1.9E-06
GCNT3	glucosaminyl (N-acetyl) transferase 3, mucin type	-2.4	6.8E-09	2.0E-07
GDF15	growth differentiation factor 15	1.5	1.5E-08	3.6E-07
GHSROS	Growth Hormone Secretagogue Receptor Opposite Strand	5.3	3.4E-13	4.3E-10
GJB3	gap junction protein beta 3	1.7	6.0E-10	3.8E-08
GNAI1	G protein subunit alpha i1	1.5	1.6E-10	1.6E-08
GPR153	G protein-coupled receptor 153	1.6	5.7E-13	6.1E-10
GPR63	G protein-coupled receptor 63	-2.3	2.5E-09	9.7E-08
GRID2	glutamate ionotropic receptor delta type subunit 2	1.7	1.5E-07	2.1E-06
GRIN2D	glutamate ionotropic receptor NMDA type subunit 2D	2.0	1.6E-08	3.7E-07
GRTP1	growth hormone regulated TBC protein 1	2.1	6.0E-08	1.0E-06
GUCA1B	guanylate cyclase activator 1B	1.5	6.7E-07	6.5E-06
HEPH	hephaestin	-2.4	2.4E-09	9.3E-08

HR	hair growth associated	2.2	5.3E-09	1.7E-07
HRASLS	HRAS like suppressor	-1.9	2.7E-07	3.2E-06
HSPA12A	heat shock protein family A (Hsp70) member 12A	-3.7	2.7E-11	5.1E-09
HSPB8	heat shock protein family B (small) member 8	-3.5	9.9E-10	5.3E-08
HTR7	5-hydroxytryptamine receptor 7	-2.0	2.4E-07	2.9E-06
HTRA3	HtrA serine peptidase 3	-1.8	1.5E-08	3.6E-07
IFI16	interferon gamma inducible protein 16	-2.2	9.4E-13	7.5E-10
IFITM1	interferon induced transmembrane protein 1	1.6	3.6E-06	2.5E-05
IGFBP5	insulin like growth factor binding protein 5	1.6	2.4E-12	1.5E-09
IGFBP6	insulin like growth factor binding protein 6	1.9	3.8E-11	6.3E-09
IL13RA2	interleukin 13 receptor subunit alpha 2	-3.0	6.4E-10	4.0E-08
ITGB2	integrin subunit beta 2	2.2	6.1E-11	8.4E-09
ITGB4	integrin subunit beta 4	1.9	9.2E-13	7.5E-10
ITM2A	integral membrane protein 2A	-2.7	7.3E-10	4.4E-08
JAM3	junctional adhesion molecule 3	-1.8	1.3E-08	3.3E-07
JUP	junction plakoglobin	1.5	5.9E-12	2.0E-09
KCNJ12	potassium voltage-gated channel subfamily J member 12	-2.2	4.3E-09	1.4E-07
KCNJ3	potassium voltage-gated channel subfamily J member 3	1.5	2.4E-05	1.2E-04
KCNN3	potassium calcium-activated channel subfamily N member 3	-2.3	5.9E-07	5.9E-06
KIAA0319	KIAA0319	-3.6	4.6E-11	6.9E-09
KIAA1210	KIAA1210	-1.7	2.9E-07	3.4E-06
KIAA1211	KIAA1211	-3.8	2.7E-12	1.5E-09
KIAA1644	KIAA1644	2.0	2.6E-07	3.1E-06
KIF26A	kinesin family member 26A	-1.7	4.5E-08	8.3E-07
KIF5C	kinesin family member 5C	-2.7	1.6E-11	3.5E-09
KLF9	Kruppel like factor 9	-3.3	2.5E-10	2.1E-08
KRT6B	keratin 6B	-2.2	1.7E-08	3.9E-07
KRT7	keratin 7	2.6	1.9E-14	6.7E-11
KRT75	keratin 75	-5.5	3.5E-16	2.5E-12
KRT81	keratin 81	1.5	3.1E-12	1.5E-09
LAMA1	laminin subunit alpha 1	-2.1	1.6E-08	3.8E-07
LAMC3	laminin subunit gamma 3	-1.7	2.1E-09	8.5E-08
LARGE2	LARGE xylosyl- and glucuronyltransferase 2	1.8	4.3E-08	8.0E-07
LCK	LCK proto-oncogene, Src family tyrosine kinase	1.5	2.6E-06	2.0E-05
LCP1	lymphocyte cytosolic protein 1	-2.3	3.4E-12	1.6E-09
LEF1	lymphoid enhancer binding factor 1	-1.5	6.7E-07	6.5E-06
LGR5	leucine rich repeat containing G protein-coupled receptor 5	-1.7	3.9E-09	1.3E-07
LIMCH1	LIM and calponin homology domains 1	2.2	6.1E-10	3.8E-08
LIMS2	LIM zinc finger domain containing 2	1.7	3.1E-09	1.2E-07
LINC00346	long intergenic non-protein coding RNA 346	1.5	8.0E-07	7.4E-06
LINC01133	long intergenic non-protein coding RNA 1133	1.5	4.1E-06	2.8E-05
LITAF	lipopolysaccharide induced TNF factor	3.1	1.1E-10	1.3E-08

LOC100506123	uncharacterized LOC100506123	-1.6	1.4E-09	6.7E-08
LOC101927870	uncharacterized LOC101927870	1.5	5.2E-09	1.6E-07
LOXL4	lysyl oxidase like 4	1.7	4.4E-12	1.8E-09
LRCH2	leucine rich repeats and calponin homology domain containing 2	-2.4	3.7E-09	1.3E-07
LRIG1	leucine rich repeats and immunoglobulin like domains 1	-2.0	1.6E-08	3.7E-07
LRP4	LDL receptor related protein 4	-1.5	1.8E-05	9.3E-05
LRRN2	leucine rich repeat neuronal 2	-1.5	8.3E-07	7.7E-06
MAGEH1	MAGE family member H1	-1.9	1.1E-08	2.8E-07
MAP2	microtubule associated protein 2	-1.5	3.0E-08	6.0E-07
MAP3K15	mitogen-activated protein kinase kinase kinase 15	-1.5	8.5E-09	2.3E-07
MARCH3	membrane associated ring-CH-type finger 3	1.5	2.2E-06	1.7E-05
MARK1	microtubule affinity regulating kinase 1	-2.9	2.7E-10	2.2E-08
MCOLN3	mucolipin 3	-1.8	2.1E-06	1.7E-05
MCTP2	multiple C2 domains, transmembrane 2	-3.0	3.1E-10	2.3E-08
MEGF6	multiple EGF like domains 6	2.0	4.0E-12	1.7E-09
MEST	mesoderm specific transcript	1.7	7.0E-09	2.0E-07
MFAP3L	microfibrillar associated protein 3 like	-2.5	1.3E-09	6.3E-08
MIR31HG	MIR31 host gene	1.7	2.4E-09	9.3E-08
MISP	mitotic spindle positioning	1.7	1.0E-10	1.2E-08
MLLT11	myeloid/lymphoid or mixed-lineage leukemia; translocated to, 11	-3.2	3.1E-16	2.5E-12
MMRN1	multimerin 1	-1.8	1.1E-08	2.9E-07
MN1	meningioma (disrupted in balanced translocation) 1	-2.6	1.2E-10	1.3E-08
MSX2	msh homeobox 2	-2.1	1.3E-08	3.3E-07
MTSS1	metastasis suppressor 1	-1.5	4.2E-07	4.4E-06
MUC2	mucin 2, oligomeric mucus/gel-forming	2.0	1.3E-08	3.3E-07
MUC3A	mucin 3A, cell surface associated	3.7	7.5E-12	2.4E-09
MUC5B	mucin 5B, oligomeric mucus/gel-forming	2.8	2.3E-09	9.2E-08
MUM1L1	MUM1 like 1	-3.5	1.1E-09	5.6E-08
MYT1	myelin transcription factor 1	-1.6	4.8E-06	3.2E-05
NACAD	NAC alpha domain containing	2.9	4.0E-09	1.4E-07
NAP1L2	nucleosome assembly protein 1 like 2	-1.7	1.4E-11	3.3E-09
NAP1L6	nucleosome assembly protein 1 like 6	-1.8	2.0E-06	1.6E-05
NAV3	neuron navigator 3	-1.6	4.3E-07	4.6E-06
NBEAP1	neurobeachin pseudogene 1	-1.8	6.9E-07	6.6E-06
NCR3LG1	natural killer cell cytotoxicity receptor 3 ligand 1	-1.7	8.9E-06	5.3E-05
NEK3	NIMA related kinase 3	2.0	1.4E-08	3.4E-07
NELL2	neural EGFL like 2	-4.3	2.6E-12	1.5E-09
NEO1	neogenin 1	-1.5	3.2E-06	2.3E-05
NFASC	neurofascin	-2.3	7.1E-11	9.5E-09
NLGN1	neuroligin 1	-1.7	1.9E-06	1.5E-05
NLRC5	NLR family CARD domain containing 5	-1.5	3.9E-07	4.2E-06
NOG	noggin	-1.5	1.3E-09	6.4E-08
NPR3	natriuretic peptide receptor 3	1.6	1.2E-07	1.7E-06

NPY1R	neuropeptide Y receptor Y1	1.9	3.0E-11	5.4E-09
NRXN3	neurexin 3	-1.9	1.2E-07	1.7E-06
NTSR1	neurotensin receptor 1 (high affinity)	4.0	1.4E-14	6.3E-11
NUDT10	nudix hydrolase 10	-2.6	9.7E-10	5.3E-08
NUDT11	nudix hydrolase 11	-4.9	2.4E-13	3.4E-10
OASL	2'-5'-oligoadenylate synthetase like	-1.6	1.8E-10	1.6E-08
OCLN	occludin	1.7	4.0E-09	1.4E-07
OPN3	opsin 3	1.5	5.9E-09	1.8E-07
OSBP2	oxysterol binding protein 2	1.8	1.5E-12	1.0E-09
OXTR	oxytocin receptor	1.7	7.0E-12	2.3E-09
PALD1	phosphatase domain containing, paladin 1	-2.2	2.0E-08	4.5E-07
PALM2	paralemmin 2	-2.1	5.0E-07	5.2E-06
PAQR8	progestin and adipoQ receptor family member 8	1.7	3.1E-09	1.1E-07
PARM1	prostate androgen-regulated mucin-like protein 1	-4.4	3.2E-12	1.5E-09
PARP8	poly(ADP-ribose) polymerase family member 8	-1.9	4.0E-09	1.4E-07
PCDH19	protocadherin 19	-1.7	2.0E-06	1.6E-05
PCDHGB2	protocadherin gamma subfamily B, 2	1.7	3.4E-07	3.8E-06
PCSK5	proprotein convertase subtilisin/kexin type 5	-1.9	2.4E-07	2.9E-06
PCSK9	proprotein convertase subtilisin/kexin type 9	1.7	4.8E-08	8.7E-07
PDGFA	platelet derived growth factor subunit A	1.6	1.9E-08	4.3E-07
PDLIM2	PDZ and LIM domain 2	1.9	8.0E-09	2.3E-07
PELI2	pellino E3 ubiquitin protein ligase family member 2	-1.6	2.3E-06	1.8E-05
PI3	peptidase inhibitor 3	1.7	5.8E-10	3.7E-08
PIANP	PILR alpha associated neural protein	1.6	8.1E-07	7.5E-06
PLAT	plasminogen activator, tissue type	1.8	1.9E-13	3.4E-10
PLBD1	phospholipase B domain containing 1	-1.5	4.1E-06	2.8E-05
PLCH2	phospholipase C eta 2	1.7	8.4E-10	4.8E-08
PLD5	phospholipase D family member 5	-2.1	4.5E-08	8.2E-07
PLEKHG6	pleckstrin homology and RhoGEF domain containing G6	1.5	3.3E-06	2.3E-05
PLLP	plasmolipin	1.5	9.7E-07	8.7E-06
PLXNA4	plexin A4	2.6	1.9E-07	2.4E-06
POF1B	premature ovarian failure, 1B	-1.5	1.6E-06	1.3E-05
POU3F2	POU class 3 homeobox 2	-3.6	2.7E-11	5.1E-09
PPL	periplakin	2.2	1.7E-10	1.6E-08
PPP1R1B	protein phosphatase 1 regulatory inhibitor subunit 1B	3.2	5.9E-10	3.7E-08
PPP1R3G	protein phosphatase 1 regulatory subunit 3G	2.3	4.3E-09	1.4E-07
PPP2R2C	protein phosphatase 2 regulatory subunit Bgamma	-4.9	1.9E-13	3.4E-10
PREX2	phosphatidylinositol-3,4,5-trisphosphate dependent Rac exchange factor 2	-1.6	8.3E-07	7.7E-06
PRKXP1	protein kinase, X-linked, pseudogene 1	-1.5	6.6E-06	4.2E-05
PRR15	proline rich 15	1.8	4.8E-08	8.6E-07
PTGER2	prostaglandin E receptor 2	1.9	1.5E-09	6.9E-08

PTGFRN	prostaglandin F2 receptor inhibitor	-1.6	4.6E-10	3.2E-08
PTGS2	prostaglandin-endoperoxide synthase 2	1.7	4.9E-07	5.1E-06
PTPN20	protein tyrosine phosphatase, non-receptor type 20	1.8	5.1E-08	9.0E-07
PTPRG	protein tyrosine phosphatase, receptor type G	-2.5	5.3E-09	1.7E-07
RAB39B	RAB39B, member RAS oncogene family	-2.1	9.3E-08	1.4E-06
RASD1	ras related dexamethasone induced 1	2.4	4.9E-09	1.6E-07
RASEF	RAS and EF-hand domain containing	-1.8	3.6E-07	4.0E-06
RASL11A	RAS like family 11 member A	1.9	6.8E-11	9.2E-09
RBM11	RNA binding motif protein 11	-3.2	1.4E-10	1.5E-08
RBP4	retinol binding protein 4	1.6	1.3E-11	3.2E-09
RCOR2	REST corepressor 2	1.6	1.3E-06	1.1E-05
REG4	regenerating family member 4	2.2	5.1E-09	1.6E-07
RFTN1	raftlin, lipid raft linker 1	-1.8	6.6E-09	1.9E-07
RGAG4	retrotransposon gag domain containing 4	-1.6	5.0E-06	3.3E-05
RGCC	regulator of cell cycle	1.7	3.3E-06	2.3E-05
RHOU	ras homolog family member U	1.7	1.5E-07	2.0E-06
RIMKLB	ribosomal modification protein rimK-like family member B	-1.6	1.5E-08	3.6E-07
RNASEL	ribonuclease L	-2.4	1.4E-09	6.6E-08
RNF128	ring finger protein 128, E3 ubiquitin protein ligase	-3.8	1.5E-11	3.5E-09
RNF152	ring finger protein 152	-1.5	2.7E-06	2.0E-05
ROBO4	roundabout guidance receptor 4	-2.1	2.0E-11	4.1E-09
RPS6KA2	ribosomal protein S6 kinase A2	1.5	6.3E-08	1.0E-06
RRAGD	Ras related GTP binding D	-3.0	8.0E-11	1.0E-08
RUNDC3B	RUN domain containing 3B	-1.8	2.8E-06	2.0E-05
RYR2	ryanodine receptor 2	-2.9	3.2E-09	1.2E-07
S100A2	S100 calcium binding protein A2	2.1	5.4E-11	7.7E-09
S100A9	S100 calcium binding protein A9	-1.5	8.9E-06	5.3E-05
S100P	S100 calcium binding protein P	1.9	9.6E-07	8.6E-06
SCIN	scinderin	1.5	7.2E-07	6.8E-06
SCN3A	sodium voltage-gated channel alpha subunit 3	-1.9	2.4E-08	5.1E-07
SEMA3B	semaphorin 3B	1.9	3.4E-10	2.5E-08
SEMA6B	semaphorin 6B	2.3	5.3E-10	3.5E-08
SERPINA1	serpin family A member 1	-2.1	3.2E-08	6.4E-07
SERPINB2	serpin family B member 2	-2.9	2.4E-11	4.7E-09
SERTAD4	SERTA domain containing 4	-1.6	2.3E-06	1.7E-05
SESN3	sestrin 3	-2.6	5.4E-10	3.5E-08
SGK494	uncharacterized serine/threonine-protein kinase SgK494	-1.5	3.1E-08	6.2E-07
SH2D1B	SH2 domain containing 1B	-2.2	1.5E-08	3.5E-07
SIRPB1	signal regulatory protein beta 1	-2.3	6.3E-11	8.7E-09
SIRPB2	signal regulatory protein beta 2	-1.6	3.2E-06	2.3E-05
SLC16A9	solute carrier family 16 member 9	1.7	4.0E-11	6.5E-09
SLC1A3	solute carrier family 1 member 3	-3.7	4.2E-11	6.6E-09
SLC25A25-AS1	SLC25A25 antisense RNA 1	-1.5	3.2E-08	6.3E-07
SLC26A10	solute carrier family 26 member 10	-1.8	1.6E-10	1.6E-08
SLC26A5	solute carrier family 26 member 5	1.5	1.4E-05	7.6E-05
SLC29A4	solute carrier family 29 member 4	1.6	2.6E-08	5.4E-07

SLC38A11	solute carrier family 38 member 11	1.7	2.7E-07	3.2E-06
SLC44A5	solute carrier family 44 member 5	-2.1	6.3E-08	1.1E-06
SLC47A1	solute carrier family 47 member 1	1.8	2.6E-07	3.1E-06
SLC6A11	solute carrier family 6 member 11	-2.3	4.9E-08	8.8E-07
SLC7A8	solute carrier family 7 member 8	-3.4	4.0E-10	2.8E-08
SLC9A2	solute carrier family 9 member A2	-3.6	2.1E-11	4.2E-09
SLFN13	schlafen family member 13	-2.3	2.9E-10	2.2E-08
SLITRK4	SLIT and NTRK like family member 4	-1.8	1.7E-09	7.5E-08
SOD3	superoxide dismutase 3, extracellular	1.7	7.5E-09	2.1E-07
SPDEF	SAM pointed domain containing ETS transcription factor	1.5	2.3E-10	2.0E-08
SPOCK3	sparc/osteonectin, cwcv and kazal-like domains proteoglycan (testican) 3	1.5	7.9E-08	1.3E-06
SPTB	spectrin beta, erythrocytic	-1.7	1.0E-09	5.5E-08
SRPX	sushi repeat containing protein, X-linked	-1.5	1.2E-09	6.1E-08
ST6GAL1	ST6 beta-galactoside alpha-2,6-sialyltransferase 1	-3.8	2.8E-12	1.5E-09
ST6GAL2	ST6 beta-galactoside alpha-2,6-sialyltransferase 2	2.0	9.2E-09	2.5E-07
ST6GALNAC2	ST6 N-acetylgalactosaminide alpha-2,6-sialyltransferase 2	2.4	1.6E-09	7.2E-08
STARD8	StAR related lipid transfer domain containing 8	-1.8	1.7E-07	2.2E-06
STAT6	signal transducer and activator of transcription 6	1.9	1.3E-11	3.2E-09
STC1	stanniocalcin 1	-1.5	4.5E-08	8.3E-07
STMN3	stathmin 3	1.5	3.8E-08	7.3E-07
STOX2	storkhead box 2	-2.6	5.3E-09	1.7E-07
SUSD3	sushi domain containing 3	1.8	1.9E-07	2.5E-06
SYT14	synaptotagmin 14	-2.2	1.0E-07	1.5E-06
TACSTD2	tumor-associated calcium signal transducer 2	-2.0	3.0E-09	1.1E-07
TAGLN3	transgelin 3	-1.5	5.2E-09	1.6E-07
TBC1D30	TBC1 domain family member 30	-1.8	7.1E-08	1.2E-06
TCN1	transcobalamin 1	-5.4	1.7E-13	3.4E-10
TDO2	tryptophan 2,3-dioxygenase	-2.0	1.3E-06	1.1E-05
TENM1	teneurin transmembrane protein 1	-1.8	7.8E-09	2.2E-07
TFF1	trefoil factor 1	3.6	5.2E-12	1.9E-09
TFF2	trefoil factor 2	3.4	3.4E-10	2.5E-08
TGFBI	transforming growth factor beta induced	-1.6	2.2E-07	2.7E-06
THBS1	thrombospondin 1	1.5	5.5E-09	1.7E-07
TLR3	toll like receptor 3	-1.9	2.1E-07	2.6E-06
TMC6	transmembrane channel like 6	1.7	2.4E-09	9.3E-08
TMEM108-AS1	TMEM108 antisense RNA 1	-3.1	9.8E-11	1.2E-08
TMEM229B	transmembrane protein 229B	-1.5	8.4E-08	1.3E-06
TMEM27	transmembrane protein 27	-1.7	4.4E-11	6.8E-09
TMEM74	transmembrane protein 74	-1.8	1.7E-07	2.2E-06
TMOD2	tropomodulin 2	-2.3	3.0E-10	2.3E-08
TMPRSS15	transmembrane protease, serine 15	2.4	2.8E-08	5.7E-07
TMPRSS3	transmembrane protease, serine 3	2.1	3.3E-07	3.8E-06
TMX4	thioredoxin related transmembrane protein 4	-1.7	8.7E-12	2.6E-09

TNFRSF11B	tumor necrosis factor receptor superfamily member 11b	-1.9	8.9E-08	1.4E-06
TNFRSF14	tumor necrosis factor receptor superfamily member 14	1.7	1.0E-08	2.7E-07
TNFSF9	tumor necrosis factor superfamily member 9	-1.5	1.5E-07	2.0E-06
TNXB	tenascin XB	2.6	2.8E-10	2.2E-08
TP53I11	tumor protein p53 inducible protein 11	2.5	1.0E-08	2.7E-07
TPTE	transmembrane phosphatase with tensin homology	-2.1	2.4E-08	5.1E-07
TSPEAR	thrombospondin type laminin G domain and EAR repeats	1.9	3.8E-08	7.2E-07
TSPOAP1	TSPO associated protein 1	1.7	4.7E-07	4.9E-06
TTC3P1	tetratricopeptide repeat domain 3 pseudogene 1	-1.8	9.6E-08	1.5E-06
TTC9	tetratricopeptide repeat domain 9	1.6	6.7E-07	6.5E-06
UBE2QL1	ubiquitin conjugating enzyme E2 Q family like 1	-2.4	1.3E-11	3.2E-09
UNC80	unc-80 homolog, NALCN activator	-3.6	3.0E-11	5.4E-09
VASH1	vasohibin 1	-1.6	2.8E-10	2.2E-08
VAV3	vav guanine nucleotide exchange factor 3	-1.6	2.5E-07	3.0E-06
VSTM2L	V-set and transmembrane domain containing 2 like	2.0	1.2E-08	3.1E-07
VWA5A	von Willebrand factor A domain containing 5A	-3.4	1.5E-10	1.6E-08
WDR72	WD repeat domain 72	-3.2	3.7E-11	6.2E-09
WNT2B	Wnt family member 2B	-1.5	2.1E-06	1.7E-05
YPEL2	yippee like 2	-1.5	1.7E-07	2.3E-06
ZFPM2	zinc finger protein, FOG family member 2	-3.8	5.1E-12	1.9E-09
ZG16B	zymogen granule protein 16B	1.6	8.2E-08	1.3E-06
ZNF334	zinc finger protein 334	3.1	4.5E-09	1.5E-07
ZNF415	zinc finger protein 415	2.5	2.0E-10	1.8E-08
ZNF43	zinc finger protein 43	2.0	2.5E-07	3.0E-06
ZNF467	zinc finger protein 467	3.5	1.7E-10	1.6E-08
ZNF470	zinc finger protein 470	2.5	5.3E-09	1.7E-07
ZNF521	zinc finger protein 521	-1.5	7.8E-07	7.3E-06
ZNF585B	zinc finger protein 585B	-2.3	2.9E-08	5.9E-07
ZNF607	zinc finger protein 607	2.4	3.0E-09	1.1E-07
ZNF702P	zinc finger protein 702, pseudogene	2.2	3.2E-09	1.2E-07
ZNF818P	zinc finger protein 818, pseudogene	2.0	1.5E-07	2.0E-06
ZNF85	zinc finger protein 85	3.9	1.6E-11	3.5E-09

Supplementary Table S4. Enrichment for GO terms in the category 'biological process' for genes upregulated in PC3-GHSROS cells (compared to empty-vector control). $P \leq 0.01$, Fisher's exact test.

GO term	Description	Count	%	Genes	Fold Enrichment	Fisher Exact P-value
GO:0010669	epithelial structure maintenance	4	2.6	*MUC2, RBP4, MUC3A, TFF1*	70	1.1E-07
GO:0030277	maintenance of gastrointestinal epithelium	4	2.6	*MUC2, RBP4, MUC3A, TFF1*	70	1.1E-07
GO:0070482	response to oxygen levels	9	5.9	*PLAT, CAV1, CA9, PDGFA, OXTR, CD24, THBS1, SOD3, ANGPTL4*	7	7.5E-06
GO:0009725	response to hormone stimulus	13	8.5	*RBP4, CAV1, PTGS2, PDGFA, FBP1, OXTR, NPY1R, ABCG1, CA9, PCSK9, CD24, TFF1, THBS1*	4	4.4E-05
GO:0001666	response to hypoxia	8	5.2	*PLAT, CAV1, CA9, PDGFA, CD24, THBS1, SOD3, ANGPTL4*	6	4.0E-05
GO:0022600	digestive system process	5	3.3	*MUC2, RBP4, MUC3A, OXTR, TFF1*	16	1.6E-05
GO:0009719	response to endogenous stimulus	13	8.5	*RBP4, CAV1, PTGS2, PDGFA, FBP1, OXTR, NPY1R, ABCG1, CA9, PCSK9, CD24, TFF1, THBS1*	3	1.2E-04
GO:0048545	response to steroid hormone stimulus	9	5.9	*CAV1, PTGS2, CA9, PDGFA, OXTR, TFF1, NPY1R, CD24, THBS1*	5	8.6E-05
GO:0043627	response to estrogen stimulus	7	4.6		7	6.1E-05
GO:0008285	negative regulation of cell proliferation	12	7.8	*MUC2, RBP4, CAV1, TP53I11, IFITM1, PTGS2, IGFBP6, SCIN, TNFRSF14, CD24, THBS1, IGFBP5*	4	1.6E-04
GO:0051241	negative regulation of multicellular organismal process	8	5.2	*RBP4, CAV1, ACHE, PTGS2, PDGFA, PCSK9, CD24, THBS1*	5	1.6E-04
GO:0042493	response to drug	9	5.9	*CAV1, PTGS2, CA9, PDGFA, LCK, OXTR, CDH1, CDH3, SLC47A1*	4	2.1E-04
GO:0032355	response to estradiol stimulus	5	3.3	*PTGS2, PDGFA, OXTR, TFF1, NPY1R*	10	1.5E-04
GO:0007586	digestion	6	3.9	*MUC2, RBP4, MUC3A, TFF2, OXTR, TFF1*	7	2.2E-04
GO:0042127	regulation of cell proliferation	17	11.1	*MUC2, RBP4, CAV1, PTGER2, TP53I11, PTGS2, IFITM1, CXCL5, PDGFA, CRIP2, IGFBP6, TNFRSF14, STAT6, SCIN, CD24, THBS1, IGFBP5*	2	1.2E-03

GO:0010033	response to organic substance	16	10.5	*RBP4, CAV1, PTGS2, PDGFA, FBP1, OXTR, CDH1, NPY1R, ABCG1, STAT6, CA9, PCSK9, CREB3L1, CD24, TFF1, THBS1*	2	1.3E-03
GO:0031644	regulation of neurological system process	7	4.6	*PLAT, ACHE, S100P, PTGS2, GRIN2D, OXTR, CALB1*	5	6.2E-04
GO:0050730	regulation of peptidyl-tyrosine phosphorylation	5	3.3	*CAV1, PDGFA, TNFRSF14, ITGB2, CD24*	8	4.5E-04
GO:0007267	cell-cell signaling	14	9.2	*PLAT, GUCA1B, ACHE, CXCL5, PDGFA, OXTR, ITGB2, NTSR1, GRIN2D, GRID2, CEACAM6, SEMA3B, CD24, GDF15*	2	1.6E-03
GO:0042632	cholesterol homeostasis	4	2.6	*CAV1, PCSK9, CD24, ABCG1*	11	4.4E-04
GO:0055092	sterol homeostasis	4	2.6	*CAV1, PCSK9, CD24, ABCG1*	11	4.4E-04
GO:0007155	cell adhesion	15	9.8	*CLDN7, ACHE, CADM4, TNXB, ITGB4, ITGB2, CDH1, CDH3, PCDHGB2, COL5A1, JUP, CD24, ADAM8, THBS1, MUC5B*	2	2.5E-03
GO:0022610	biological adhesion	15	9.8	*CLDN7, ACHE, CADM4, TNXB, ITGB4, ITGB2, CDH1, CDH3, PCDHGB2, COL5A1, JUP, CD24, ADAM8, THBS1, MUC5B*	2	2.6E-03
GO:0045907	positive regulation of vasoconstriction	3	2.0	*CAV1, PTGS2, NPY1R*	24	2.2E-04
GO:0035249	synaptic transmission, glutamatergic	3	2.0	*PLAT, GRIN2D, GRID2*	23	2.8E-04
GO:0044057	regulation of system process	9	5.9	*PLAT, CAV1, ACHE, S100P, PTGS2, GRIN2D, OXTR, NPY1R, CALB1*	3	2.7E-03
GO:0048878	chemical homeostasis	12	7.8	*RBP4, CAV1, LCK, GRID2, PCSK9, OXTR, PLLP, NPY1R, CD24, ABCG1, TMPRSS3, CKB*	2	3.4E-03
GO:0050804	regulation of synaptic transmission	6	3.9	*PLAT, ACHE, S100P, PTGS2, OXTR, CALB1*	5	1.8E-03
GO:0042592	homeostatic process	15	9.8	*RBP4, MUC2, CAV1, OXTR, NPY1R, TMPRSS3, ABCG1, CKB, MUC3A, LCK, GRID2, PCSK9, PLLP, CD24, TFF1*	2	4.9E-03

GO:0055088	lipid homeostasis	4	2.6	*CAV1, PCSK9, CD24, ABCG1*	8	1.4E-03
GO:0051969	regulation of transmission of nerve impulse	6	3.9	*PLAT, ACHE, S100P, PTGS2, OXTR, CALB1*	4	2.7E-03
GO:0007610	behavior	11	7.2	*S100P, PTGS2, CXCL5, PDGFA, PPP1R1B, GRIN2D, OXTR, ITGB2, NPY1R, NTSR1, CALB1*	2	4.9E-03
GO:0032570	response to progesterone stimulus	3	2.0	*CAV1, OXTR, THBS1*	16	8.4E-04
GO:0016337	cell-cell adhesion	8	5.2	*JUP, CLDN7, CDH1, ITGB2, CD24, ADAM8, CDH3, PCDHGB2*	3	4.7E-03
GO:0032101	regulation of response to external stimulus	6	3.9	*CAV1, PTGS2, PDGFA, GRID2, CD24, THBS1*	4	4.0E-03
GO:0051050	positive regulation of transport	7	4.6	*RBP4, CAV1, ACHE, SCIN, PCSK9, OXTR, CDH1*	3	5.3E-03
GO:0001894	tissue homeostasis	4	2.6	*MUC2, RBP4, MUC3A, TFF1*	7	3.0E-03
GO:0048167	regulation of synaptic plasticity	4	2.6	*PLAT, S100P, PTGS2, CALB1*	7	3.1E-03
GO:0033273	response to vitamin	4	2.6	*RBP4, PTGS2, PDGFA, MEST*	6	3.5E-03
GO:0050865	regulation of cell activation	6	3.9	*STAT6, PDGFA, LCK, TNFRSF14, CD24, THBS1*	4	6.4E-03
GO:0006873	cellular ion homeostasis	9	5.9	*CAV1, LCK, GRID2, OXTR, PLLP, NPY1R, CD24, TMPRSS3, CKB*	3	9.1E-03
GO:0051480	cytosolic calcium ion homeostasis	5	3.3	*CAV1, LCK, OXTR, NPY1R, CD24*	4	5.2E-03
GO:0007618	mating	3	2.0	*PPP1R1B, PI3, OXTR*	12	2.0E-03
GO:0055082	cellular chemical homeostasis	9	5.9	*CAV1, LCK, GRID2, OXTR, PLLP, NPY1R, CD24, TMPRSS3, CKB*	3	1.0E-02
GO:0001568	blood vessel development	7	4.6	*PLAT, CAV1, PDGFA, CCBE1, THBS1, COL5A1, ANGPTL4*	3	8.7E-03
GO:0010648	negative regulation of cell communication	7	4.6	*CBLC, CAV1, ACHE, PTGS2, STMN3, THBS1, IGFBP5*	3	9.3E-03
GO:0008544	epidermis development	6	3.9	*PTGS2, PDGFA, PPL, CRABP2, GJB3, COL5A1*	3	8.1E-03
GO:0043588	skin development	3	2.0	*PDGFA, GJB3, COL5A1*	11	2.5E-03
GO:0001944	vasculature development	7	4.6	*PLAT, CAV1, PDGFA, CCBE1, THBS1, COL5A1, ANGPTL4*	3	9.9E-03
GO:0010038	response to metal ion	5	3.3	*CAV1, PTGS2, TFF1, THBS1, SOD3*	4	7.6E-03
GO:0007270	nerve-nerve synaptic transmission	3	2.0	*PLAT, GRIN2D, GRID2*	10	3.1E-03

GO:0006875	cellular metal ion homeostasis	6	3.9	*CAV1, LCK, OXTR, NPY1R, CD24, TMPRSS3*	3	1.1E-02
GO:0044092	negative regulation of molecular function	8	5.2	*CBLC, CAV1, GNAI1, HR, PCSK9, NPY1R, NPR3, ANGPTL4*	3	1.4E-02
GO:0031667	response to nutrient levels	6	3.9	*RBP4, CAV1, PTGS2, PDGFA, PCSK9, MEST*	3	1.1E-02
GO:0032526	response to retinoic acid	3	2.0	*RBP4, PDGFA, MEST*	10	3.7E-03

Supplementary Table S5. Enrichment for GO terms in the category 'biological process' for genes downregulated in PC3-GHSROS cells (compared to empty-vector control). $P \leq 0.01$, Fisher's exact test.

GO term	Description	Count	%	Genes	Fold Enrichment	Fisher Exact *P*-value
GO:0007155	cell adhesion	22	1.1	*MTSS1, COL21A1, ADAM23, NRXN3, LRRN2, NELL2, NLGN1, NFASC, LEF1, NEO1, MMRN1, CXADR, PCDH19, CDH12, LAMA1, SRPX, LAMC3, CD33, TGFBI, CNTN1, FCGBP, CXADRP2, EDA*	3	5.8E-06
GO:0022610	biological adhesion	22	1.1	*MTSS1, COL21A1, ADAM23, NRXN3, LRRN2, NELL2, NLGN1, NFASC, LEF1, NEO1, MMRN1, CXADR, PCDH19, CDH12, LAMA1, SRPX, LAMC3, CD33, TGFBI, CNTN1, FCGBP, CXADRP2, EDA*	3	6.0E-06
GO:0007267	cell-cell signaling	16	0.8	*AR, NRXN3, S100A9, NLGN1, CD70, FGF13, GAL, TNFSF9, SLC1A3, KCNN3, HTR7, CD33, DMD, TMOD2, STC1, PCSK5*	2	7.6E-04
GO:0000904	cell morphogenesis involved in differentiation	9	0.4	*NOG, SLITRK4, SLC1A3, NRXN3, KIF5C, NFASC, EOMES, LEF1, EPHB2*	3	1.3E-03
GO:0000902	cell morphogenesis	11	0.5	*LAMA1, NOG, SLITRK4, SLC1A3, NRXN3, DMD, KIF5C, NFASC, EOMES, LEF1, EPHB2*	3	1.7E-03
GO:0001655	urogenital system development	6	0.3	*AGTR1, EYA1, AR, NOG, LEF1, PCSK5*	5	1.2E-03
GO:0043009	chordate embryonic development	10	0.5	*EYA1, AR, NOG, CHD7, ARNT2,*	3	3.2E-03

				EOMES, LEF1, AMOT, ZFPM2, PCSK5		
GO:0009792	embryonic development ending in birth or egg hatching	10	0.5	*EYA1, AR, NOG, CHD7, ARNT2, EOMES, LEF1, AMOT, ZFPM2, PCSK5*	3	3.4E-03
GO:0032989	cellular component morphogenesis	11	0.5	*LAMA1, NOG, SLITRK4, SLC1A3, NRXN3, DMD, KIF5C, NFASC, EOMES, LEF1, EPHB2*	3	3.8E-03
GO:0030509	BMP signaling pathway	4	0.2	*MSX2, NOG, CHRDL1, BMP6*	8	1.3E-03
GO:0006928	cell motion	12	0.6	*LAMA1, MTSS1, VAV3, NRXN3, KIF5C, S100A9, NFASC, AMOT, POU3F2, DNAH5, EPHB2, ARHGDIB*	2	5.4E-03
GO:0003013	circulatory system process	7	0.3	*AGTR1, CHD7, HTR7, RYR2, AMOT, KCNJ12, PCSK5*	3	4.0E-03
GO:0008015	blood circulation	7	0.3	*AGTR1, CHD7, HTR7, RYR2, AMOT, KCNJ12, PCSK5*	3	4.0E-03
GO:0048732	gland development	6	0.3	*EYA1, AR, NOG, LEF1, POU3F2, EDA*	4	3.4E-03
GO:0001837	epithelial to mesenchymal transition	3	0.1	*NOG, EOMES, LEF1*	15	8.9E-04
GO:0021545	cranial nerve development	3	0.1	*SLC1A3, CHD7, EPHB2*	15	1.1E-03
GO:0030182	neuron differentiation	11	0.5	*SLITRK4, SLC1A3, MCOLN3, NRXN3, DGKG, DMD, KIF5C, MAP2, NFASC, POU3F2, EPHB2*	2	7.9E-03
GO:0001822	kidney development	5	0.2	*AGTR1, EYA1, NOG, LEF1, PCSK5*	5	3.8E-03
GO:0001501	skeletal system development	9	0.4	*MSX2, EYA1, TNFRSF11B, NOG, CHD7, CHRDL1, STC1, PCSK5, BMP6*	3	7.8E-03
GO:0035108	limb morphogenesis	5	0.2	*MSX2, NOG, CHD7, LEF1, PCSK5*	5	4.3E-03
GO:0035107	appendage morphogenesis	5	0.2	*MSX2, NOG, CHD7, LEF1, PCSK5*	5	4.3E-03

GO:0048736	appendage development	5	0.2	*MSX2*, *NOG*, *CHD7*, *LEF1*, *PCSK5*	4	5.1E-03
GO:0060173	limb development	5	0.2	*MSX2*, *NOG*, *CHD7*, *LEF1*, *PCSK5*	4	5.1E-03
GO:0043627	response to estrogen stimulus	5	0.2	*TNFRSF11B*, *ARNT2*, *ANGPT1*, *SERPINA1*, *GAL*	4	5.6E-03
GO:0021675	nerve development	3	0.1	*SLC1A3*, *CHD7*, *EPHB2*	11	2.4E-03

Supplementary Table S6. Oncomine concepts analysis of positively and negatively correlated PC3-*GHSROS* gene signature. Red: positively correlated gene signature; Black: negatively correlated gene signature. $P \leq 0.01$, Fisher's exact test.

Concept 1 ID	Concept 1 Name	Concept 2 ID	Concept 2 Name	P-value	Odds Ratio	Overlap Size
C41610	PC3 GHSROS downregulated gene list	17697	Cancer Type: Prostate Cancer - Top 10% Over-expressed (Bittner Multi-cancer)	2.17E-08	3.7	32
C41610	PC3 GHSROS downregulated gene list	122189617	Prostate Cancer - Metastasis - Top 10% Under-expressed (Taylor Prostate 3)	3.14E-06	3.1	28
C41610	PC3 GHSROS downregulated gene list	122210891	Cancer Type: Prostate Cancer - Top 5% Under-expressed (Garnett CellLine)	3.94E-06	4.5	16
C41610	PC3 GHSROS downregulated gene list	122208916	Cancer Type: Prostate Cancer - Top 5% Under-expressed (Barretina CellLine)	3.55E-05	3.5	17
C41610	PC3 GHSROS downregulated gene list	122213069	Prostate Cancer - Metastasis - Top 5% Under-expressed (Grasso Prostate)	9.84E-05	3.3	16
C41610	PC3 GHSROS downregulated gene list	28483	Prostate Cancer - Metastasis - Top 5% Under-expressed (Varambally Prostate)	4.13E-04	3	15
C41610	PC3 GHSROS downregulated gene list	23100	Prostate Cancer - Metastasis - Top 10% Under-expressed (LaTulippe Prostate)	4.20E-04	3	16
C41610	PC3 GHSROS downregulated gene list	28344	Prostate Cancer - Metastasis - Top 10% Under-expressed (Vanaja Prostate)	0.001	2.3	21
17697	Cancer Type: Prostate Cancer - Top 10% Over-expressed (Bittner Multi-cancer)	122189617	Prostate Cancer - Metastasis - Top 10% Under-expressed (Taylor Prostate 3)	1.55E-120	4.2	559
17697	Cancer Type: Prostate Cancer - Top 10% Over-expressed (Bittner Multi-cancer)	122213069	Prostate Cancer - Metastasis - Top 5% Under-expressed (Grasso Prostate)	1.33E-120	6.4	356
17697	Cancer Type: Prostate Cancer - Top 10% Over-expressed (Bittner Multi-cancer)	28483	Prostate Cancer - Metastasis - Top 5% Under-expressed (Varambally Prostate)	3.67E-134	6.8	377
17697	Cancer Type: Prostate Cancer - Top 10% Over-expressed (Bittner Multi-cancer)	23100	Prostate Cancer - Metastasis - Top 10% Under-expressed (LaTulippe Prostate)	1.22E-54	4.1	250
17697	Cancer Type: Prostate Cancer - Top 10% Over-expressed (Bittner Multi-cancer)	28344	Prostate Cancer - Metastasis - Top 10% Under-expressed (Vanaja Prostate)	3.10E-189	6.1	619
122189617	Prostate Cancer - Metastasis - Top 10% Under-expressed (Taylor Prostate 3)	122210891	Cancer Type: Prostate Cancer - Top 5% Under-expressed (Garnett CellLine)	1.63E-12	2.1	143

122189617	Prostate Cancer - Metastasis - Top 10% Under-expressed (Taylor Prostate 3)	122208916	Cancer Type: Prostate Cancer - Top 5% Under-expressed (Barretina CellLine)	1.94E-26	2.5	218
122189617	Prostate Cancer - Metastasis - Top 10% Under-expressed (Taylor Prostate 3)	122213069	Prostate Cancer - Metastasis - Top 5% Under-expressed (Grasso Prostate)	6.85E-300	15.4	554
122189617	Prostate Cancer - Metastasis - Top 10% Under-expressed (Taylor Prostate 3)	28483	Prostate Cancer - Metastasis - Top 5% Under-expressed (Varambally Prostate)	1.26E-181	8.7	446
122189617	Prostate Cancer - Metastasis - Top 10% Under-expressed (Taylor Prostate 3)	23100	Prostate Cancer - Metastasis - Top 10% Under-expressed (LaTulippe Prostate)	7.69E-149	8.1	422
122189617	Prostate Cancer - Metastasis - Top 10% Under-expressed (Taylor Prostate 3)	28344	Prostate Cancer - Metastasis - Top 10% Under-expressed (Vanaja Prostate)	1.66E-141	4.8	574
122210891	Cancer Type: Prostate Cancer - Top 5% Under-expressed (Garnett CellLine)	122208916	Cancer Type: Prostate Cancer - Top 5% Under-expressed (Barretina CellLine)	6.57E-135	13.7	232
122210891	Cancer Type: Prostate Cancer - Top 5% Under-expressed (Garnett CellLine)	122213069	Prostate Cancer - Metastasis - Top 5% Under-expressed (Grasso Prostate)	4.37E-06	1.9	65
122210891	Cancer Type: Prostate Cancer - Top 5% Under-expressed (Garnett CellLine)	23100	Prostate Cancer - Metastasis - Top 10% Under-expressed (LaTulippe Prostate)	3.26E-04	1.6	73
122208916	Cancer Type: Prostate Cancer - Top 5% Under-expressed (Barretina CellLine)	122213069	Prostate Cancer - Metastasis - Top 5% Under-expressed (Grasso Prostate)	9.74E-20	2.9	118
122208916	Cancer Type: Prostate Cancer - Top 5% Under-expressed (Barretina CellLine)	28483	Prostate Cancer - Metastasis - Top 5% Under-expressed (Varambally Prostate)	1.44E-09	2.1	93
122208916	Cancer Type: Prostate Cancer - Top 5% Under-expressed (Barretina CellLine)	23100	Prostate Cancer - Metastasis - Top 10% Under-expressed (LaTulippe Prostate)	1.04E-05	1.7	87
122213069	Prostate Cancer - Metastasis - Top 5% Under-expressed (Grasso Prostate)	28483	Prostate Cancer - Metastasis - Top 5% Under-expressed (Varambally Prostate)	1.06E-199	14.8	332
122213069	Prostate Cancer - Metastasis - Top 5% Under-expressed (Grasso Prostate)	23100	Prostate Cancer - Metastasis - Top 10% Under-expressed (LaTulippe Prostate)	5.82E-85	7.7	221
122213069	Prostate Cancer - Metastasis - Top 5% Under-expressed (Grasso Prostate)	28344	Prostate Cancer - Metastasis - Top 10% Under-expressed (Vanaja Prostate)	1.21E-75	4.7	288
28483	Prostate Cancer - Metastasis - Top 5%	23100	Prostate Cancer - Metastasis - Top 10%	1.59E-59	5.7	192

	Under-expressed (Varambally Prostate)		Under-expressed (LaTulippe Prostate)			
28483	Prostate Cancer - Metastasis - Top 5% Under-expressed (Varambally Prostate)	28344	Prostate Cancer - Metastasis - Top 10% Under-expressed (Vanaja Prostate)	3.84E-80	4.7	302
23100	Prostate Cancer - Metastasis - Top 10% Under-expressed (LaTulippe Prostate)	28344	Prostate Cancer - Metastasis - Top 10% Under-expressed (Vanaja Prostate)	2.79E-54	4	258
C41610	PC3 GHSROS downregulated gene list	122199554	Prostate Carcinoma - Dead at 3 Years - Top 10% Under-expressed (Setlur Prostate)	0.003	2.9	12
C41610	PC3 GHSROS downregulated gene list	122189630	Prostate Carcinoma - Advanced Gleason Score - Top 5% Under-expressed (Taylor Prostate 3)	0.004	2.5	13
C41610	PC3 GHSROS downregulated gene list	122189606	Prostate Carcinoma - Recurrence at 5 Years - Top 5% Under-expressed (Taylor Prostate 3)	0.004	2.5	13
122199554	Prostate Carcinoma - Dead at 3 Years - Top 10% Under-expressed (Setlur Prostate)	122189630	Prostate Carcinoma - Advanced Gleason Score - Top 5% Under-expressed (Taylor Prostate 3)	3.07E-37	4.7	141
122199554	Prostate Carcinoma - Dead at 3 Years - Top 10% Under-expressed (Setlur Prostate)	122189606	Prostate Carcinoma - Recurrence at 5 Years - Top 5% Under-expressed (Taylor Prostate 3)	3.29E-24	3.4	130
122189630	Prostate Carcinoma - Advanced Gleason Score - Top 5% Under-expressed (Taylor Prostate 3)	122189606	Prostate Carcinoma - Recurrence at 5 Years - Top 5% Under-expressed (Taylor Prostate 3)	0.00E+00	26.5	493
C41601	PC3 GHSROS upregulated gene list_RNAseq	29459	Prostate Carcinoma vs. Normal - Top 1% Over-expressed (Yu Prostate)	4.78E-04	12.5	4
C41602	PC3 GHSROS upregulated gene list_RNAseq	122189633	Prostate Carcinoma - Advanced N Stage - Top 5% Over-expressed (Taylor Prostate 3)	0.002	3.5	9
C41603	PC3 GHSROS upregulated gene list_RNAseq	17807	Prostate Adenocarcinoma - Advanced Stage - Top 1% Over-expressed (Bittner Prostate)	0.003	7.5	4
C41604	PC3 GHSROS upregulated gene list_RNAseq	23091	Prostate Carcinoma vs. Normal - Top 10% Over-expressed (LaTulippe Prostate)	0.003	3.4	10
29459	Prostate Carcinoma vs. Normal - Top 1% Over-expressed (Yu Prostate)	17807	Prostate Adenocarcinoma - Advanced Stage - Top 1% Over-expressed (Bittner Prostate)	3.33E-04	7.2	6
29459	Prostate Carcinoma vs. Normal - Top 1% Over-expressed (Yu Prostate)	23091	Prostate Carcinoma vs. Normal - Top 10% Over-expressed (LaTulippe Prostate)	5.61E-07	3.8	25
122189633	Prostate Carcinoma - Advanced N Stage - Top 5% Over-	23091	Prostate Carcinoma vs. Normal - Top 10% Over-	3.73E-06	2	61

	expressed (Taylor Prostate 3)		expressed (LaTulippe Prostate)			
17807	Prostate Adenocarinoma - Advanced Stage - Top 1% Over-expressed (Bittner Prostate)	23091	Prostate Carcinoma vs. Normal - Top 10% Over-expressed (LaTulippe Prostate)	6.07E-04	2.5	20

Supplementary Table S7. Differentially expressed genes in PC3-GHSROS and LNCaP-GHSROS cells compared to the Grasso Oncomine dataset. The Grasso dataset includes 59 localized and 35 metastatic prostate tumors. Red: higher expression in metastatic tumors; Black: lower expression in metastatic tumors. Fold-changes are $\log_2$ transformed; *Q*-value denotes the false discovery rate (FDR; Benjamini-Hochberg)-adjusted *P*-value.

Gene Symbol	**Gene Name**	**Reporter ID**	**Fold Change**	***P*-value**	***Q*-value**
AASS	aminoadipate-semialdehyde synthase	A_23_P8754	-1.5	6.0E-03	2.5E-02
CHRDL1	chordin-like 1	A_24_P168925	-48.0	3.6E-21	2.9E-18
CNTN1	contactin 1	A_23_P204541	-19.3	1.6E-16	3.4E-14
DIRAS1	DIRAS family, GTP-binding RAS-like 1	A_23_P386942	2.2	3.5E-07	4.4E-06
FBXL16	F-box and leucine-rich repeat protein 16	A_23_P406385	6.0	2.5E-08	4.7E-07
IFI16	interferon, gamma-inducible protein 16	A_23_P160025	-2.2	1.1E-05	8.8E-05
MUM1L1	melanoma associated antigen (mutated) 1-like 1	A_23_P73571	-8.8	7.9E-11	2.5E-09
TFF2	trefoil factor 2	A_23_P57364	1.3	6.4E-04	3.1E-03
TP53I11	tumor protein p53 inducible protein 11	A_23_P150281	1.5	4.8E-05	3.1E-04
ZNF467	zinc finger protein 467	A_23_P59470	3.5	5.4E-07	6.3E-06

Supplementary Table S8. Differentially expressed genes in PC3-GHSROS and LNCaP-GHSROS cells compared to the Taylor Oncomine dataset. The Taylor dataset includes 123 localized and 35 metastatic prostate tumors. Red: higher expression in metastatic tumors; Black: lower expression in metastatic tumors. Fold-changes are $\log_2$ transformed; *Q*-value denotes the false discovery rate (FDR; Benjamini-Hochberg)-adjusted *P*-value.

Gene Symbol	**Gene Name**	**Reported ID**	**Fold Change**	***P*-value**	***Q*-value**
AASS	aminoadipate-semialdehyde synthase	10093	-1.5	3.9E-05	1.7E-03
CHRDL1	chordin-like 1	20828	-5.0	1.6E-18	1.3E-15
CNTN1	contactin 1	6403	-3.5	4.2E-22	6.8E-19
DIRAS1	DIRAS family, GTP-binding RAS-like 1	20799	1.1	1.2E-02	1.4E-01
FBXL16	F-box and leucine-rich repeat protein 16	21824	1.1	8.0E-03	1.2E-01
IFI16	interferon, gamma-inducible protein 16	9878	-1.5	8.4E-05	3.3E-03
MUM1L1	melanoma associated antigen (mutated) 1-like 1	21313	-1.3	1.0E-02	1.3E-01
TFF2	trefoil factor 2	9774	1.1	3.6E-02	2.4E-01
TP53I11	tumor protein p53 inducible protein 11	4038	1.1	2.2E-02	1.9E-01
ZNF467	zinc finger protein 467	25037	1.3	2.8E-04	1.7E-02

Supplementary Table S9. Disease-free survival (DFS) analysis of differentially expressed genes (in PC3-GHSROS cells, LNCaP-GHSROS cells and clinical metastatic tumors) in human datasets. Patients, in the Taylor (*N*=150; *n*=123 localized and *n*=27 metastatic tumors) and TCGA-PRAD (*N*=489; localized tumors) datasets, were stratified into two groups by *k*-means clustering of gene expression (*k*=2). The log-rank test, was used to assign statistical significance, with $P \leq 0.05$ considered significant (shown in bold). The Cox *P*-value and absolute hazard ratio (HR) between *k*-means cluster 1 and 2 for each gene are indicated. Overall median disease-free survival (DFS) in days are indicated for each cluster.

	Taylor (*N*=150)					**TCGA-PRAD (*N*=489)**				
gene	**log-rank *P***	**Cox *P***	**Absolute HR**	**Overall median DFS cluster 1**	**Overall median DFS cluster 2**	**log-rank *P***	**Cox *P***	**Absolute HR**	**Overall median DFS cluster 1**	**Overall median DFS cluster 2**
ZNF467	**0.0027**	**0.0039**	2.7	174	871	**0.000050**	**0.000026**	2.5	546	685
CHRDL1	**0.0047**	**0.0062**	2.5	840	402	**0.0079**	**0.0071**	1.8	649	640
FBXL16	**0.017**	**0.020**	2.2	300	871	0.089	0.087	1.5	627	663
DIRAS1	0.09	0.099	1.7	709	329	**0.012**	**0.011**	1.7	425	723
TFF2	0.11	0.11	1.7	840	125	0.84	0.089	1.1	648	896
CNTN1	0.13	0.14	1.6	701	457	0.10	0.094	1.4	627	691
IFI16	0.27	0.28	1.5	579	181	0.95	0.95	1.0	671	648
AASS	0.62	0.63	1.2	843	348	0.35	0.35	1.2	552	697
MUM1L1	0.78	0.78	1.1	472	676	0.14	0.14	1.4	765	426
TP53I11	0.98	0.98	1.0	122	843	0.57	0.57	1.1	533	751

Supplementary Table S10. Overview of human Affymetrix exon array datasets interrogated.

resource	unique ID	tissue/cell type	type	N	reference
ArrayExpress	E-MEXP-2644	lung (18 benign and 18 cancer)	tissues	36	[68]
ArrayExpress	E-MEXP-3931	THP1 (acute monocytic leukemia)	cell lines	12	[69]
ArrayExpress	E-MTAB-1273	induced pluripotent stem (iPS) cells derived from glioblastoma-derived neural stem cells	primary cells	16	[70]
ArrayExpress	E-MTAB-2471	large B-cell lymphoma	tissues	16	[71]
Affymetrix web site	goo.gl/rBWrFv	breast, cerebellum, heart, kidney, liver, muscle, pancreas, prostate, spleen, testes, thyroid, mixture	tissues	53	-
Affymetrix web site	goo.gl/Yack5K	colon cancer (10 benign and 10 cancer)	tissues	20	-
GEO	GSE11967	thymus (4 benign and 4 cancer)	tissues	8	[72]
GEO	GSE16732	breast (cancer)	cell lines	41	[73]
GEO	GSE18927	NIH Epigenomics Roadmap Initiative (stem cells and primary *ex vivo* tissues)	tissues and primary cells	99	[74,75,76,77,78,79]
GEO	GSE19090	ENCODE Project Consortium (84 cell lines and primary cells)	cell lines and primary cells	182	[80, 81]
GEO	GSE19891	HeLa (cervical cancer)	cell lines	15	[82]
GEO	GSE20342	MCF7 (breast cancer)	cell lines	32	[83]
GEO	GSE20567	HL60, THP-1, U937 (myeloid leukemia)	cell lines	17	[84]
GEO	GSE21034	prostate (cancer)	tissues	310	[36]
GEO	GSE21163	pancreas (1 benign and 6 cancer)	cell lines	22	[85, 86]
GEO	GSE21337	acute myeloid leukemia	tissues	64	[87]
GEO	GSE21840	MCF7 (breast cancer)	cell lines	6	[87, 89]
GEO	GSE23361	lung (cancer)	tissues	12	[90]
GEO	GSE23514	HeLa S3 (cervical cancer)	cell lines	12	[91]
GEO	GSE23768	breast, lung, ovarian and prostate cancer	tissues	153	[92]
GEO	GSE24778	K562 (chronic myelogenous leukemia)	cell lines	10	[93]
GEO	GSE29682	breast, central nervous system, colon, leukemia, melanoma, lung, ovary, prostate, kidney (cancer)	cell lines	178	[94, 95]
GEO	GSE29778	HEK293 (embryonic kidney)	cell lines	12	[96]
GEO	GSE30472	brain (cancer; glioma)	tissues	55	[97]
GEO	GSE30521	prostate (benign and cancer)	tissues	23	[98]
GEO	GSE30727	stomach (cancer)	tissues	60	[99]
GEO	GSE32875	LNCaP (prostate cancer)	cell lines	8	[100]
GEO	GSE37138	lung (cancer)	tissues	117	[101]
GEO	GSE40871	acute myeloid leukemia	primary cells	67	[102]
GEO	GSE43107	brain (cancer; glioma)	tissues	95	[103, 104]
GEO	GSE43754	bone marrow stem and progenitor cells (chronic myeloid leukemia)	cells	20	[105]
GEO	GSE43830	WI38 (fetal lung fibroblasts)	cell lines	6	[106]
GEO	GSE45379	HeLa (cervical cancer)	cell lines	6	-
GEO	GSE46691	prostate (cancer)	tissues	545	[107, 108]

GEO	GSE47032	kidney (cancer)	tissues	40	[109]
GEO	GSE53405	MCF10A (benign)	cell lines	26	-
GEO	GSE57076	THP1 (acute monocytic leukemia)	cell lines	7	[110]
GEO	GSE57933	bladder (cancer)	tissues	199	[111]
GEO	GSE58598	breast (cancer)	tissues	10	-
GEO	GSE62116	prostate (cancer)	tissues	235	[112, 113, 114]
GEO	GSE62667	prostate (cancer)	tissues	182	[114, 115]
GEO	GSE67312	bladder (cancer)	primary xenografts	10	[116]
GEO	GSE68591	sarcoma (84 cancer) and 5 benign	cell lines	75	[117]
GEO	GSE71010	neutrophils (cystic fibrosis and healthy controls)	cells	93	[118]
GEO	GSE72291	prostate (cancer)	tissues	139	[114]
GEO	GSE78246	brain (schizophrenia, bipolar disorder, major depressive disorder, and controls)	tissues	20	[119]
GEO	GSE79956	prostate (cancer)	tissues	211	-
GEO	GSE79957	prostate (cancer)	tissues	260	-
GEO	GSE80683	prostate (cancer)	tissues	17	-
GEO	GSE9342	T-cell acute lymphoblastic leukaemia	cell lines	17	-
GEO	GSE9385	brain (26 glioblastomas, 22 oligodendrogliomas and 6 control brain samples)	tissues	55	[120]

Supplementary Table S11. Primers used in this study.

Primer	Gene name	Primer sequence (5'-3')
GHSROS	growth hormone secretagogue receptor opposite strand	ACATTCAGCAAATCCAGTTAATGACA
		CGACTGGAGCACGAGGACACTTGA
GHSROS-RT linker		CGACTGGAGCACGAGGACACTGACAACAGAATTCACTACTTCCCCAAA
AR	androgen receptor	CTGGACACGACAACAACCAG
		CAGATCAGGGGCGAAGTAGA
NTSR1	neurotensin receptor 1 (high affinity)	Proprietary – QIAGEN QuantiTect Primer Assay QT00018494
TFF1	trefoil factor 1	Proprietary - QIAGEN QuantiTect Primer Assay QT00209608
TFF2	trefoil factor 2	Proprietary - QIAGEN QuantiTect Primer Assay QT00001785
MUC5B	mucin 5B, oligomeric mucus/ gel-forming	Proprietary - QIAGEN QuantiTect Primer Assay QT01322818
PPP2R2C	protein phosphatase 2, regulatory subunit B, gamma	Proprietary - QIAGEN QuantiTect Primer Assay QT01006383
RPL32	ribosomal protein L32 (housekeeping gene)	CCCCTTGTGAAGCCCAAGA
		GACTGGTGCCGGATGAACTT
ACTB	actin beta (housekeeping gene)	ACTCTTCCAGCCTTCCTTCCT
		CAGTGATCTCCTTCTGCATCCT
GAPDH	glyceraldehyde-3-phosphate dehydrogenase (housekeeping gene)	AATCCCATCACCATCTTCCA
		AAATGAGCCCCAGCCTTC
HPRT	hypoxanthine phosphoribosyltransferase 1 (housekeeping gene)	CAGTCAACGGGGGACATAAA
		AGAGGTCCTTTTCACCAGCAA

Supplementary Dataset 1. Differentially expressed genes in LNCaP-GHSROS cells. Compared to empty vector control. Red: higher expression in LNCaP-GHSROS cells; Black: lower expression in LNCaP-GHSROS cells. Fold-changes are $\log_2$ transformed; *Q*-value denotes the false discovery rate (FDR; Benjamini-Hochberg)-adjusted *P*-value (cutoff ≤ 0.05).

(provided in a separate file).

Supplementary Dataset 2. Enrichment for GO terms in the category 'biological process' for genes upregulated in LNCaP-GHSROS cells (compared to empty-vector control). $P \leq 0.01$, Fisher's exact test.

(provided in a separate file).

Supplementary Dataset 3. Enrichment for GO terms in the category 'biological process' for genes downregulated in LNCaP-GHSROS cells (compared to empty-vector control). $P \leq 0.01$, Fisher's exact test.

(provided in a separate file).

SUPPLEMENTARY METHODS

Identification of *GHSROS* transcription in exon array datasets

To assess *GHSROS* expression, we interrogated Affymetrix GeneChip Exon 1.0 ST arrays, strand-specific oligonucleotide microarrays with probes for known and predicted exons (hereafter termed exon arrays). Exon arrays are comparable to RNA-seq in experiments aimed at assessing exon expression (*i.e.* gene isoforms) and suitable for experiments where the exon of interest is known[121, 122]. In the Exon 1.0 ST array, known (genes and ESTs) and putative exons are combined to form 'transcript clusters', with each exon defined as a probe set (typically, a set of 2-4 probes). By combining all probe sets, the expression of a transcript cluster (known or putative gene) can be measured (see https://goo.gl/4RSTG3). To identify probe set(s) corresponding to *GHSROS*, we downloaded the Exon 1.0 ST probe annotation file from NCBI (NCBI Gene Expression Omnibus (GEO) accession no. GPL5188). Full-length *GHSROS* (1.1 kb) was aligned to the human genome (NCBI36/hg18; March 2006 assembly) to generate genomic coordinates compatible with the probe file (chr3:173,646,439-173,647,538). Next, the probe annotation file (GPL5188) was interrogated to reveal probe sets spanning *GHSROS* by entering the following command in a UNIX terminal window:

```
sed 's/#.*//' GPL5188.txt | awk -F " " '{print $2}' $1 | grep $(echo
"chr3:173646846-173647446" | perl -ne 'print if /\bchr3\:173646[0-
9][0-9][0-9]-173647[0-9][0-9][0-9]/' $1) GPL5188.txt
```

This revealed a probe set, 2652604, consisting of 4 probes complementary to *GHSROS*.

Cell and tissue exon array data were downloaded from NCBI GEO[123], EBI ArrayExpress[124] and the Affymetrix web site (see Supplementary Table S10). GEO datasets were bulk-downloaded using v3.6.2.117442 of the Aspera Connect Linux software (Aspera, Emeryville, CA, USA). In total, 3,924 samples were downloaded, corresponding to ~46% of all exon array data deposited in the NCBI GEO database. Arrays (individual CEL files) were normalized (output on a $\log_2$ scale, centered at 0) using the *SCAN* function in the R package 'SCAN.UPC'[125, 126]. SCAN normalizes each array (sample) individually by removing background noise (probe- and array-specific) data from within the array. Next, arrays were interrogated using the *UPC* function in 'SCAN.UPC'. UPC outputs standardized expression values (UPC value), ranging from 0 to 1, which indicate whether a gene is actively transcribed in a sample of interest: higher values indicate that a gene is 'active'[126]. UPC scores are platform-independent and allow cross-experimental and cross-platform integration.

Evaluation of *GHSR/GHSROS* transcription in deep RNA-seq dataset

It has been estimated that reliable detection of low abundance transcripts in humans warrants very deep sequencing (> 200 million reads per sample[127]) – far beyond most current datasets. To illustrate, we considered the expression of *GHSR*/*GHSROS* in a comparable clinical dataset. Publicly available RNA-seq data (NCBI GEO accession no. GSE31528) from eight subjects with metastatic castration-resistant prostate cancer (bone marrow metastases)[128] were interrogated. Briefly, total RNA-seq was performed on random-primed paired end read libraries, to ensure consistent transcript coverage[128, 129], generating an average of 160M reads per sample. Paired-end FASTQ files were aligned to the human genome (UCSC build hg19) using the spliced-read mapper TopHat

(v2.0.9)[130] and reference gene annotations to guide the alignment. BigWig sequencing tracks for the UCSC genome browser[131, 132] were obtained from TopHat-generated BAM files (indexed by samtools v1.2[133]) using a local instance of the *bamCoverage* command in deepTools v2.5.4[134]. BigWig files were visualized in the UCSC genome browser (hg19). A region with less than ~10 supporting reads can be considered to have low coverage, rendering active transcription difficult to interpret[127, 135].

Cell culture, prostate cancer patient derived xenograft (PDX) models, and treatments

The cancer cell lines PC3 (ATCC CRL-1435), DU145 (ATCC HTB-81), LNCaP (ATCC CRL-1740), ES-2 (ATCC CRL-1978), A549 (ATCC CCL-185), and 22Rv1 (ATCC CRL-2505) were obtained from the American Type Culture Collection (ATCC, Rockville, MD, USA). The C4-2B[66] and DUCaP[67] prostate cancer cell lines, six LuCaP prostate derived xenograft (PDX) lines[17], and the BM18 PDX cell line[18] were available in our laboratory. All prostate cancer and ovarian cancer cell lines were maintained in Roswell Park Memorial Institute (RPMI) 1640 medium (RPMI-1640; Invitrogen, Carlsbad, CA) with 10 % Fetal Calf Serum (FCS, Thermo Fisher Scientific Australia, Scoresby, VIC, Australia), supplemented with 100 U/mL penicillin G and 100 ng/mL streptomycin (Invitrogen). The A549 lung cancer cell line was maintained in Dulbecco's Modified Eagle Medium: Nutrient Mixture F-12 (DMEM/F12) medium (Invitrogen) with 10% FCS (Thermo Fisher Scientific Australia) supplemented with 100 U/mL penicillin G and 100 ng/mL streptomycin (Invitrogen). The non-tumorigenic RWPE-1 (ATCC CRL-11609) and the transformed, tumorigenic RWPE-2 (ATCC CRL-11610) prostate epithelium-derived cell lines were cultured in keratinocyte serum-free medium (Invitrogen) supplemented with 50 µg/mL bovine pituitary extract and 5 ng/mL epidermal growth factor (Invitrogen). All cell lines were passaged at 2- to 3-day intervals on reaching 70 % confluency using TrypLE Select (Invitrogen). Cell morphology and viability were monitored by microscopic observation and regular Mycoplasma testing was performed (Universal Mycoplasma Detection Kit, ATCC). For drug treatments, cells were treated with 10 µM enzalutamide (ENZ; Selleck Chemicals, Houston, TX, USA) or 10-100 nM docetaxel (DTX; Sigma Aldrich, St. Louis, MO, USA) for 96 (functional assays) or 48 hours (qRT-PCR) and compared to dimethyl sulfoxide (DMSO) (Sigma Aldrich, St. Louis, MO, USA) vehicle control.

Production of *GHSROS* overexpressing cancer cell lines

Full-length *GHSROS* transcript was cloned into the *pTargeT* mammalian expression vector (Promega, Madison, WI). PC3, DU145, and A549 cell lines were transfected with *GHSROS-pTargeT* DNA, or vector alone (empty vector), (using Lipofectamine LTX, Invitrogen) according to the manufacturer's instructions. Cells were incubated for 24 hours in LTX and selected with geneticin (100-1500 µg/mL G418, Invitrogen). As LNCaP prostate cancer cells were difficult to transfect using lipid-mediated transfection, we employed lentiviral transduction. Briefly, *pReceiver-Lv105* vectors, expressing full length *GHSROS*, or empty control vectors, were obtained from GeneCopoeia (Rockville, MD). For stable overexpression, LNCaP cells were seeded at 50-60% confluency and transduced with *GHSROS*, or empty vector control lentiviral constructs in the presence of 8 µg/ml polybrene (Sigma Aldrich). Following a 48-hour incubation period, transduced cells were selected with 1 µg/mL puromycin (Invitrogen). *GHSROS* expression was

confirmed approximately 3 weeks after selection by qRT-PCR, every 2-3 weeks, and before every functional experiment (see Supplementary Fig. S5).

RNA extraction, reverse transcription and quantitative reverse transcription Polymerase Chain Reaction (qRT-PCR)

Total RNA was extracted from cell pellets using an RNeasy Plus Mini Kit (QIAGEN, Hilden, Germany) with a genomic DNA (gDNA) Eliminator spin column. To remove contaminating genomic DNA, 1 µg RNA was DNase treated prior to cDNA synthesis with Superscript III (Invitrogen). qRT-PCR was performed using the AB7500 FAST sequence detection thermal cycler (Applied Biosystems, Foster City, CA), or the ViiA Real-Time PCR system (Applied Biosystems) with SYBR Green PCR Master Mix (QIAGEN) using primers listed in Supplementary Table S11. A negative control (water instead of template) was used in each real-time plate for each primer set. All real-time experiments were performed in triplicate. Baseline and threshold values (C_t) were obtained using ABI 7500 Prism and the relative expression of mRNA was calculated using the comparative $2^{-\Delta\Delta Ct}$ method[136]. Expression was normalized to the housekeeping gene ribosomal protein L32 (*RPL32*). Statistical analyses were performed using GraphPad Prism v.6.01 software (GraphPad Software, Inc., San Diego, CA). Student's *t*-test or Mann-Whitney-Wilcoxon tests were used to assess the statistical significance of all the direct comparisons.

***GHSROS* qRT-PCR interrogation of human tissue specimens**

To survey the expression of *GHSROS* in cancer, we initially interrogated a TissueScan Cancer Survey Tissue qPCR panel (CSRT102; OriGene, Rockville, MD, USA); cDNA arrayed on multi-well PCR plates. Some of the samples are normal non-malignant tissue samples, making it possible to compare expression in tumor versus normal tissue. For each cancer type, data were expressed as mean fold change using the comparative $2^{-\Delta\Delta Ct}$ method against a non-malignant control tissue. Normalized to β-actin (*ACTB*).

To further investigate the expression of *GHSROS* in prostate cancer TissueScan Prostate Cancer Tissue qPCR panels (HPRT101, HPRT102, and HPRT103) were obtained from OriGene. The cDNA panels contained of a total of 24 normal prostate-derived samples, 31 abnormal prostate samples (defined as lesions), and 88 prostate tumor samples. These panels were examined by qRT-PCR, using the method described above, except that the housekeeping gene ribosomal protein L32 (*RPL32*) was employed.

An independent cohort was obtained from the Andalusian Biobank (Servicio Andaluz de Salud, Spain). It consisted of tissue from 28 patients with clinical high-grade prostate cancer (10 localized and 18 metastatic tumors) and 8 normal prostate tissue samples. RT-PCR was performed using Brilliant III SYBR Green Master Mix and a Stratagene Mx3000p instrument (both from Agilent, La Jolla, CA, USA), as previously described[137]. Briefly, samples were on the same plate were analysed with a standard curve to estimate mRNA copy number (tenfold dilutions of synthetic cDNA template for each transcript). No-RNA controls were carried out for all primer pairs. To control for variations in the amount of RNA used, and the efficiency of the reverse-transcription reaction, the expression level (copy number) of each transcript was adjusted by a normalization factor

(NF) obtained from the expression of three housekeeping genes (*ACTB*, *HPRT*, and *GAPDH*) using the geNorm algorithm[138]. Primers used are listed in Supplementary Table S11.

Locked Nucleic Acid-Antisense Oligonucleotides (LNA-ASO)

Two distinct LNA ASOs, RNV104L and RNV124, complementary to different regions of *GHSROS* (see Supplementary Fig. S6), were designed in-house and synthesized commercially (Exiqon, Vedbæk, Denmark). The ASOs contained two consecutive LNA nucleotides at the 5'-end and three consecutive LNA nucleotides at the 3'-end – in line with gapmer design principles. RNV104L contained LNA nucleotides at positions 2, 3, 16, 17, and 18; RNV124 at positions 3, 4, 18, 19, and 20. The LNA ASO sequences were as follows: scrambled control sequence: 5'-GCTTCGACTCGTAATCACCTA-3'; RNV124 (underlined bases denote LNA nucleotides): 5'-ATAAACCTGCTAGTGTCCTCC-3'; RNV104L: 5'-GTTAACTTTCTTCTTCCTTG-3'. Lyophilized oligonucleotides were resuspended in ultrapure H_2O (Invitrogen) and stored as a 100 µM stock solution at -20°C. Briefly, LNA-ASOs were diluted to 20 µM in OptiMEM I Reduced Serum Medium (Invitrogen) and cultured cells were transfected according to the manufacturer's instructions. Cultured cells were incubated at 37°C in 5% CO_2 for 4 hours, before 500 µl growth medium, containing 30% FCS, was added to the serum-free medium. The cells were transfected for 24-72 hours and *GHSROS* levels assessed by qRT-PCR.

RNA secondary structure prediction

The ViennaRNA web server was employed[139] to predict the secondary structure of *GHSROS* and its minimum free energy[140, 141].

Cell proliferation assays

Proliferation assays were performed using an xCELLigence real-time cell analyzer (RTCA) DP instrument (ACEA Biosciences, San Diego, CA). This system employs sensor impedance technology to quantify the status of the cell using a unit-less parameter termed the cell index (CI). The CI represents the status of the cell based on the measured relative changes in electrical impedance that occur in the presence and absence of cells in the wells (generated by the software, according to the formula $CI = (Z_i - Z_0)/15\ \Omega$, where Z_i is the impedance at an individual point of time during the experiment and Z_0 the impedance at the start of the experiment). Impedance is measured at three different frequencies (10, 25 or 50 kHz). Briefly, 5×10^3 cells were trypsinized and seeded into a 96 well plate (E-plate) and grown for 48 hours in 150 µl growth media. Cell index was measured every 15 minutes and all experiments were performed in triplicate, with at least three independent repeats. Because cells did not attach well to the gold microelectrodes of the xCELLigence instrument, LNCaP proliferation was quantified by measuring the cleavage of WST-1 (Roche, Basel, Switzerland). Briefly, 5×10^4 cells/ well were seeded in 96-well plates (BD Biosciences, Franklin Lakes, NJ) and propagated for 72 hours in complete medium. To determine cell number, absorbance was measured using the FLUOstar Omega spectrophotometer (BMG, Ortenberg, Germany) at 440 nm using a reference wavelength of 600 nm. All proliferation experiments were performed independently three times, with 8 replicates each.

Cell Viability Assay
LNCaP and PC3 vector or *GHSROS* over-expressing cells (5000 cells/well) were seeded in 96-well plates (BD Biosciences) and propagated overnight in complete medium. LNCaP cells were treated with standard doses of test compounds in both charcoal stripped FCS (CSS) or 2% FCS. PC3 cells were treated with increasing doses of docetaxel in 2% FCS. After a 96-hour period cell viability was measured using a WST-1 cell proliferation assay (Roche, Nonnenwald, Penzberg, Germany) according to the manufacturer's instructions. All viability experiments were performed independently three times, with 4 replicates each.

Cell Migration assays
Migration assays were performed using an xCELLigence RTCA DP instrument (ACEA Biosciences). Briefly, 5×10^4 cells/well were seeded on the top chamber in 150 µl serum-free media. The lower chamber contained 160 µl media with 10% FCS as a chemo-attractant. Cell index was measured every 15 minutes for 24 hours to indicate the rate of cell migration to the lower chamber. All experiments were performed in triplicate with at least 3 independent repeats. Because cells did not attach well to the gold microelectrodes of the xCELLigence instrument, LNCaPs migration was assessed using a transwell assay. Briefly, 6×10^5 cells were suspended in serum-free medium and added to the upper chamber of inserts coated with a polycarbonate membrane (8 µm pore size; BD Biosciences). Cells in 12-well plates were allowed to migrate for 24 h in response to a chemoattractant (10% FBS) in the lower chamber. After 24 h, cells remaining in the upper chamber were removed. Cells that had migrated to the lower surface of the membrane were fixed with methanol (100%) and stained with 1% crystal violet. Acetic acid (10%, v/v) was used to extract the crystal violet and absorbance was measured at 595 nm. Each experiment consisted of three replicates and was repeated independently three times.

Mouse subcutaneous *in vivo* xenograft models
All mouse studies were carried out with approval from the University of Queensland and the Queensland University of Technology Animal Ethics Committees. PC3-GHSROS, PC3-vector, DU145-GHSROS, DU145-vector, LNCaP-GHSROS, and LNCaP-vector cell lines were injected subcutaneously into the flank of 4-5-week-old male NSG mice[142] (obtained from Animal Resource Centre, Murdoch, WA, Australia). Cells were injected in a 1:1 ratio with growth factor-reduced Matrigel (Thermo Fisher) (n=8-10 per cell line) and tumors measured twice weekly with digital calipers (ProSciTech, Kirwan, QLD, Australia). Neither randomization nor blinding for animal use was performed because we commercially obtained these mice with the same genetic background. Animals were euthanized once tumor volume reached 1,000 mm^3, or at other ethical endpoints. At the experimental endpoint, the primary tumor was resected, divided in half, snap frozen and stored at -80°C.

Histology and immunohistochemistry
For histological analysis, cryosections (6-10 µm thick) were prepared using a Leica CM1850 cryotome (Wetzlar, Germany). Sections were collected onto warm, charged Menzel Superfrost slides (Thermo Fisher), fixed in ice-cold 100% acetone, air dried and

stored at -80 ºC. For immunohistochemistry, tissues were fixed in paraformaldehyde and dehydrated through a graded series of ethanol and xylene, before being embedded in paraffin. Sections (5µm) were mounted on to glass Menzel Superfrost slides ThermoFisher Scientific). Immunohistochemistry was performed using antibodies for the proliferation marker Ki67 (rabbit anti-human Ki67, Abcam, Cambridge, UK) and for the infiltration of murine blood vessels using rabbit anti-murine CD31 antibody (Abcam). Tissue sections were incubated with HRP-polymer conjugates (SuperPicture, Thermo Fisher Scientific), and incubated with the chromagen diaminobenzidine (DAB) (Dako, Glostrup, Denmark), as per manufacturer's specifications. Slides were counterstained with Mayer's hematoxylin, dehydrated, and mounted with coverslips using D.P.X neutral mounting medium (Sigma-Aldrich). All sections were counterstained with Mayer's hematoxylin (Sigma Aldrich) and mounted with coverslips using D.P.X with Colourfast (Fronine, ThermoFisher Scientific).

RNA sequencing of PC3-GHSROS cells

RNA was extracted from *in vitro* cultured PC3-GHSROS cells and controls, as outlined in the manuscript body. RNA purity was analysed using an Agilent 2100 Bioanalyzer, and RNA with an RNA Integrity Number (RIN) above 7 used for RNA-seq. Strand-specific RNA-sequencing (RNA-seq) was performed by Macrogen, South Korea. A TruSeq stranded mRNA library (Illumina) was constructed and RNA sequencing performed (50 million reads) on a HiSeq 2000 instrument (Illumina) with 100bp paired end reads. Pre-processing of raw FASTQ reads, including elimination of contamination adapters, was performed with scythe v0.994 (https://github.com/vsbuffalo/scythe). Paired-end human FASTQ files were aligned to the human genome, UCSC build hg19 using the spliced-read mapper TopHat (v2.0.9)[130] and reference gene annotations to guide the alignment.

Raw gene counts were computed from TopHat-generated BAM files using featureCounts v1.4.5-p1[143], counting coding sequence (CDS) features of the UCSC hg19 gene annotation file (gtf). FeatureCounts output files were analysed using the R programming language (v.3.2.2). Briefly, raw counts were normalized by Trimmed Mean of M-values (TMM) correction[144, 145]. Library size-normalized read counts (per million; CPM) were subjected to the voom function (variance modelling at the observation-level) in limma v3.22.1 (Linear Models for Microarray Data)[146, 147], with trend=TRUE for the eBayes function and correction for multiple testing (Benjamini-Hochberg false discovery rate of cut-off, *Q*-value, set at 0.05). Genes with at least a 1.5 $\log_2$ fold-change difference in expression between PC3-GHSROS and PC3-vector (empty vector) cells were defined as differentially expressed. Although validation is not required, as RNA-seq gives very accurate measurements of relative expression across a broad dynamic range[148], selected differentially regulated genes were validated using quantitative reverse-transcription PCR (qRT-PCR) (see manuscript body and table S11).

Detailed gene annotations were obtained by querying Ensembl with the R/Bioconductor package 'biomaRt'[149]. Gene Ontology (GO) term analyses were performed using DAVID (Database for Annotation, Visualization and Integrated Discovery)[150]. Briefly, to test for enrichment we interrogated DAVID's GO FAT database with genes differentially

expressed in PC3-*GHSROS* cells. The DAVID functional annotation tool categorizes GO terms and calculates an 'enrichment score' or EASE score (a modified Fisher's exact test-derived *P*-value). Categories with smaller *P*-values ($P \leq 0.01$) and larger fold-enrichments (≥ 2.0) were considered interesting and most likely to convey biological meaning[150].

To perform Oncomine meta-analysis, genes differentially expressed in PC3-GHSROS were separated into 'over-expressed' and 'under-expressed' gene sets. The Oncomine database[27] was interrogated by importing these genes, and enriched concepts were generated and ordered by *P*-values (calculated using Fisher's exact test). Only datasets with an odds ratio ≥ 3.0 and a *P*-value ≤ 0.01 were retained. The datasets were exported as nodes and edges for network visualization in Cytoscape[151] (v3.4.0). The network layout and node position were generated using the Force-Directed Layout algorithm[152], with odds ratio as the leading parameter for the edge weight. Using our custom concept generated lists, we next sought to assess the differential expression of our gene lists in two prostate cancer microarray datasets: Grasso[35] (59 localized and 35 metastatic prostate tumors) and Taylor[36] (123 localized and 27 metastatic prostate tumors). Differentially expressed genes were ranked and results exported as fold change ($\log_2$ transformed, median centered). Data was filtered for significance with *P*-value set at ≤ 0.05 and Benjamini-Hochberg false discovery rate (FDR) *Q*-value[153] at ≤ 0.25; a threshold deemed suitable to find biologically relevant transcriptional signatures[154, 155].

RNA sequencing of LNCaP-GHSROS cells

RNA was extracted from LNCaP-GHSROS xenograft tumors and controls (empty vector control lentiviral constructs), as outlined in the manuscript body. RNA purity was analysed using an Agilent 2100 Bioanalyzer, and RNA with an RNA Integrity Number (RIN) above 7 used for RNA-seq. Strand-specific RNA-seq was performed by the South Australian Health and Medical Research Institute (SAHMRI, Adelaide, SA, Australia). A TruSeq stranded mRNA library (Illumina) was constructed and RNA sequencing performed (35 million reads) on a Nextseq 500 instrument (Illumina) with 75bp single end reads. Pre-processing of raw FASTQ reads, including elimination of contamination adapters, was performed with scythe v0.994 (https://github.com/vsbuffalo/scythe). Human (xenograft tumor; the graft) and mouse (the host) RNA-seq reads were separated using Xenome[156] on the trimmed FASTQ files, leaving ~20M human reads. Reads were aligned to the human genome and processed as described for PC3-GHSROS cells above. Genes differentially expressed in LNCaP-GHSROS cells (cutoff set at $\log_2$ 1.5-fold-change and $Q \leq 0.05$) were imported into the GSEA (Gene Set Enrichment Analysis) program[157].

LP50 prostate cancer cell line *AR* knockdown microarray

Publicly available Affymetrix HG-U133 Plus 2.0 microarray data (NCBI GEO accession no. GSE22483) from a substrain of the LNCaP cell line: androgen-independent late passage LNCaP cells (LP50) was interrogated. This cell line was subjected to androgen receptor (*AR*) knockdown by shRNA[64]. The array (n=2, of AR shRNA and scrambled control) was normalized to housekeeping genes using the Affymetrix Gene Chip Operating System v1.4[64]. Prior to differential expression analysis, the probe set was pre-

filtered, using the R statistical programming language, as follows: probes with mean expression values in the lowest 20th percentile of the array was removed. Differential expression was determined by the R package 'limma'[139] and probes with a Benjamini-Hochberg adjusted *P*-value (*Q*; BH-FDR) ≤ 0.05 considered significant. Gene annotations were obtained using the R/Bioconductor packages 'Biobase'[158] and 'GEOquery'[159].

Survival analysis

Two datasets were interrogated: Taylor[36](123 localized and 27 metastatic prostate tumors) and TCGA-PRAD from The Cancer Genomics Atlas (TCGA) consortium, which contains tumors from patients with moderate- (~39% Gleason 6 and 3 + 4) and high- (~61% Gleason 4+3 and Gleason 8-10) risk localized prostate carcinoma[37]. Briefly, in the case of TCGA-PRAD, the UCSC Xena Browser[160] was used to obtain normalized gene expression values, represented as $\log_2$(normalized counts+1), from the 'TCGA TARGET GTeX' dataset consisting of ~12,000 tissue samples from 31 cancers[161]. To obtain up-to-date overall survival (OS) and disease-free survival (DFS) information, we manually queried cBioPortal for Cancer Genomics[162, 163] (last accessed 05.08.16).

We performed non-hierarchical *k*-means clustering[164] to partition patients into groups with similar gene expression patterns[165]. The following 10 genes obtained by Oncomine meta-analysis (see above) were assessed: *AASS*, *CHRDL1*, *CNTN1*, *DIRAS1*, *FBXL16*, *IFI16*, *MUM1L1*, *TP53I11*, *TFF2*, and *ZNF467*. Clustering was performed using the *kmeans* function in the R package 'stats' with two clusters/groups (*k=2*) and the best cluster pair after 500 runs (*nstart=500*) was retained[166]. Kaplan-Meier survival analysis[167] was performed with the R package 'survival'[168], fitting survival curves (*survfit*) and computing log-rank *P*-values using the *survdiff* function, with *rho=0* (equivalent to the method employed by UCSC Xena; see https://goo.gl/4knf62). Survival curves were plotted when survival was significantly different between two groups (log-rank $P \leq 0.05$). We used the *coxph* function in the R package 'survival' to test the prognostic significance of genes (that is: we implemented the Cox proportional hazard model to analyze the association of gene expression with patient survival)[169, 170], with $P \leq 0.05$ (Wald test) considered significant. Because there is a single categorical covariate (*k*-means cluster; group), the *P*-values from the log-rank and the Cox regression tests are comparable. We considered groups (clusters) that had fewer than 10 samples with a recorded event unreliable.

A scaled heat map (unsupervised hierarchical clustering by Euclidean distance) was generated in R using heatmap.3 (available at https://goo.gl/Yd9aTY) and a custom R script.

Statistical analyses

Data values were expressed as mean ± s.e.m. of at least two independent experiments and evaluated using Student's *t*-test for unpaired samples, or otherwise specified. Mean differences were considered significant when $P \leq 0.05$. *Q*-values denote multiple testing correction (Benjamini-Hochberg) adjusted *P*-values[153]. Normalized high-throughput gene expression data were analyzed using LIMMA, employing a modified version of the

Student's *t*-test (moderated *t*-test) where the standard errors are reduced toward a common value using an empirical Bayesian model robust for datasets with few biological replicates[147]. Statistical analyses were performed using GraphPad Prism v.6.01 software (GraphPad Software, Inc., San Diego, CA), or the R statistical programming language.

Code

Selected R code is available in a repository at https://github.com/sciseim/GHSROS_MS. Additional R and bash scripts can be obtained by contacting the corresponding authors.

SUPPLEMENTARY REFERENCES

68 Langer W. *et al*. Exon array analysis using re-defined probe sets results in reliable identification of alternatively spliced genes in non-small cell lung cancer. *BMC Genomics* 2010; **11**: 676.

69 Folkard D.L. *et al*. Suppression of LPS-induced transcription and cytokine secretion by the dietary isothiocyanate sulforaphane. *Mol Nutr Food Res* 2014; **58**: 2286-2296.

70 Stricker S.H. *et al*. Widespread resetting of DNA methylation in glioblastoma-initiating cells suppresses malignant cellular behavior in a lineage-dependent manner. *Genes Dev* 2013; **27**: 654-669.

71 Riihijarvi S. *et al*. Prognostic influence of macrophages in patients with diffuse large B-cell lymphoma: a correlative study from a Nordic phase II trial. *Haematologica* 2015; **100**: 238-245.

72 Soreq L. *et al*. Identifying alternative hyper-splicing signatures in MG-thymoma by exon arrays. *PLoS One* 2008; **3**: e2392.

73 Riaz M. *et al*. Low-risk susceptibility alleles in 40 human breast cancer cell lines. *BMC Cancer* 2009; **9**: 236.

74 Bernstein B.E. *et al*. The NIH Roadmap Epigenomics Mapping Consortium. *Nat Biotechnol* 2010; **28**: 1045-1048.

75 Maurano M.T. *et al*. Systematic localization of common disease-associated variation in regulatory DNA. *Science* 2012; **337**: 1190-1195.

76 Neph S. *et al*. An expansive human regulatory lexicon encoded in transcription factor footprints. *Nature* 2012; **489**: 83-90.

77 Polak P. *et al*. Cell-of-origin chromatin organization shapes the mutational landscape of cancer. *Nature* 2015; **518**: 360-364.

78 Polak P. *et al*. Reduced local mutation density in regulatory DNA of cancer genomes is linked to DNA repair. *Nat Biotechnol* 2014; **32**: 71-75.

79 Schultz M.D. *et al*. Human body epigenome maps reveal noncanonical DNA methylation variation. *Nature* 2015; **523**: 212-216.

80 Hansen R.S. *et al*. Sequencing newly replicated DNA reveals widespread plasticity in human replication timing. *Proc Natl Acad Sci U S A* 2010; **107**: 139-144.

81 Thurman R.E. *et al*. The accessible chromatin landscape of the human genome. *Nature* 2012; **489**: 75-82.

82 Younis I. *et al*. Rapid-response splicing reporter screens identify differential regulators of constitutive and alternative splicing. *Mol Cell Biol* 2010; **30**: 1718-1728.

83 Dutertre M. *et al*. Estrogen regulation and physiopathologic significance of alternative promoters in breast cancer. *Cancer Res* 2010; **70**: 3760-3770.

84 Kitamura H. *et al*. Ubiquitin-specific protease 2-69 in macrophages potentially modulates metainflammation. *FASEB J* 2013; **27**: 4940-4953.

85 Omura N. *et al*. Cyclooxygenase-deficient pancreatic cancer cells use exogenous sources of prostaglandins. *Mol Cancer Res* 2010; **8**: 821-832.

86 Vincent A. *et al*. Genome-wide analysis of promoter methylation associated with gene expression profile in pancreatic adenocarcinoma. *Clin Cancer Res* 2011; **17**: 4341-4354.

87 Risueno A. *et al*. A robust estimation of exon expression to identify alternative spliced genes applied to human tissues and cancer samples. *BMC Genomics* 2014; **15**: 879.

88 Dutertre M. *et al*. A recently evolved class of alternative 3'-terminal exons involved in cell cycle regulation by topoisomerase inhibitors. *Nat Commun* 2014; **5**: 3395.

89 Dutertre M. *et al*. Cotranscriptional exon skipping in the genotoxic stress response. *Nat Struct Mol Biol* 2010; **17**: 1358-1366.

90 Calverley D.C. *et al*. Significant downregulation of platelet gene expression in metastatic lung cancer. *Clin Transl Sci* 2010; **3**: 227-232.

91 Llorian M. *et al*. Position-dependent alternative splicing activity revealed by global profiling of alternative splicing events regulated by PTB. *Nat Struct Mol Biol* 2010; **17**: 1114-1123.

92 Kan Z. *et al*. Diverse somatic mutation patterns and pathway alterations in human cancers. *Nature* 2010; **466**: 869-873.

93 Pencovich N., Jaschek R., Tanay A., Groner Y. Dynamic combinatorial interactions of RUNX1 and cooperating partners regulates megakaryocytic differentiation in cell line models. *Blood* 2011; **117**: e1-e14.

94 Kohn K.W., Zeeberg B.M., Reinhold W.C., Pommier Y. Gene expression correlations in human cancer cell lines define molecular interaction networks for epithelial phenotype. *PLoS One* 2014; **9**: e99269.

95 Reinhold W.C. *et al*. Exon array analyses across the NCI-60 reveal potential regulation of TOP1 by transcription pausing at guanosine quartets in the first intron. *Cancer Res* 2010; **70**: 2191-2203.

96 Mukherjee N. *et al*. Integrative regulatory mapping indicates that the RNA-binding protein HuR couples pre-mRNA processing and mRNA stability. *Mol Cell* 2011; **43**: 327-339.

97 Gravendeel L.A. *et al*. Gene expression profiles of gliomas in formalin-fixed paraffin-embedded material. *Br J Cancer* 2012; **106**: 538-545.

98 Agell L. *et al*. A 12-gene expression signature is associated with aggressive histological in prostate cancer: SEC14L1 and TCEB1 genes are potential markers of progression. *Am J Pathol* 2012; **181**: 1585-1594.

99 Hong S.H. *et al*. Upregulation of adenylate cyclase 3 (ADCY3) increases the tumorigenic potential of cells by activating the CREB pathway. *Oncotarget* 2013; **4**: 1791-1803.

100 Rajan P. *et al*. Identification of novel androgen-regulated pathways and mRNA isoforms through genome-wide exon-specific profiling of the LNCaP transcriptome. *PLoS One* 2011; **6**: e29088.

101 Baty F. *et al*. EGFR exon-level biomarkers of the response to bevacizumab/erlotinib in non-small cell lung cancer. *PLoS One* 2013; **8**: e72966.

102 Klco J.M. *et al*. Genomic impact of transient low-dose decitabine treatment on primary AML cells. *Blood* 2013; **121**: 1633-1643.

103 Erdem-Eraslan L. *et al*. Intrinsic molecular subtypes of glioma are prognostic and predict benefit from adjuvant procarbazine, lomustine, and vincristine chemotherapy in combination with other prognostic factors in anaplastic oligodendroglial brain tumors: a report from EORTC study 26951. *J Clin Oncol* 2013; **31**: 328-336.

104 Mack S,C. *et al*. Epigenomic alterations define lethal CIMP-positive ependymomas of infancy. *Nature* 2014; **506**: 445-450.

105 Gerber J.M. *et al*. Genome-wide comparison of the transcriptomes of highly enriched normal and chronic myeloid leukemia stem and progenitor cell populations. *Oncotarget* 2013; **4**: 715-728.

106 Tripathi V. *et al*. Long noncoding RNA MALAT1 controls cell cycle progression by regulating the expression of oncogenic transcription factor B-MYB. *PLoS Genet* 2013; **9**: e1003368.

107 Erho N. *et al*. Discovery and validation of a prostate cancer genomic classifier that predicts early metastasis following radical prostatectomy. *PLoS One* 2013; **8**: e66855.

108 Zhao S.G. *et al*. The Landscape of Prognostic Outlier Genes in High-Risk Prostate Cancer. *Clin Cancer Res* 2016; **22**: 1777-1786.

109 Valletti A. *et al*. Genome-wide analysis of differentially expressed genes and splicing isoforms in clear cell renal cell carcinoma. *PLoS One* 2013; **8**: e78452.

110 Silva-Martinez G.A. *et al*. Arachidonic and oleic acid exert distinct effects on the DNA methylome. *Epigenetics* 2016; **11**: 321-334.

111 Mitra A.P. *et al*. Discovery and validation of novel expression signature for postcystectomy recurrence in high-risk bladder cancer. *J Natl Cancer Inst* 2014; **106**.

112 Karnes R.J. *et al*. Validation of a genomic classifier that predicts metastasis following radical prostatectomy in an at risk patient population. *J Urol* 2013; **190**: 2047-2053.

113 Tsai H. *et al*. Cyclin D1 Loss distinguishes prostatic small-cell carcinoma from most prostatic adenocarcinomas. *Clin Cancer Res* 2015; **21**: 5619-5629.

114 Zhao S.G. *et al*. The Landscape of Prognostic Outlier Genes in High-Risk Prostate Cancer. *Clin Cancer Res* 2016; **22**: 1777-1786.

115 Klein E.A. *et al*. A genomic classifier improves prediction of metastatic disease within 5 years after surgery in node-negative high-risk prostate cancer patients managed by radical prostatectomy without adjuvant therapy. *Eur Urol* 2015; **67**: 778-786.

116 Jager W. *et al*. Patient-derived bladder cancer xenografts in the preclinical development of novel targeted therapies. *Oncotarget* 2015; **6**: 21522-21532.

117 Teicher B.A. *et al*. Sarcoma cell line screen of oncology drugs and investigational agents identifies patterns associated with gene and microRNA expression. *Mol Cancer Ther* 2015; **14**: 2452-2462.

118 Hu Z., Jiang K., Frank M.B., Chen Y., Jarvis J.N. Complexity and specificity of the neutrophil transcriptomes in juvenile idiopathic arthritis. *Sci Rep* 2016; **6**: 27453.

119 Morgan L.Z. *et al*. Quantitative trait locus and brain expression of HLA-DPA1 offers evidence of shared immune alterations in psychiatric disorders. *Microarrays (Basel)* 2016; **5**: 6.

120 French P.J. *et al*. Identification of differentially regulated splice variants and novel exons in glial brain tumors using exon expression arrays. *Cancer Res* 2007; **67**: 5635-5642.

121 Dapas M., Kandpal M., Bi Y., Davuluri R.V. Comparative evaluation of isoform-level gene expression estimation algorithms for RNA-seq and exon-array platforms. *Brief Bioinform* 2017; **18**: 260-269.

122 Griffith M. *et al*. Alternative expression analysis by RNA sequencing. *Nat Methods* 2010; **7**: 843-847.

123 Barrett T. *et al*. NCBI GEO: archive for functional genomics datasets--update. *Nucleic Acids Res* 2013; **41**: D991-995.

124 Brazma A. *et al*. ArrayExpress--a public repository for microarray gene expression data at the EBI. *Nucleic Acids Res* 2003; **31**: 68-71.

125 Piccolo S.R. *et al*. A single-sample microarray normalization method to facilitate personalized-medicine workflows. *Genomics* 2012; **100**: 337-344.

126 Piccolo S.R., Withers M.R., Francis O.E., Bild A.H., Johnson W.E. Multiplatform single-sample estimates of transcriptional activation. *Proc Natl Acad Sci U S A* 2013; **110**: 17778-17783.

127 Tarazona S., Garcia-Alcalde F., Dopazo J., Ferrer A., Conesa A. Differential expression in RNA-seq: a matter of depth. *Genome Res* 2011; **21**: 2213-2223.

128 Sowalsky AG. *et al*. Whole transcriptome sequencing reveals extensive unspliced mRNA in metastatic castration-resistant prostate cancer. *Mol Cancer Res* 2015; **13**: 98-106.

129 Adiconis X. *et al*. Comparative analysis of RNA sequencing methods for degraded or low-input samples. *Nat Methods* 2013; **10**: 623-629.

130 Kim D. *et al*. TopHat2: accurate alignment of transcriptomes in the presence of insertions, deletions and gene fusions. *Genome Biol* 2013; **14**: R36.

131 Kent W.J. *et al*. The human genome browser at UCSC. *Genome Res* 2002; **12**: 996-1006.

132 Karolchik D. *et al*. The UCSC Table Browser data retrieval tool. *Nucleic Acids Res* 2004; **32**: D493-496.

133 Li H. *et al*. The Sequence Alignment/Map format and SAMtools. *Bioinformatics* 2009; **25**: 2078-2079.

134 Ramirez F. *et al*. deepTools2: a next generation web server for deep-sequencing data analysis. *Nucleic Acids Res* 2016; **44**: W160-W165.

135 Sims D., Sudbery I., Ilott N.E., Heger A., Ponting C.P. Sequencing depth and coverage: key considerations in genomic analyses. *Nat Rev Genet* 2014; **15**: 121-132.

136 Livak K.J., Schmittgen T.D. Analysis of relative gene expression data using real-time quantitative PCR and the 2(-Delta Delta C(T)) Method. *Methods* 2001; **25**: 402-408.

137 Hormaechea-Agulla D. *et al*. Ghrelin *O*-acyltransferase (GOAT) enzyme is overexpressed in prostate cancer, and its levels are associated with patient's metabolic status: Potential value as a non-invasive biomarker. *Cancer Lett* 2016; **383**: 125-134.

138 Vandesompele J. *et al*. Accurate normalization of real-time quantitative RT-PCR data by geometric averaging of multiple internal control genes. *Genome Biol* 2002; **3**: research0034.1-research0034.11.

139 Gruber A.R., Bernhart S.H., Lorenz R. The ViennaRNA web services. *Methods Mol Biol* 2015; **1269**: 307-326.

140 Wan Y., Kertesz M., Spitale R.C., Segal E., Chang H.Y. Understanding the transcriptome through RNA structure. *Nat Rev Genet* 2011; **12**: 641-655.

141 Zuker M., Stiegler P. Optimal computer folding of large RNA sequences using thermodynamics and auxiliary information. *Nucleic Acids Res* 1981; **9**: 133-148.

142 Shultz L.D. *et al*. Human lymphoid and myeloid cell development in NOD/LtSz-scid IL2R gamma null mice engrafted with mobilized human hemopoietic stem cells. *J Immunol* 2005; **174**: 6477-6489.

143 Liao Y., Smyth G.K., Shi W. featureCounts: an efficient general purpose program for assigning sequence reads to genomic features. *Bioinformatics* 2014; **30**: 923-930.

144 Robinson M.D., McCarthy D.J., Smyth G.K. edgeR: a Bioconductor package for differential expression analysis of digital gene expression data. *Bioinformatics* 2010; **26**: 139-140.

145 Robinson M.D., Oshlack A. A scaling normalization method for differential expression analysis of RNA-seq data. *Genome Biol* 2010; **11**: R25.

146 Law C.W., Chen Y., Shi W., Smyth G.K. voom: Precision weights unlock linear model analysis tools for RNA-seq read counts. *Genome Biol* 2014; **15**: R29.

147 Ritchie M.E. *et al*. limma powers differential expression analyses for RNA-sequencing and microarray studies. *Nucleic Acids Res* 2015; **43**: e47.

148 Wang E.T. *et al*. Alternative isoform regulation in human tissue transcriptomes. *Nature* 2008; **456**: 470-476.

149 Durinck S., Spellman P.T., Birney E., Huber W. Mapping identifiers for the integration of genomic datasets with the R/Bioconductor package biomaRt. *Nat Protoc* 2009; **4**: 1184-1191.

150 Huang da W., Sherman B.T., Lempicki R.A. Systematic and integrative analysis of large gene lists using DAVID bioinformatics resources. *Nat Protoc* 2009; **4**: 44-57.

151 Shannon P. *et al*. Cytoscape: a software environment for integrated models of biomolecular interaction networks. *Genome Res* 2003; **13**: 2498-2504.

152 Suderman M., Hallett M. Tools for visually exploring biological networks. *Bioinformatics* 2007; **23**: 2651-2659.

153 Benjamini Y., Hochberg Y. Controlling the false discovery rate: a practical and powerful approach to multiple testing. *J R Stat Soc Series B Stat Methodol* 1995; **1**: 289-300.

154 Luck S., Thurley K., Thaben P.F., Westermark P.O. Rhythmic degradation explains and unifies circadian transcriptome and proteome data. *Cell Rep* 2014; **9**: 741-751.

155 Simola D.F. *et al*. A chromatin link to caste identity in the carpenter ant *Camponotus floridanus*. *Genome Res* 2013; **23**: 486-496.

156 Conway T. *et al*. Xenome--a tool for classifying reads from xenograft samples. *Bioinformatics* 2012; **28**: i172-178.

157 Subramanian A. *et al*. Gene set enrichment analysis: a knowledge-based approach for interpreting genome-wide expression profiles. *Proc Natl Acad Sci U S A* 2005; **102**: 15545-15550.

158 Huber W. *et al*. Orchestrating high-throughput genomic analysis with Bioconductor. *Nat Methods* 2015; **12**: 115-121.

159 Davis S., Meltzer P.S. GEOquery: a bridge between the Gene Expression Omnibus (GEO) and BioConductor. *Bioinformatics* 2007; **23**: 1846-1847.

160 Goldman M. *et al*. The UCSC Cancer Genomics Browser: update 2015. *Nucleic Acids Res* 2015; **43**: D812-817.

161 Vivian J. *et al*. Toil enables reproducible, open source, big biomedical data analyses. *Nat Biotechnol* 2017; **35**: 314-316.

162 Cerami E. *et al*. The cBio cancer genomics portal: an open platform for exploring multidimensional cancer genomics data. *Cancer Discov* 2012; **2**: 401-404.

163 Gao J. *et al*. Integrative analysis of complex cancer genomics and clinical profiles using the cBioPortal. *Sci Signal* 2013; **6**: pl1.

164 Hartigan J.A., Wong M.A. Algorithm AS 136: A k-means clustering algorithm. *J R Stat Soc Ser C Appl Stat* 1979; **28**: 100-108.

165 Quackenbush J. Computational analysis of microarray data. *Nat Rev Genet* 2001; **2**: 418-427.

166 Weichselbaum R.R. *et al*. An interferon-related gene signature for DNA damage resistance is a predictive marker for chemotherapy and radiation for breast cancer. *Proc Natl Acad Sci* U S A 2008; **105**: 18490-18495.

167 Rich J.T. *et al*. A practical guide to understanding Kaplan-Meier curves. *Otolaryngol Head Neck Surg* 2010; **143**: 331-336.

168 Therneau T. *A package for survival analysis in S*, doi: 10.1093/survival/43.3.1 (2015).

169 Cox D.R. Regression models and life-tables. *Breakthroughs in Statistics*. 527-541 (Springer, 1992).

170 Efron B. The efficiency of Cox's likelihood function for censored data. *J Am Stat Assoc* 1977; **72**: 557-565.